الجـــــــــــــــــــــمهـوريـــــة الجـــــــــــــزائـريـة الديمـــــــقـراطيـة الـشـــــــــعبيـة

**REPUBLIQUE ALGERIENNE DEMOCRATIQUE ET POPULAIRE**

وزارة التـــــــــــــــــــــــــــعـليـم العـــــــالي و البـــــــــحث العـــــلـمـــي

**Ministère de l'Enseignement Supérieur et de la Recherche Scientifique**

جـــــــــــــــامعة أبي بكـــر بـلـقـايد – تـلمســـــــــــــــان –

Université Aboubakr Belkaïd – Tlemcen –

Faculté de TECHNOLOGIE

# THESE

Présentée pour l'obtention du **grade** de **DOCTORAT 3ème Cycle**

**En** : Génie Mécanique

**Spécialité** : Energétique

**Par** : MEDJAHED Lamia

**Sujet**

# Combustion Study of Biofuel Derived from Waste Fish Oils in Internal Combustion Engines

Soutenue publiquement, le 15 / 02 / 2026 , devant le jury composé de :

| | | | |
|---|---|---|---|
| Mr Rachid Saim | Professeur | Univ. Tlemcen | Président |
| Mr Hamza Bousbaa | Professeur | ENPO-MA | Directeur de thèse |
| Mr Mohammed Benramdane | Professeur | Univ.Tlemcen | Co- Directeur de thèse |
| Mr Mohamed Bencherif | Professeur | Univ. USTO-Oran | Examinateur 1 |
| Mr Zakaria Sari Hassoun | MCA | Univ.Tlemcen | Examinateur 2 |

الجمهورية الجزائرية الديمقراطية الشعبية

**REPUBLIQUE ALGERIENNE DEMOCRATIQUE ET POPULAIRE**

وزارة التعليم العالي و البحث العلمي

**Ministère de l'Enseignement Supérieur et de la Recherche Scientifique**

جامعة أبي بكر بلقايد – تلمسان –

Université Aboubakr Belkaïd – Tlemcen –

Faculté de TECHNOLOGIE

# THESE

Présentée pour l'obtention du **grade** de **DOCTORAT 3ème Cycle**

**En** : Génie Mécanique

**Spécialité** : Energétique

**Par** : MEDJAHED Lamia

**Sujet**

# Etude de la combustion d'un biocarburant à base des huiles usagées de poisson dans les moteurs à combustion interne

Soutenue publiquement, le 15 / 02 / 2026 , devant le jury composé de :

| | | | |
|---|---|---|---|
| Mr Rachid Saim | Professeur | Univ. Tlemcen | Président |
| Mr Hamza Bousbaa | Professeur | ENPO-MA | Directeur de thèse |
| Mr Mohammed Benramdane | Professeur | Univ.Tlemcen | Co- Directeur de thèse |
| Mr Mohamed Bencherif | Professeur | Univ. USTO-Oran | Examinateur 1 |
| Mr Zakaria Sari Hassoun | MCA | Univ.Tlemcen | Examinateur 2 |

# Table of Contents

# Acknowledgements

All praise is due to Allah, the Most Merciful and the Most Compassionate, whose guidance and countless blessings sustained me throughout my academic journey and enabled me to complete this humble work. I ask Allah to send His peace and blessings upon His final Messenger, Prophet Muhammad (peace be upon him), and upon his family and companions.

I would like to express my deepest gratitude to my thesis director, Dr. Hamza Bousbaa, for his dedicated support, guidance, and trust throughout this journey. His perseverance, scientific rigor, and constant encouragement have been essential in bringing this work to completion. I am sincerely grateful for the time, patience, and commitment he devoted to this research.

My appreciation goes to my co-supervisor also, Dr. Mohammed Benramdane, who enriched this thesis with his insightful advice and invaluable assistance greatly. His expertise and availability were of tremendous help at every stage.

I am equally thankful to my peers at the LTE Laboratory, in particular Msemen Bachir and Boumaza Ali, whose collaborative spirit made this experience both meaningful and motivating. My thanks also extend to the faculty and staff of the Department of Mechanical Engineering at Abu Bakr Belkaid University, for the supportive academic system that enabled this research.

This thesis is also a reflection of the steady support and boundless love I have received from my family.I wish to sincerely thank my parents, who nurtured my curiosity, encouraged my ambitions, and supported my educational journey from the very beginning. Their constant prayers have been my greatest source of strength.

I have a special acknowledgement for my husband, *Choukri*. Thank you for being my steadfast source of strength. Your patience, constant encouragement, and unwavering belief in me carried me through the most challenging moments. This thesis would not have reached this stage without your support.

I am deeply grateful to have shared this PhD journey with my journey as a mother. To my boys, *Ihsane* and *Diaa*, you have been my endless source of motivation and joy. Your smiles and your innocent faith in me gave meaning to every step of this path. I truly hope I have made you proud.

My heartfelt thanks also go to my sister and brothers, whose love and encouragement have always been a source of strength. I am equally grateful to my family-in-law for their support, especially *Serina*, whose kindness and encouragement accompanied me throughout this journey.

To my solid support system ,  my dear friends *Imene*, *Nassima*, *Asmaa*, and *Amira* , thank you for being there in moments of doubt, for pushing me to do more, and for their belief in me, even at times when I lacked confidence in myself..

Finally, it is my hope that this work may serve as a meaningful contribution and to be beneficial and useful to anyone interested in this field. This work reflects not just my efforts, but also the encouragement and support I have received from everyone who has shaped my academic and personal journey. For that, I am profoundly grateful.

## Nomenclature

| | |
|---|---|
| $A$ | Control surface |
| $a$ | Thermal diffusivity |
| $a_r$ , $b_r$ | Empirical coefficients |
| $B_{rd}$ | Spalding transfer number |
| $b_{cr}$ | Critical collision impact parameter |
| $a_m$ , $b_m$ | Integral stoichiometric coefficients for reaction r |
| $C_p$ | Specific heat of the fluid |
| $C_{pm}$ | Specific heat of species m |
| $C_1$ | Constant of k–ε and RNG k–ε models |
| $C_2$ | Constant of k–ε and RNG k–ε models |
| $D$ | Diffusion coefficient |
| $F$ | Time rate of change of an individual droplet |
| $f$ | Probability distribution function of droplets |
| $\dot{f}_{bu}$ | Breakup source term |
| $\dot{f}_{coll}$ | Collision source term |
| $f_w$ | Wall heat flux per unit surface |
| $g$ | Inertial force |
| $\Delta h_f^0$ | Standard formation enthalpy of species m at absolute zero |
| $h_m$ | Specific enthalpy of species m |
| $I$ | Identity matrix |
| $I$ | Turbulence intensity |
| $I_m$ | Specific internal energy of species m |
| $J$ | Heat flux vector |
| $k$ | Turbulent kinetic energy |
| $K$ | Transport coefficient |
| $K_c^t(T)$ | Equilibrium constant |
| $K_{fr}$ , $K_{br}$ | Forward and backward reaction rate constants |

| | |
|---|---|
| $L$ | Latent heat |
| $m_f$ | Fuel mass in the considered zone |
| $m_{fg}$ | Vaporized fuel mass |
| $m_a$ | Air mass in this zone |
| $N$ | Engine rotational speed |
| $n$ | Normal vector to the wall surface |
| $P$ | Fluid pressure |
| $P_{ch}$ | Chamber pressure |
| $P_{inj}$ | Injection pressure |
| $P_{ox}$ | Oxygen partial pressure |
| $R$ | Droplet velocity |
| $R_C$ | Critical Reynolds number |
| $R_0$ | Universal gas constant |
| $R^*$ | Radical |
| $r$ | Droplet radius |
| $S$ | Spray/jet penetration |
| $T$ | Fluid temperature |
| $\dot{T}$ | Droplet temperature rate |
| $t$ | Time |
| $\Delta t$ | Time step |
| $T_{cu}$ | Cylinder head temperature |
| $T_{cy}$ | Cylinder temperature |
| $T_p$ | Wall temperature |
| $T_f$ | Fuel temperature |
| $u$ | Gas velocity |
| $u$ | Mean linear piston speed |
| $u^*$ | Shear velocity |
| $u''$ | Turbulent velocity fluctuation |
| $u_i$ | Fuel injection velocity |
| $u$ , $v$ , $w$ | Velocity vector components |

| | |
|---|---|
| $V$ | Control volume |
| $W_m$ | Molecular weight of species m |
| $W_{wall}$ | Wall velocity |
| $x$ , $y$ , $z$ | Cartesian coordinates |
| $\ddot{y}$ | Droplet oscillation velocity |
| $\dot{y}$ | Droplet time rate of change |
| $Y^*{}_m$ | Equilibrium mass fraction value |
| $Y_m$ | Mass fraction of species m |
| $\overline{\dot{Y_m}}$ | Mean source term |
| $\vec{\imath}, \vec{\jmath}, \vec{k}$ | Cartesian unit vectors |
| $\nabla$ | Laplacian |

## Greek Symbols

| | |
|---|---|
| $\sigma$ | Viscous stress tensor |
| $\varepsilon$ | Dissipation rate of turbulent kinetic energy |
| $\lambda$ | Thermal conductivity |
| $\mu$ | Dynamic viscosity |
| $\mu_t$ | Turbulent dynamic viscosity |
| $\nu$ | Kinematic viscosity |
| $\nu_t$ | Turbulent kinematic viscosity |
| $\nu'_{m,r}$, $\nu''_{m,r}$ | Stoichiometric coefficients for reactants and products |
| $\rho$ | Density |
| $\rho_m$ | Species density |
| $\rho_s$ | Soot density |
| $\tau_c$ | Characteristic chemical reaction time scale |
| $\tau_l$ | Laminar characteristic time scale |
| $\tau_t$ | Turbulent characteristic time scale |
| $w_r$ | Reaction rate |
| $\widetilde{\emptyset}$ | Favre-averaged quantity |

| | |
|---|---|
| $\Omega_{KH}$ | Kelvin–Helmholtz growth rate |
| $\dot{\rho}_{chem}$ | Jet source term |
| $\dot{\rho}$ | Chemical source term |
| Δθ | Injection duration |
| Λ | Wavelength |

## Dimensioless Numbers

| | |
|---|---|
| *We* | Weber Number |
| *Z* | Ohnesorge Number |
| *Ta* | Taylor Number |
| $We_L$ | Liquid Weber Number |
| $Re_L$ | Reynolds Number |
| *Nu* | Nusselt Number |
| *Pr* | Prandtl Number |
| *Sc* | Nombre de Schmidt |
| *Sh* | Nombre de de Sherwood |

## Abbreviations

| | |
|---|---|
| AMR | Adaptive Mesh Refinement |
| ASCII | American Standard Code for Information Interchange |
| ASTM | American Society for Testing and Materials |
| B100 | 100% Neat Biodiesel |
| B20 | 20% Biodiesel Blend |
| B30 | 30% Biodiesel Blend |
| BC | Bottom Center |
| BDC | Bottom Dead Center |
| BP | Brake Power |
| BSFC | Brake Specific Fuel Consumption |
| BTE | Brake Thermal Efficiency |

| | |
|---|---|
| °CA | crank angle degree |
| CaBIO | Canola Biodiesel |
| CAD | Computer Aided Design |
| CAD | crank angle degree |
| CB10 | 10% Canola Biodiesel Blend |
| CB20 | 20% Canola Biodiesel Blend |
| CEQ | Chemical Equilibrium |
| CFD | Computational Fluid Dynamic |
| CFPP | Cold Filter Plugging Point |
| CI | Compression-Ignition |
| CN | Cetane Index |
| CO | Carbon Monoxide |
| CO2 | Carbon Dioxide |
| CP | Cloud Point |
| CTC | Characteristic Time Combustion |
| D75BWP25 | Diesel 75% + (Waste Cooking Oil + Pongamia Oil) 25% |
| D80BWP20 | Diesel 80% + (Waste Cooking Oil + Pongamia Oil) 20% |
| D85BWP15 | Diesel 85% + (Waste Cooking Oil + Pongamia Oil) 15% |
| D90BWP10 | Diesel 90% + (Waste Cooking Oil + Pongamia Oil) 10% |
| D95BWP5 | Diesel 95% + (Waste Cooking Oil + Pongamia Oil) 5% |
| DI | Direct Injection |
| DPF | Diesel Particulate Filter |
| E10 | Ethanol Blend containing 10% Ethanol |
| E85 | Ethanol Blend containing 85% Ethanol |
| ECM | Engine Control Module |

| | |
|---|---|
| EGR | Exhaust Gas Recirculation |
| EN 14214 | European Biodiesel Standard |
| FAMEs | Fatty Acid Methyl Esters |
| FFAs | Free Fatty Acids |
| GM | Genetically Modified |
| GMV | General Mesh Viewer |
| GUI | Graphical User Interface |
| HC | Unburned Hydrocarbons |
| ICE | Internal Combustion Engines |
| IEA | International Energy Agency |
| KH | Kelvin-Helmholtz |
| KH | Kolmogorov Hinze |
| LHV | Lower Heating Value |
| LTE | Laboratoire de recherché en Technologie de l'environnement |
| NOx | Nitrogen Oxides |
| ONM | Office Nationale de la Météorologie |
| PaBIO | Palm Biodiesel |
| PB30 | Palm Biodiesel Blend 30% |
| PM | Particulate Matter |
| PO20 | Palm Oil Biodiesel Blend 20% |
| PP | Pour Point |
| RANS | Reynolds Averaged Navier-Stokes |
| RK | Redlich-Kwong |
| RKS | Redlich-Kwong-Soave |
| RNG | ReNormalization Group |

| | |
|---|---|
| RPM | Round Per Minute |
| RT | Rayleigh-Taylor |
| RT | Reynolds Transport |
| SAGE | Stochastic Algebraic Gas-phase Equations |
| STL | Standard Tessellation Language |
| TC | Top Center |
| TDC | Top Dead Center |
| TPC | Total Polar Compounds |
| TPM | Total Polar Materials |
| UCO | Used Cooking Oil |
| WB10 | 10% Waste Cooking Oil Biodiesel Blend |
| WB20 | 20%Waste Cooking Oil Biodiesel Blend |
| WCO | Waste Cooking Oil |

## List of Figures

# List of Tables

## Abstract

The rising global energy demand, the depletion of fossil fuel reserves, and the environmental challenges associated with waste cooking oil disposal highlight the need for cleaner and more sustainable fuel alternatives. This thesis investigates the production, characterization, and engine application of biodiesel derived from waste cooking oil, aiming to establish an efficient and environmentally responsible pathway for its utilization in existing diesel engines.

Waste cooking oil was collected, stored, and pretreated following proper handling practices to ensure feedstock quality. Biodiesel was produced through an optimized transesterification process in which the effects of alcohol-to-oil ratio, catalyst concentration, reaction time, and reaction temperature were evaluated. The produced biodiesel was purified and assessed according to ASTM D6751 and EN 14214 standards to verify its physicochemical suitability as a diesel substitute. Fuel blends of B5, B10, B20, and B30 were then formulated and evaluated to enhance fuel stability and better understand the influence of biodiesel concentration on engine behaviour.

Engine tests were conducted on a Deutz Z-MWM D302-1 single-cylinder, naturally aspirated, direct-injection diesel engine. Performance characteristics, fuel consumption, and pollutant emissions were examined across the different biodiesel blends. The validated experimental data were further used to develop a combustion model in CONVERGE CFD, providing numerical access to key spray and combustion characteristics such as in-cylinder pressure, temperature, heat release rate, and ignition delay.

The optimized production process yielded high-quality biodiesel fully compliant with ASTM D6751 and EN 14214 specifications. Engine results showed stable operation for all blends, with a modest increase in CO emissions and a clear reduction in NOx, attributed to the intrinsic oxygenated nature of biodiesel and its lower combustion temperature. The modelling results supported and deepened the experimental findings, overcoming limitations in available measurement techniques. Overall, this work demonstrates the viability of waste cooking oil biodiesel as a sustainable fuel and provides both experimental and computational contributions to the understanding of its combustion behaviour in diesel engines, confirming that WCO biodiesel and its blends represent an efficient, low-cost, and environmentally responsible fuel pathway with strong potential for real-world implementation.



## Keywords

Waste cooking oil, biodiesel, transesterification, diesel engine, performance, combustion, pollutant emissions, modelling, CONVERGE.

## الملخص

يشهد العالم تزايدًا مستمرًا في الطلب على الطاقة، في وقت تتراجع فيه احتياطيات الوقود الأحفوري وتتفاقم الآثار البيئية الناتجة عن التخلص غير السليم من زيوت القلي المستعملة. وفي هذا السياق، تهدف هذه الأطروحة إلى دراسة إنتاج البيوديزل من زيت الطهي المستعمل، وتوصيف خصائصه، وتقييم أدائه عند استخدامه في محركات الديزل، من أجل اعتماد مسار طاقوي مستدام وقابل للتطبيق في المحركات الحالية.

تم جمع زيت الطهي المستعمل وتخزينه ومعالجته أوليًا وفق إجراءات تضمن جودة المادة الأولية. ثم جرى إنتاج البيوديزل عبر عملية أسترة تبادلية محسّنة، شملت دراسة تأثير نسبة الكحول إلى الزيت، وتركيز الحفاز، وزمن التفاعل ودرجة حرارته. التنقية، وبعد خضع الوقود المنتج لتقييم شامل وفق مواصفات ASTM D6751 و .EN 14214 كما جرى تحضير خلطات B5 و B10 و B20و B30لتحليل تأثير نسبة البيوديزل على أداء المحرك.

أُجريت الاختبارات التجريبية على محرك ديزل أحادي الأسطوانة من نوع Deutz Z-MWM D302-1يعمل بالحقن المباشر والسحب الطبيعي. وشملت القياسات أداء المحرك، واستهلاك الوقود، والانبعاثات الغازية. واستُخدمت النتائج الموثوقة لتطوير نموذج عددي للاحتراق باستخدام برنامجCFD CONVERGE ، مما أتاح دراسة خصائص الرذاذ والاحتراق داخل الأسطوانة مثل الضغط والحرارة ومعدل إطلاق الحرارة وزمن الاشتعال.

أظهرت النتائج أن البيوديزل المنتج ذو جودة عالية ومطابق تمامًا للمعايير الدولية. كما أظهرت التجارب استقرارًا تشغيليًا لجميع الخلطات، مع ارتفاع طفيف في انبعاثات CO وانخفاض واضح في NOx، نتيجة التركيب المؤكسج للبيوديزل ودرجات حرارة الاحتراق المنخفضة. وقد أتاحت النمذجة العددية فهماً أعمق للظواهر الفيزيائية والكيميائية، متجاوزة حدود القياسات التقليدية. وتؤكد هذه الدراسة أن بيوديزل زيت الطهي
المستعمل يقدم خيارًا فعالًا ومنخفض التكلفة وصديقًا للبيئة، مع إمكانات قوية للتطبيق العملي.



## الكلمات المفتاحية

زيوت الطهي المستعملة ، الديزل الحيوي ، عملية الأسترة التبادلية ، محركات الديزل ، أداء ، انبعاثات العادم ، نمذجة الاحتراق،CONVERGE .

## Résumé

La croissance soutenue de la demande énergétique mondiale, l'épuisement progressif des ressources fossiles et les impacts environnementaux liés à l'élimination des huiles de cuisson usagées soulignent l'importance de développer des carburants alternatifs plus propres et durables. Dans cette optique, cette thèse porte sur la production, la caractérisation et l'application moteur d'un biodiesel issu d'huiles de friture usagées, dans le but de proposer une filière énergétique performante et respectueuse de l'environnement, compatible avec les moteurs diesel actuels.
Les huiles collectées ont été stockées et prétraitées selon des protocoles garantissant la qualité de la matière première. Le biodiesel a été obtenu par un procédé de transestérification optimisé, tenant compte du rapport alcool/huile, de la concentration en catalyseur ainsi que du temps et de la température de réaction. Après purification, le carburant a été évalué conformément aux normes ASTM D6751 et EN 14214. Des mélanges B5, B10, B20 et B30 ont été élaborés afin d'étudier l'influence de la teneur en biodiesel sur le comportement moteur.
Les essais expérimentaux ont été réalisés sur un moteur diesel monocylindre à injection directe et aspiration naturelle de type Deutz Z-MWM D302-1. Les performances, la consommation de carburant et les émissions polluantes ont été analysées pour chaque mélange. Les données validées ont ensuite servi à développer un modèle de combustion sous CONVERGE CFD, offrant un accès détaillé aux phénomènes de pulvérisation et d'auto-inflammation, ainsi qu'aux évolutions de pression, de température et de dégagement de chaleur dans le cylindre.
Les résultats montrent que le procédé optimisé permet d'obtenir un biodiesel de haute qualité conforme aux exigences internationales. Les tests moteur révèlent un fonctionnement stable des différents mélanges, accompagné d'une légère augmentation du CO et d'une réduction marquée des NOx, attribuées à la nature oxygénée du biodiesel et à ses températures de combustion plus faibles. La modélisation numérique a apporté un éclairage plus approfondi que les mesures expérimentales seules, dépassant leurs limitations. Globalement, ce travail confirme que le biodiesel issu des huiles de cuisson usagées constitue une solution énergétique efficace, économique et écologique, présentant un fort potentiel d'application réelle.



## Mots-clés

Huiles usagées, biodiesel, transestérification, moteur diesel, combustion, performances, émissions polluantes, modélisation, CONVERGE.

## Background and Context

The global energy landscape is under increasing strain due to the depletion of fossil fuel reserves, price instability, and geopolitical tensions. Despite the growing availability of alternative energy sources, fossil fuels continue to meet approximately 80% of worldwide energy demand, with diesel consumption rising from 3.5 million tonnes in 2010 to 3.9 million tonnes in 2019 (Ali Ijaz Malik et al., 2024). This reliance, coupled with the volatility of global oil markets, underscores the urgent need for locally available and sustainable energy alternatives.

Algeria's economy is particularly dependent on fossil fuel exports, with oil and natural gas representing 93.6% of its total export revenue. The sharp fluctuations in crude oil prices over the past decade have negatively impacted national economic stability. In response, the Algerian government has prioritized the transition toward renewable energy technologies and the green economy, aiming to secure future energy supply while mitigating environmental risks.

Among potential renewable options, biodiesel derived from waste cooking oil (WCO) emerges as a promising solution. It offers dual benefits: mitigating environmental pollution associated with WCO disposal and enhancing energy security (Maheshwari et al., 2022; Ali & Akbar, 2020). Improper management of WCO is a pressing issue worldwide and in Algeria, where the food industry and domestic sectors collectively produced around 469,332 metric tons of WCO in 2020, a figure projected to reach 561,286 metric tons by 2028 (Agence Nationale des Déchets, 2021). Improper disposal (through sewer systems or landfills) can lead to serious consequences, including water contamination, soil degradation, sewer blockages, and broader ecosystem disruption. For instance, China has faced long-standing challenges with "gutter oil" management, generating approximately five million tonnes of WCO annually, a significant portion of which re-enters the food supply or pollutes urban infrastructures. Similar issues are observed in Europe, the United States, Malaysia, and the United Kingdom, where fats, oils, and greases are major contributors to sewer blockages, imposing substantial economic burdens ( Lopresto et al., 2024).

Converting WCO into biodiesel provides a sustainable and circular solution, simultaneously promoting energy independence, reducing waste, and safeguarding public health. Developed regions such as the European Union, the United States, Japan, and Korea have implemented policies to encourage biodiesel production from WCO, including bans on its use in animal feed and mandates for renewable energy integration in the transport sector. Notably, the EU Renewable Energy Directive targeted a 10% share of renewable energy in transport by 2020, with WCO-based biodiesel expected to replace up to 1.5% of diesel consumption.

Biodiesel, as a renewable and environmentally friendly fuel, can be produced from a variety of lipid feedstocks, including WCO, palm oil, soybean oil, rapeseed oil, and microalgae (Tabatabaei et al., 2019). Research on WCO-based biodiesel has expanded due to its potential to address energy scarcity, reduce greenhouse gas emissions, promote sustainable economic growth, and prevent the illegal reuse of WCO in food production (Hosseinzadeh-Bandbafha et al., 2022). Historically, interest in WCO biodiesel intensified alongside global environmental awareness and renewable energy policies, with significant research developments occurring in the early 2000s, particularly in countries seeking to integrate circular economy principles into energy production.

From a technical perspective, biodiesel production from WCO is comparable to conventional biodiesel processes, involving alkaline, acidic, or enzymatic transesterification. However, it often requires additional steps for collection, pretreatment, and quality control, which can increase energy and material inputs, thereby influencing the overall sustainability and economic feasibility of the process. Nevertheless, the multiple benefits, which extend from environmental protection to energy security, make WCO-based biodiesel a compelling focus for both research and industrial development.

## Problem Statement

Despite growing awareness of the environmental and economic implications of fossil fuel dependence, diesel remains a dominant energy source for transportation and industrial sectors. The persistent rise in diesel demand, coupled with the depletion of petroleum reserves and fluctuations in global oil prices, continues to challenge the stability of energy systems, particularly in economies reliant on fossil fuel exports such as Algeria. This dependence limits progress toward sustainable energy diversification and exposes the national economy to external market vulnerabilities.

At the same time, the management of waste cooking oil (WCO) represents a significant environmental and public health concern. In Algeria, large quantities of WCO are generated annually from domestic and industrial activities, yet systematic collection and valorization practices remain underdeveloped. Improper disposal of WCO through drainage systems or landfills contributes to water and soil contamination, sewer blockages, and the emission of harmful degradation by-products. Furthermore, the absence of structured recycling mechanisms results in the loss of a potentially valuable energy resource.

Although converting WCO into biodiesel presents a technically viable and environmentally responsible alternative, several challenges persist. The variability in WCO composition, its high

free fatty acid content, and the presence of impurities complicate the transesterification process and can reduce biodiesel yield and quality. In addition, production costs associated with collection, pretreatment, and processing may affect the overall economic feasibility of WCO-based biodiesel compared with conventional diesel.

Existing research on biodiesel production from various feedstocks has established its potential as a clean and renewable substitute for fossil fuels; however, localized optimization that considers feedstock quality, reaction conditions, and process-specific limitations remains necessary to ensure its practical application. For Algeria, in particular, there is a lack of comprehensive studies addressing the optimization of WCO transesterification, the physicochemical characterization of the produced biodiesel, and its performance and emission behaviour in diesel engines. Thus, there is a clear need to investigate the potential of WCO as a sustainable feedstock for biodiesel production under local conditions, to develop optimized conversion methods, and to evaluate the resulting fuel's suitability for engine applications. Addressing these gaps would contribute not only to waste management and energy diversification in Algeria but also to the broader global effort toward cleaner and more sustainable fuel technologies.

## Research work motivation

The motivation for this study arises from the combined challenges of energy security, environmental protection, and sustainable waste management. Algeria's dependence on fossil fuels for both domestic consumption and export leaves its economy highly vulnerable to price fluctuations and market instabilities. At the same time, the growing generation of waste cooking oil presents an environmental burden but also an underutilized opportunity for renewable energy production.

Valorizing WCO as a feedstock for biodiesel production represents a practical pathway toward achieving national and global sustainability objectives. This approach aligns with the Algerian government's strategic vision to diversify energy sources and promote a green economy. By transforming waste into energy, WCO-based biodiesel production can simultaneously address waste management concerns, mitigate environmental pollution, and enhance local energy independence. Biodiesel provides a practical and adaptable energy option that does not require the large-scale infrastructure typical of solar, wind, or hydroelectric systems. Its flexibility makes it suitable for powering small, distributed energy setups for homes, community facilities, and essential services such as schools, clinics, or farms. This capability is particularly valuable in rural, remote, or disaster-affected areas where deploying conventional renewable energy technologies may be challenging.

From a scientific perspective, this research is motivated by the need to establish an integrated understanding of the entire WCO-to-biodiesel chain. While numerous studies have optimized the transesterification reaction, fewer have systematically examined the upstream variables (feedstock characterization, collection, storage, and pretreatment) that determine the quality and yield of the final product. Furthermore, comprehensive evaluation of biodiesel-diesel blends, combining experimental investigations with modeling analysis, is indispensable for validating their applicability under real engine operating conditions.

This study therefore contributes to filling critical research and practical gaps by:

- Emphasizing the significance of upstream processing in achieving consistent biodiesel quality;
- Optimizing transesterification conditions tailored to locally sourced WCO;
- Evaluating the performance of biodiesel–diesel blends in engine operation; and
- Promoting a circular economy model that integrates waste recovery with renewable fuel production.

By addressing these dimensions in a unified framework, this research aims to support Algeria's transition toward cleaner, more sustainable energy systems while providing insights relevant to other regions facing similar challenges.

## Thesis Objectives and Methodology

This PhD research aligns with the global vision of promoting sustainable waste-to-energy processes as a viable pathway to mitigate the dual challenges of waste accumulation and energy scarcity. As global waste generation continues to increase due to economic and demographic growth, the transformation of waste streams into renewable energy carriers becomes an imperative component of the circular economy. In this context, waste cooking oil (WCO) represents a promising renewable resource that can be converted into biodiesel, thereby addressing both waste management and sustainable energy production goals.

**General Objective**

The overarching objective of this thesis is to develop and assess an integrated framework for the production, optimization, and utilization of biodiesel derived from waste cooking oil. The study seeks to simplify the biodiesel production process while ensuring that the resulting fuel meets international standards of quality and performance. Furthermore, it aims to evaluate the potential of biodiesel-diesel blends as a technically feasible and environmentally sustainable alternative to conventional diesel.

**Specific Objectives**

To achieve the general aim, the following specific objectives were established:

1. *Waste Characterization and Pre-treatment*

   To investigate and establish procedures for the efficient collection, controlled storage, and pre-treatment of locally sourced waste cooking oil, ensuring feedstock consistency and suitability for biodiesel conversion.

2. *Optimization of the Transesterification Process*

   To determine the optimal reaction parameters, such as catalyst concentration, molar ratio, temperature, and reaction time, for maximizing biodiesel yield and purity using both experimental and statistical tools.

3. *Physicochemical Characterization of Biodiesel*

   To evaluate the produced biodiesel against international quality standards (ASTM D6751 and EN 14214) and analyse its physicochemical properties in comparison with conventional diesel.

4. *Blend Formulation and Performance Assessment*

   To formulate different biodiesel-diesel blends and assess their combustion, performance, and emission characteristics through experimental engine testing under various operating conditions.

5. *Computational Modeling and Simulation*

   To complement the experimental study with numerical simulations using CONVERGE software, enabling the prediction and analysis of in-cylinder phenomena such as spray behaviour, combustion dynamics, and emission formation, as well as the impact of engine parameters (e.g., EGR rate, injection timing).

6. *Evaluation of Environmental and Practical Implications*

   To analyse the potential of WCO biodiesel as a scalable and practical energy solution for decentralized applications, particularly in regions with limited access to conventional renewable systems.

**Methodological Approach**

The methodological framework of this research integrates experimental investigation and computational modelling to ensure comprehensive analysis and validation. The experimental phase involves the production of biodiesel from locally collected WCO, followed by characterization according to ASTM and EN standards. Subsequently, various biodiesel–diesel blends are prepared and tested in a single-cylinder, four-stroke compression ignition engine to evaluate key

performance parameters such as brake thermal efficiency, fuel consumption, and exhaust emissions (CO and $NO_x$).

In parallel, computational fluid dynamics (CFD) simulations are performed using CONVERGE software to model the in-cylinder combustion process of biodiesel-diesel blends. This simulation approach allows for the exploration of parameters that are difficult or costly to measure experimentally, offering detailed insight into spray evolution, ignition delay, and emission formation mechanisms. Together, the experimental and computational analyses provide a robust understanding of biodiesel behaviour under real-world engine conditions and contribute to the advancement of predictive models for renewable fuel performance.

## Thesis Outline

The thesis begins with a general introduction, which situates the research within the broader global and local context. It discusses the pressing challenges of fossil fuel dependence, environmental pollution, and the growing need for renewable energy solutions. Within this framework, the introduction presents the problem statement, research motivation, objectives, and methodology, establishing the foundation for the subsequent chapters and clarifying the rationale behind the study.

The first chapter provides a comprehensive literature review. It examines the global energy situation, presenting quantitative data and trends to illustrate the scale of energy demand and the environmental consequences of conventional fuels. Biofuels are defined and classified as a renewable energy source, with particular emphasis on waste cooking oil (WCO) as a promising feedstock for alternative fuel production. The chapter presents a holistic approach to biodiesel production, detailing the critical stages from collection and storage to transesterification and final biodiesel recovery. Issues and considerations at each stage, including quality control and characterization according to international standards, are discussed. Furthermore, the chapter reviews studies on engine performance and emissions when using biodiesel, providing a foundation for interpreting experimental results. In addition, it identifies limitations in current studies and highlights gaps that the present research aims to address.

The second chapter is dedicated to the case study of WCO biodiesel production. It presents an integrated valorisation of waste cooking oil into biodiesel covering all stages of the production process, including feedstock collection, storage, pre-treatment, transesterification, and biodiesel recovery. Detailed descriptions of the materials, experimental procedures, and methods are provided, and the physicochemical properties of the produced biodiesel are characterized according to international standards such as ASTM and EN. This chapter critically discusses

the challenges encountered, the optimization strategies employed, and the practical feasibility of WCO biodiesel production, emphasizing the scalability of the process and its potential for sustainable waste-to-energy applications.

The third chapter focuses on the experimental evaluation of engine performance and emissions using WCO biodiesel–diesel blends. It describes the engine test bench, instrumentation, and experimental protocols, followed by a presentation and discussion of the results. Key performance indicators, such as brake thermal efficiency and fuel consumption, as well as emission parameters, including CO and $NO_x$ are analysed to understand the practical implications of biodiesel blending on engine operation. This chapter provides insights into the real-world applicability of WCO biodiesel as an alternative fuel in conventional compression-ignition engines.

The fourth chapter transitions to computational modeling and simulation of biodiesel combustion. Using CONVERGE software, the study models in-cylinder phenomena including spray dynamics, turbulence, combustion, and emissions. The chapter details the mathematical models, boundary conditions, and validation procedures used to ensure accuracy. Simulation results are compared with the experimental findings from Chapter 3 to confirm model reliability. Once validated, the simulations explore different biodiesel–diesel blend ratios and engine operating conditions, offering predictive insights that complement the experimental observations and further inform optimization strategies.

Finally, the thesis concludes with conclusions and future perspectives section. This section summarizes the key findings of the research, highlighting both technical contributions and practical implications. It discusses the limitations of the experimental and computational approaches, and provides recommendations for future work, including potential scale-up, exploration of alternative feedstocks, different engine configurations, and the broader environmental and socio-economic impacts of WCO biodiesel adoption.

# CHAPTER 1

# Research Context: From Waste Cooking Oil to Engine Applications

This chapter provides a comprehensive overview of existing knowledge relevant to biodiesel production from waste cooking oil (WCO). It examines the global energy context, the classification and significance of biofuels as renewable energy sources, and the specific advantages of WCO as a feedstock for alternative fuels. The chapter further reviews previous studies on biodiesel production processes, feedstock characterization, fuel quality assessment, and engine performance and emissions. By identifying gaps and limitations in the current literature, this chapter establishes the foundation for the experimental and computational investigations presented in the subsequent chapters.

## 1.1 Global Energy and Economic Development

Energy is widely acknowledged as a fundamental driver of modern development and prosperity. It is not only a fuel source but also a determinant of economic resilience, technological progress, and social well-being. Historically, the large-scale discovery and exploitation of fossil fuels reshaped the economic landscape of nations, enabling industrialization, mechanization, and urbanization. Countries with access to abundant energy resources were able to accelerate growth, strengthen their industrial capacity, and consolidate geopolitical influence.

In contemporary times, the interdependence between energy and economic performance remains central to global power dynamics. Energy availability and affordability directly affect productivity, trade, and social stability. The persistent rise in global energy demand underscores this relationship, as rapid industrial expansion, urban population growth, and rising living standards drive increasing consumption. Major producers such as the United States, China, and Russia together account for nearly 38% of the global energy supply, illustrating how resource control translates into economic leverage and strategic influence. At the same time, the volatility of energy markets highlights the vulnerability of economies dependent on fossil fuel revenues, with fluctuations in oil and gas prices often triggering broad economic consequences.

## 1.2 Energy Resources and the Rising Demand

The increasing demand for energy is one of the defining challenges of the twenty-first century. With global population growth, industrialization in emerging economies, and the expansion of energy-intensive technologies, the pressure on available resources continues to intensify. This has amplified concerns about the long-term security of energy supply and its implications for both economic stability and environmental sustainability.

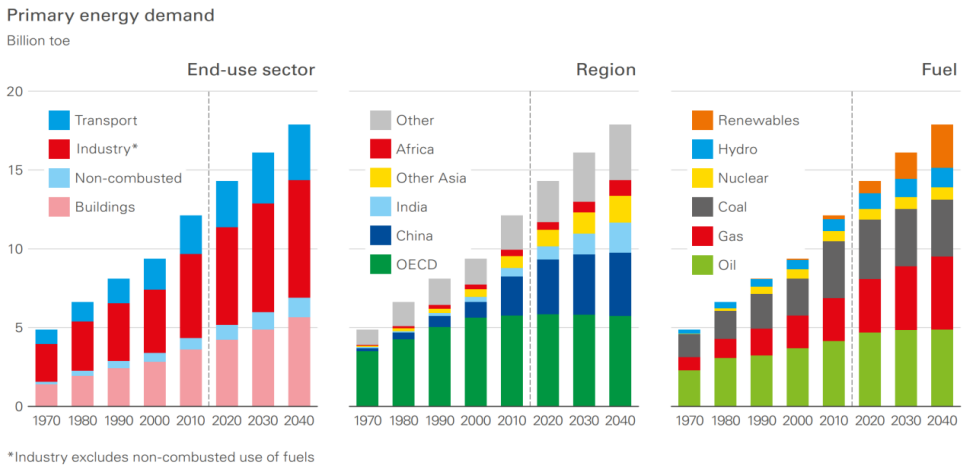


**Figure 1.1** Global primary energy demand by sector, region, and fuel type, 1970–2040 (BP, 2019b)

Energy resources are generally divided into two main categories: non-renewable and renewable. Non-renewable sources, such as crude oil, natural gas, coal, and nuclear power, have historically dominated the global energy system (Figure 1.1). Their high energy density and established infrastructure enabled the industrial revolution and sustained modern economic growth. However, these resources are finite, formed over geological timescales, and their depletion is inevitable. This raises questions about the ability of future generations to meet rising energy needs with diminishing reserves.

In contrast, renewable sources such as hydropower, biomass, solar, wind, and marine energy are replenishable on much shorter timescales. Their availability is more compatible with the objectives of long-term sustainability, and their share in the global mix has grown steadily in recent years as shown in.

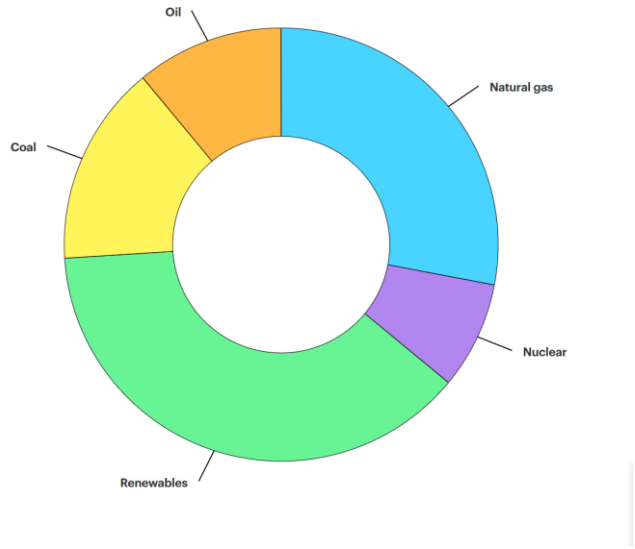


**Figure 1.2** Share of energy demand growth by source, 2024

Advances in technology, coupled with policy incentives, have accelerated their integration, positioning them as essential components of the energy transition.

Nevertheless, fossil fuels are expected to remain the cornerstone of global energy in the near future, particularly in sectors such as transport and heavy industry where alternatives are not yet widely scalable. This continued reliance highlights the dual challenge of meeting immediate demand while simultaneously preparing for a long-term shift to sustainable energy.

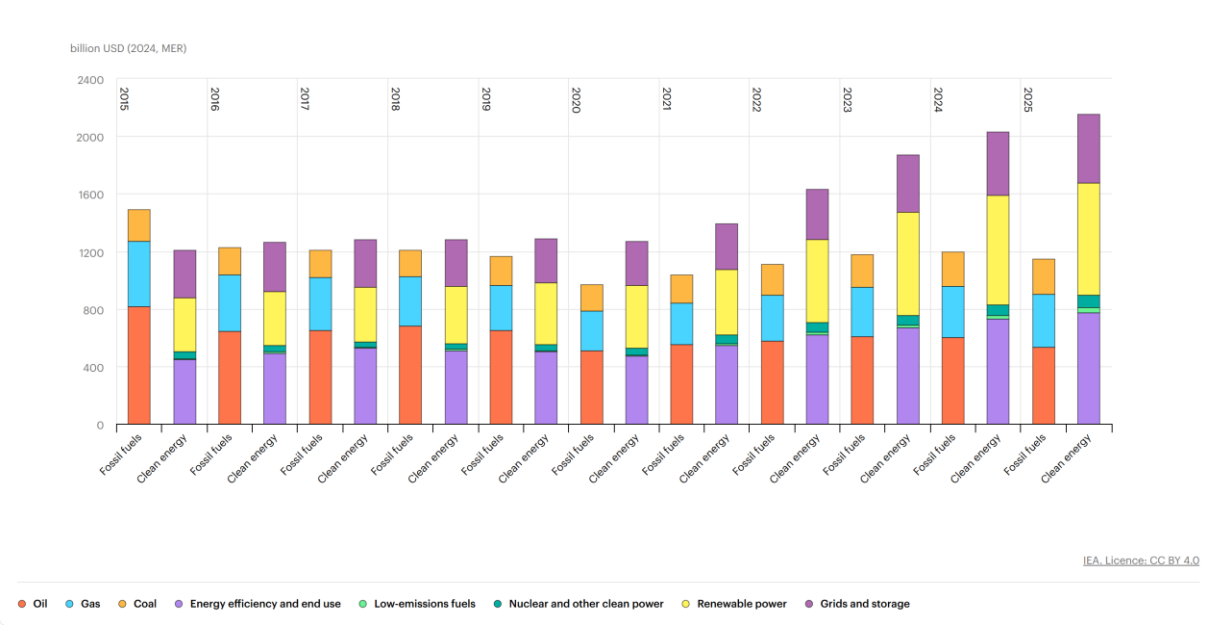


**Figure 1.3** Global investment in clean energy and fossil fuels, 2015-2025

The Global investment in clean energy and fossil fuels, 2015-2025 as shown by Figure 1.3 Global investment in clean energy and fossil fuels, 2015-2025underscores a dual reality: fossil fuels remain indispensable in the short term, but renewables are shaping the long-term path of energy diversification.

## 1.3 Emissions and Global Regulatory Responses

The increase in atmospheric greenhouse gas levels is largely attributable to the extensive combustion of fossil fuels. This accumulation, carbon dioxide ($CO_2$) particularly, has intensified global warming and contributed to climate-related challenges such as sea-level rise, extreme weather events, and long-term ecological disruptions. The environmental cost of continued dependence on coal, oil, and natural gas has therefore become a central concern of the international community.

In response, governments and multilateral organisations have established regulatory frameworks aimed at mitigating harmful emissions from industry, transport, and energy production. Policy interventions include mechanisms for carbon pricing, emissions trading schemes, mandates for renewable energy adoption, and efficiency regulations applied across multiple sectors. Collectively, such policies form the foundation of global climate governance, shaping both national energy strategies and international cooperation.

A landmark development in this regard was the adoption of the Paris Agreement in 2015, under which participating countries committed to limiting the global temperature increase to well below 2 °C above pre-industrial levels, with efforts to restrict the rise to 1.5 °C. To achieve these objectives, nations have submitted Nationally Determined Contributions (NDCs)**,** outlining their specific emission reduction targets and timelines.

The pursuit of global emission reduction targets requires not only efficiency improvements and stricter controls on fossil fuel use but also the integration of alternative energy sources capable of meeting rising demand without worsening environmental degradation. Among these alternatives, biofuels have emerged as a strategic option. As renewable and replenishable energy carriers, they reduce greenhouse gas emissions, lessen dependence on imported fossil resources, and contribute to agricultural and rural development.

## 1.4 Biofuels

Biofuels can provide both power and transport fuel, positioning them as a viable substitute for conventional fossil fuels. Unlike finite reserves of oil, coal, and natural gas, they can be replenished within relatively short cycles, supporting long-term sustainability. Their adoption also addresses a key challenge of the twenty-first century: meeting the vast and growing energy requirements of industrial, transport, and residential sectors while safeguarding energy security. Governments and international agencies have promoted supportive policies and invested in research to accelerate biofuel deployment as a means of reducing oil dependence and mitigating climate change impacts.

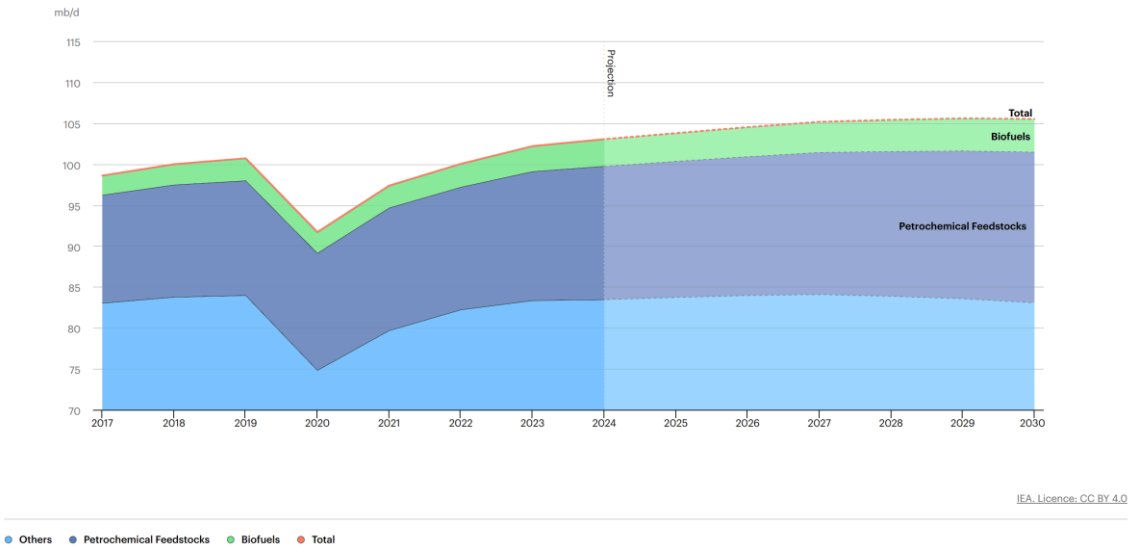


**Figure 1.4** Global oil demand forecast, 2017-2030 (IEA, 2024).

Since the early 2000s, the biofuel market has expanded steadily, driven by the need to diversify energy sources and enhance rural economies. A prominent example is Brazil, where large-scale biodiesel and bioethanol production has demonstrated the viability of biofuels as both an energy strategy and a development pathway. Data from the International Energy Agency illustrated by Figure 0.5 (IEA, 2024) confirm the consistent rise in demand for biodiesel and biogasoline between 1980 and 2022, underscoring their growing role in the global energy mix.

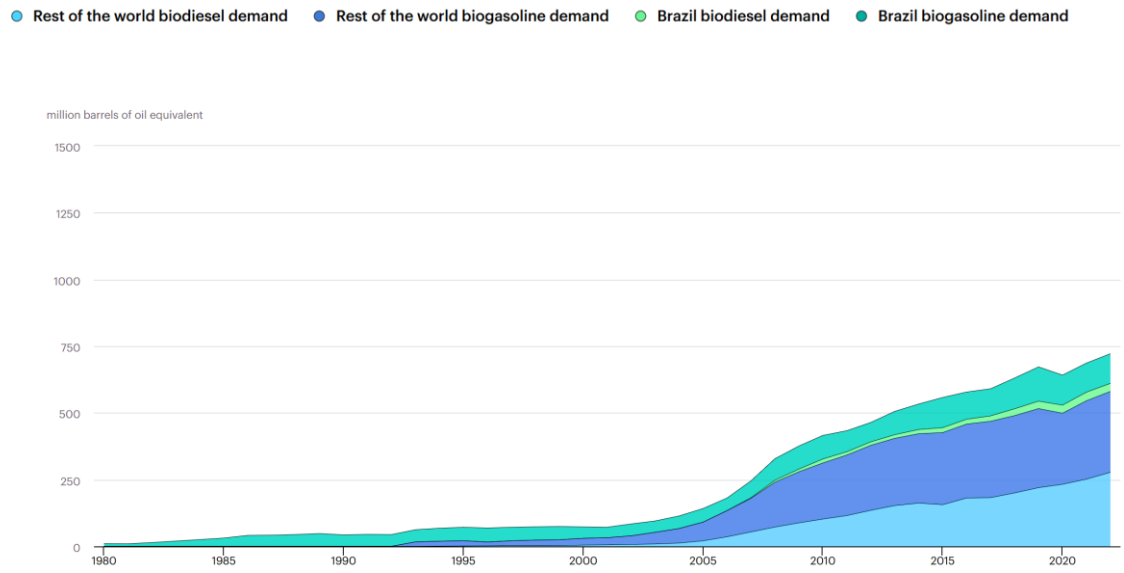


**Figure 1.5** demand for biodiesel and biogasoline between 1980 and 2022

Biofuels are fuels obtained from plant-based biomass, which includes both recently deceased organic matter and metabolic by-products of living organisms (Bungay, 1982; Demirbas, 2009). Such biomass can be transformed into usable fuels through thermal, chemical, or biochemical conversion processes. Human societies have relied on biomass as an energy source for centuries, with its use passing through successive generations.

### 1.4.1 Types of Biofuels

Biofuels can be broadly classified into liquid, gaseous, and solid forms, each with distinct applications and production pathways.

#### 1.4.1.1 Liquid Biofuels

These are the most practical substitutes for fossil fuels because they can be transported and stored within existing infrastructure. The two major liquid biofuels are bioethanol and biodiesel. Bioethanol, derived from sugar- and starch-based feedstocks such as sugarcane or maize, has

long been used as a gasoline additive due to its high octane rating and cleaner combustion (Park et al., 2012). Its blends, such as E10 and E85, are already widespread in global markets, with Brazil standing out as a pioneer in large-scale ethanol adoption (Sunggyu & Shah, 2012). Biodiesel, in contrast, is a diesel substitute produced mainly through transesterification of plant oils, animal fats, or waste oils. It is renewable, biodegradable, and has combustion properties similar to petroleum diesel, making it suitable for use either in pure form or in blends (Eevera et al., 2009; Bashir et al., 2022). Importantly, feedstock selection influences production cost and sustainability, with waste oils offering significant advantages over edible crops.

#### 1.4.1.2 Gaseous Biofuels

These include biogas and syngas, both obtained from the decomposition or gasification of organic matter. Biogas, composed mainly of methane and carbon dioxide, is generated via anaerobic digestion of agricultural residues, manures, and organic wastes, offering both energy recovery and waste management benefits. Syngas, rich in hydrogen and carbon monoxide, is produced through gasification processes and can serve as an intermediate for fuels and chemicals (Singh et al., 2016).

#### 1.4.1.3 Solid Biofuels

Traditional forms such as wood and charcoal remain in use, but modern applications rely on biochar and pellets made from agricultural residues or forestry by-products. These denser, standardised fuels provide higher energy content and greater efficiency in heating and electricity generation (Singh et al., 2016).

Overall, while a variety of biofuels exist, biodiesel and bioethanol dominate the current market, with biodiesel receiving particular attention due to its compatibility with diesel engines and potential to reduce greenhouse gas emissions.

### 1.4.2 Generations of Biofuels

Biofuels are commonly categorized into four generations based on the type of feedstock and the conversion technologies employed. Each generation reflects a step forward in addressing the limitations of its predecessor while attempting to balance energy security, environmental sustainability, and economic feasibility.

#### 1.4.2.1 First-Generation Biofuels (G1) (Sunggyu & Shah, 2012)

G1 biofuels are derived from edible crops, including starchy feedstocks such as cereals, cassava, and potatoes, sugar crops like sugarcane, sugar beet, and sorghum, and oilseed crops such as rapeseed, soybean, and sunflower .Bioethanol is typically produced from starch and sugar

crops via fermentation, while biodiesel is produced from vegetable oils through transesterification. The dominant feedstocks vary by region, with corn widely used in the United States, wheat in the European Union, and sugarcane in Brazil. Today, nearly 99% of biofuels used in EU road transport are first generation. Despite their established technologies and large-scale production, G1 biofuels face criticism for competing directly with food production and requiring extensive cultivation areas, and sometimes offering limited energy gains. Even when non-edible grades such as animal feed wheat or broken rice are used, these resources still represent a diversion of potential food supply, raising concerns for global food security.

#### 1.4.2.2 Second-Generation Biofuels (G2)

To overcome the food vs fuel competition, G2 biofuels utilize non-edible biomass such as lignocellulosic residues, dedicated energy crops, wood, and municipal solid waste. Their feedstocks are composed mainly of cellulose, hemicellulose, and lignin, which require pre-treatment to disrupt the plant matrix before enzymatic hydrolysis can release fermentable sugars. While offering a more sustainable alternative, the complexity of processing lignocellulosic material increases production costs and remains a barrier to large-scale commercialization.

#### 1.4.2.3 Third-Generation Biofuels (G3) (Abomohra et al., 2022)

G3 biofuels are based on algal biomass, which does not compete for arable land or freshwater and can grow in diverse environments ranging from oceans and rivers to wastewater systems. Algae are categorized into macroalgae (seaweeds) and microalgae, the latter including both prokaryotic cyanobacteria and eukaryotic green algae.Seaweeds, rich in carbohydrates, are primarily investigated for bioethanol production via fermentation, although they can also be processed into syngas or biodiesel through pyrolysis, gasification, or hydrothermal liquefaction. Microalgae, by contrast, are widely studied for biodiesel due to their ability to accumulate high lipid contents, but they can also yield bioethanol, biogas, and hydrogen depending on the conversion pathway. Their versatility and productivity make them a promising feedstock, though economic and technical barriers persist.

#### 1.4.2.4 Fourth-Generation Biofuels (G4) (Sunggyu & Shah, 2012)

Building on the potential of microalgae, G4 biofuels involve genetically modified (GM) strains designed to enhance photosynthetic efficiency, $CO_2$ fixation, and accumulation of lipids or carbohydrates. Genetic and metabolic engineering of species such as *Chlamydomonas reinhardtii* has demonstrated substantial improvements. Cultivation systems include closed photobioreactors, which reduce contamination risks but require high capital costs, and open raceway ponds,

which are cheaper but carry environmental risks of GM organism release. Although laboratory studies show promising results for biodiesel, biohydrogen, and bioethanol production, the complexity of algal genomes and unresolved biosafety issues remain major challenges. Addressing these constraints is crucial for scaling up G4 biofuels while ensuring environmental and health safety.

## 1.5 Waste Cooking Oil as a Biodiesel Feedstock

Waste cooking oil (WCO) has gained recognition as a valuable feedstock for biodiesel production due to its classification as an advanced biofuel resource derived from waste streams rather than primary agricultural crops. Unlike edible vegetable oils, WCO utilization does not compete with food supplies, thereby avoiding the food-versus-fuel dilemma and contributing to more sustainable biofuel development (Singh & Guldhe, 2022). Although Many authors classify WCO-based biodiesel as “advanced biofuel” or under second-generation biofuels in policy frameworks (e.g., the EU Renewable Energy Directive) underscoring its role in waste valorization, greenhouse gas mitigation, and sustainable energy generation (Singh et al., 2020).

WCO is widely available from households, restaurants, and the food industry, where it has traditionally been discarded through improper disposal methods or reused in applications such as soap making or animal feed. However, health and environmental concerns have led to regulatory restrictions to avoid the reintroduction of harmful substances into the food chain. For instance, the European Union banned the blending of WCO into animal feed in 2002, thereby reinforcing biodiesel production as the most appropriate recycling pathway (Singh, Pandey, & Gnansounou, 2016).

From a market perspective, WCO represents a significant and underutilized resource. Estimates suggest that the United States, Japan, China, Europe, and Malaysia together generate around 15 million tonnes annually, while India alone produces approximately 9.2 million tonnes per year. Converting this readily available waste into biodiesel offers cost-effective, technically feasible, and environmentally benign solutions to energy and waste management challenges. As illustrated in Figure 1.6, WCO is not only generated at large volumes but is also collected and utilized across diverse regions worldwide, ranging from North America and Europe to Asia and Oceania. This global distribution highlights its omnipresence and underscores its potential as a unifying feedstock for biodiesel production.

Overall, WCO offers a dual benefit: it addresses waste disposal challenges while contributing to affordable and sustainable biodiesel production. Its classification as an advanced biofuel

highlights its central role in strategies aimed at reducing dependence on fossil fuels, cutting emissions, and supporting the circular economy.

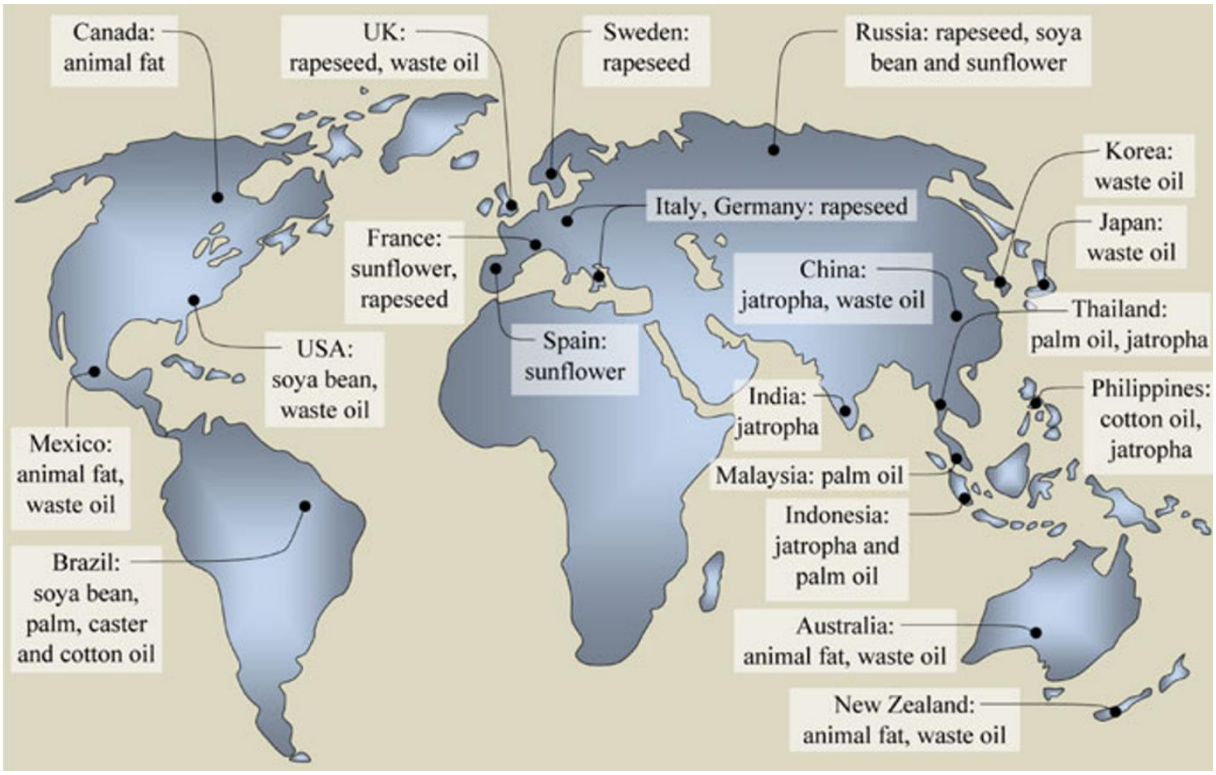


**Figure 1.6** Biodiesel sources around the world (Kegl, Kegl, & Pehan, 2013)

### 1.5.1 Quality Changes in cooking oils

The waste cooking oil (WCO) for biodiesel production is considered suitable depending on the physicochemical transformations it undergoes during frying. A process typically conducted at temperatures between 160 °C and 190 °C under atmospheric conditions, often over prolonged periods and repeated use cycles. Exposure to heat, oxygen, and moisture from food initiates a series of complex reactions; oxidation, polymerization, and hydrolysis (see figure 1.7). Choe & Min (2007) and Awogbemi et al.( 2021) asses that these reactions progressively impair oil quality. Hydrolysis occurs when water from the food reacts with triglycerides, producing free fatty acids (FFAs), mono- and diglycerides, and glycerol,with reaction rates accelerated by high temperatures, extended heating, and catalytic metal ions. Oxidation involves the reaction of unsaturated fatty acids with oxygen during repeated heating, leading to hydroperoxides and secondary products such as aldehydes and ketones, which contribute to darkening, off-odors,

and reduced oxidative stability. Polymerization results from the recombination of oxidized radicals to form high-molecular-weight compounds, including dimers and oligomers, which increase viscosity, promote foaming, and generate sticky residues. These chemical processes collectively alter critical fuel-related properties, reducing the suitability of WCO for direct transesterification without pre-treatment (Kulkarni & Dalai, 2006). Physically, frying induces marked increases in viscosity, color changes, and the formation of polar compounds and polymerized triglycerides, alongside shifts in key indicators such as iodine value, peroxide value, acidity, and total polar compounds (TPC), which rise with extended use as a result of oxidative and hydrolytic deterioration (Awogbemi et al., 2021). Oxidative cleavage of double bonds reduces the degree of unsaturation, potentially lowering the cetane number of the derived biodiesel, although density changes are often reported to be insignificant (Kulkarni & Dalai, 2006). Prolonged frying also promotes the accumulation of hazardous substances such as polycyclic aromatic hydrocarbons (Kalogianni et al., 2011), raising both fuel quality and environmental safety concerns. The rate and severity of these changes depend on the fatty acid composition of the oil, with polyunsaturated-rich oils being less stable than those rich in monounsaturated or saturated fatty acids. They are also influenced by frying conditions such as temperature, duration, and reuse cycles, while intermittent frying further exacerbates oxidation because oxygen solubility increases during cooling. Additional factors include the properties of the fried food, which can introduce moisture, starch, proteins, and catalytic metals, and fryer design, as high surface-to-volume ratios and metallic surfaces, particularly copper and iron, accelerate oxidative reactions. Empirical studies confirm that repeated frying increases viscosity, decreases unsaturated fatty acid content, and elevates degradation product concentrations, reinforcing the necessity for pre-treatment to restore oil quality before its conversion into biodiesel (Awogbemi et al., 2021; Kalogianni et al., 2011).

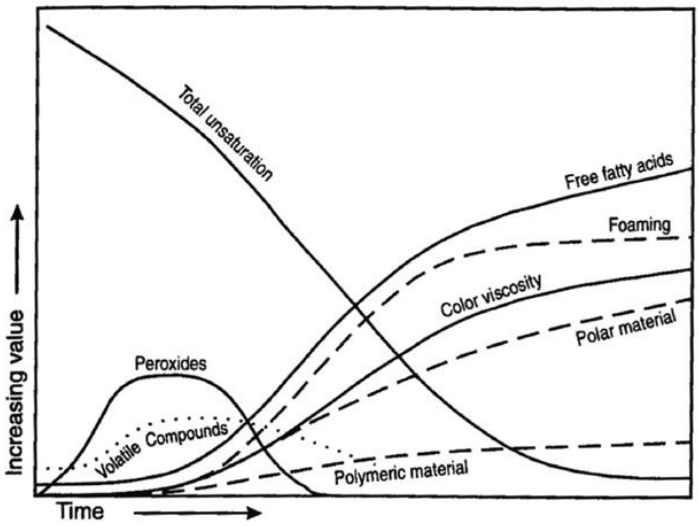


**Figure 1.7** Physical and chemical changes of oil during deep-fat frying (Choe & Min, 2007)

### 1.5.2 Suitable Waste Cooking Oils for Biodiesel: Key Indicators

The quality of waste cooking oils (WCOs) is a decisive factor in the cost-effectiveness and technical feasibility of biodiesel production. Pre-treatment processes can substantially increase production costs, potentially rendering WCOs economically uncompetitive. To reduce these burdens, the feedstock should be of the highest possible quality, with minimal degradation caused by inappropriate collection or prolonged storage. This section outlines the key indicators used to assess the suitability of WCOs for biodiesel production via alkaline transesterification, drawing attention to the underlying degradation mechanisms and acceptable threshold values.

#### *1.5.2.1* Chemical Quality Indicators

Chemical degradation in WCOs arises primarily from hydrolysis**,** oxidation, and polymerization, processes that occur during frying and storage.

- **Acidity and Moisture Content**

  Hydrolysis of acylglycerols produces polar compounds such as monoglycerides, diglycerides, and free fatty acids (FFAs). These changes are typically quantified by measuring FFA content and water content.Elevated moisture accelerates hydrolysis, as water promotes triglyceride breakdown, and is often correlated with increased FFA levels resulting from thermal and oxidative decomposition of long-chain fatty acids. High water content also promotes microbial growth during storage. For optimal biodiesel yield and quality, WCOs should have an acidity number below 4 mg KOH/g

and a moisture content below 0.2% w/w (Ujong et al., 2023 ; Cordero-Ravelo & Schallenberg-Rodriguez, 2018).

- **Oxidative Stability**

  Oxidation originates from the double bonds in unsaturated fatty acids, forming unstable hydroperoxides that subsequently degrade into aldehydes, ketones, and polymers. This process is accelerated by air exposure and the depletion of natural antioxidants such as polyphenols and flavonoids. Two key parameters are used to track oxidative changes (Catia Giovanna Lopresto et al., 2024):

  - Iodine number that reflects the degree of unsaturation and thus susceptibility to rancidity. A reduction in iodine value during frying indicates deterioration due to loss of double bonds via thermolysis and oxidation.
  - Peroxide number measures primary oxidation products (hydroperoxides), which initially increase and then decline as these compounds decompose.

- **Viscosity**

  Polymeric degradation, driven by the formation of oil oligomers and polymers during frying, results in higher viscosity. Fresh oil viscosity depends on fatty acid chain length and degree of unsaturation, but polymerization significantly increases this parameter (Cordero-Ravelo & Schallenberg-Rodriguez, 2018). For efficient single-stage alkaline transesterification, the kinematic viscosity at 40 °C should be below 38.46 $mm^2/s$. WCOs with viscosities between 39.74 and 56.04 $mm^2/s$ have been shown to produce substandard biodiesel (Adhikesavan et al., 2022).

- **Total Polar Materials (TPM)**

  TPM is a comprehensive measure of degradation, encompassing polar compounds from both hydrolytic and oxidative reactions, including FFAs, monoglycerides, diglycerides, and oxidation derivatives. TPM increases with frying time, temperature, and the moisture content of the cooked food. In many jurisdictions, frying oil is considered unsuitable for further use when TPM exceeds 25%. For reference, fresh sunflower and palm oils have TPM values of ~4% and 9.3%, respectively, which can rise to 29-43% and 27-42.5% after frying (Sanli et al., 2011)Elevated TPM affects kinematic viscosity, which in turn influences engine performance and emissions of WCO derived biodiesel, though it does not significantly alter properties such as flash point, pour point, or density.

#### 1.5.2.2 Biological Quality Indicators

Biological contamination can accelerate WCO degradation during storage. Oils stored under non-refrigerated, humid conditions are susceptible to microbial growth, particularly fungi. Some species produce lipases that hydrolyze triglycerides, increasing acidity and peroxide values Thermoresistant spores enable these microorganisms to survive the anaerobic conditions typical of stored oils, making hygienic handling and airtight storage essential (Catia Giovanna Lopresto et al., 2024).

#### 1.5.2.3 Physical Quality Indicators

Density is a further critical parameter for assessing WCO suitability. Oil density tends to increase with repeated frying cycles and decrease during transesterification. WCOs with densities below 930 kg/m³ at 15 °C yield biodiesel that meets the European standard, ensuring acceptable combustion characteristics and fuel performance (Cordero-Ravelo & Schallenberg-Rodriguez, 2018).

In summary, the suitability of WCOs for biodiesel production can be reliably determined through a combination of chemical, biological, and physical indicators. Maintaining low acidity and moisture levels, controlling oxidative and polymeric degradation, preventing microbial contamination, and ensuring compliant density values are essential to producing high-quality biodiesel while minimizing costly pre-treatments

### 1.5.3 Collection and Storage of Waste Cooking Oil for Biodiesel Production

The preservation of WCO quality depends heavily on how the oil is collected and stored prior to processing. Even when initial quality indicators such as acidity, moisture content, viscosity, and total polar materials (TPM) are within acceptable limits, improper handling during these stages can accelerate hydrolytic, oxidative, polymeric, and microbial degradation. Such deterioration increases pre-treatment requirements, reduces biodiesel yield, and raises production costs.

Waste cooking oils (WCOs) can be classified into two main categories: household WCOs and commercial WCOs collected from sources such as restaurants, hotels, fast-food outlets, hospitals, schools, universities, prisons, and workplace canteens. These two types differ notably in their characteristics. Household WCOs are typically exposed to shorter frying durations and fewer reuse cycles, whereas commercial WCOs undergo longer and more frequent frying. As a result, commercial WCOs generally contain higher levels of saturated fatty acids, which enhance their oxidative stability and improve fuel qualities such as flash point and cetane number.

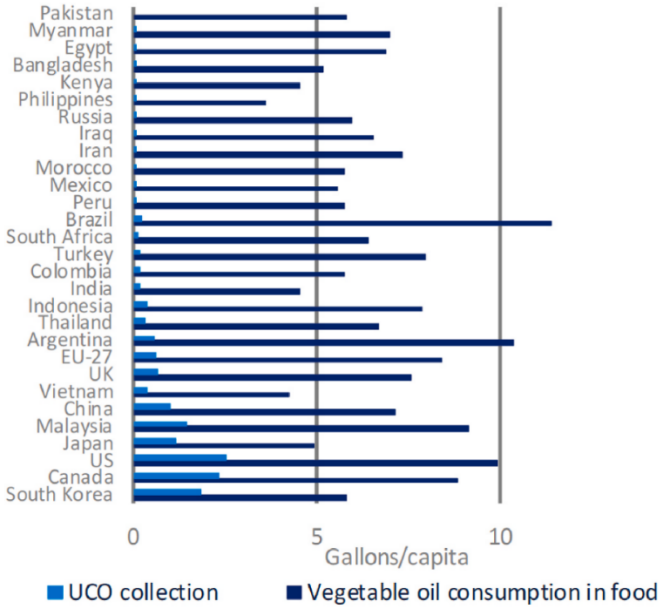


**Figure 1.8** Per capita vegetable oil consumption and used cooking oil (UCO) collection rates in 2022 (GlobalData, 2023).

#### 1.5.3.1 Waste Cooking Oil Collection Practices

The collection of waste cooking oil (WCO) varies widely across countries, influenced by vegetable oil consumption patterns and the existence of collection networks. Despite significant consumption, the proportion of WCO collected remains low worldwide as shown in Figure 1.8. Two main approaches to WCO management are evident. The first relies on second-generation economic instruments, where targeted regulations and subsidies stimulate private sector involvement in collection and valorization, as observed in countries such as the United States, Brazil, Singapore, Australia, and New Zealand. The second employs third-generation instruments, such as environmental taxes applied to consumer products, which encourage recovery and recycling in regions like the European Union, Argentina, and Japan (Teixeira et al., 2018). However, available data on WCO collection, particularly outside Europe, remain limited and fragmented.

Domestic WCO collection is generally underdeveloped. For example, in the United States, household collection systems are virtually absent due to economic constraints. In most countries, no dedicated recycling infrastructure exists for individuals, and WCO from households is typically stored in plastic containers and deposited at collection points or bins, later retrieved by specialized vehicles. Alternative models, such as door-to-door collection, are practiced in some municipalities with varying frequencies (from weekly to on-demand) depending on local waste policies. However, household WCO is often stored under uncontrolled conditions, with

food residues and moisture contributing to microbial growth and degradation. Certification of household WCO for sustainability is also challenging, as the fragmented supply chain and risk of contamination increase treatment and cleaning costs.

By contrast, commercial and industrial WCO streams are more accessible and of higher quality. Restaurants, hotels, and catering outlets are usually served by collection companies that integrate the supply of fresh oil with the removal and recycling of used oil. These companies often provide standardized, food-grade storage containers tailored to kitchen requirements. Regulatory enforcement and economic incentives are key factors influencing proper disposal practices in the commercial sector. Additionally, professional kitchens equipped with thermostatically controlled fryers and outlet filters can produce higher-quality WCO, provided that excessive frying cycles are avoided.

Several studies have sought to optimize WCO collection networks. For example, mathematical modeling has been applied to determine optimal locations for collection centers, household assignments, container numbers, and vehicle routing to biodiesel facilities (Olmez et al., 2018). Caldeira et al. (2015) in Portugal have assessed household and catering collection systems using Life Cycle Assessment (LCA) and have indicated that door-to-door collection systems had the highest climate change impact, while street-container systems had the lowest. In the catering sector, monthly collection from restaurants using plastic containers was identified as a viable model.

Despite progress, substantial gaps remain in the literature concerning WCO collection and storage practices for biodiesel conversion. Most research to date has concentrated on designing efficient local or national collection networks, leaving broader questions on long-term sustainability, quality assurance, and household participation insufficiently addressed.

#### 1.5.3.2 Current Storage Practices and Recommended Methods

After collection, waste cooking oils (WCOs) are often stored under uncontrolled conditions, frequently in containers that are neither airtight nor protected from light. Traditional storage in metal drums remains common, but it presents several challenges. These drums are inefficient in terms of space and are highly vulnerable to environmental factors. In hot climates, thermal expansion increases the likelihood of leaks, while exposure to rain can lead to water infiltration. During daily heating and cooling cycles, air exchange between the drum and the atmosphere can draw water into the oil. Over time, this water settles at the bottom, increasing the liquid

level and potentially deforming the container. Such conditions not only accelerate the degradation of WCO but also increase the risk of costly spills.

To address these issues, high-quality storage solutions are recommended. Stainless steel tanks, for example, offer durability and minimize risks of corrosion, leakage, and water contamination, making them more suitable for outdoor storage.

Maintaining hygienic conditions in storage containers is essential to prevent microbial contamination, which can compromise oil quality

### 1.5.4 Pretreatment of Waste Cooking Oil

The quality of waste cooking oil (WCO) plays a decisive role in obtaining biodiesel of acceptable standards. Due to repeated thermal exposure and food contact, WCO is often heterogeneous and contains significant levels of suspended solids, free fatty acids (FFAs), water, and degradation products. Such impurities can hinder the efficiency of transesterification, reduce biodiesel yield, and promote the formation of undesirable by-products. Consequently, adequate pretreatment is essential prior to the reaction stage. The main pretreatment steps include filtration**,** deacidification or neutralization**,** and water removal**.**

**a) Filtration and removal of suspended solids** (Cárdenas et al., 2021)

The initial pretreatment of waste cooking oil (WCO) aims to eliminate suspended food particles and other insoluble contaminants. This typically starts with a coarse filtration using fabric bags or stainless-steel strainers with openings of 150–200 μm. The oil is then gently heated to around 60–65 °C to melt solidified fats, release entrapped materials, lower viscosity, and enhance flow. A subsequent fine filtration through stainless-steel meshes of 70–100 μm is performed, followed by storage at 60 °C to facilitate emulsion breaking, water separation, and sedimentation. Finally, the oil undergoes a polishing filtration using a 5 μm mesh to obtain a clarified product.

For the removal of solids, conventional filtration is commonly employed. This approach uses cellulose filters or stainless-steel screens. Cellulose filters are inexpensive and suitable for laboratory-scale work but have limited durability, higher oil retention, and lower mechanical strength. Stainless-steel filters, although more expensive, can be reused indefinitely and withstand industrial conditions. Filtration efficiency can be further improved by adding filter aids (materials such as diatomaceous earth, clays, silicates, or activated carbon) which adsorb fine particles and, in some cases, help remove free fatty acids. While these

inorganic aids generally have macroporous structures and moderate surface areas, mesoporous and microporous materials (e.g., certain metals like aluminum, zinc, or titanium) can capture ultrafine particles smaller than 0.5 μm.

Industrial-scale processes may employ multi-stage setups, such as an electronically controlled self-cleaning steel filter for gross separation (>100 μm), followed by deep-bed filtration using clays in fiberglass containers to remove pigments and trace metals. Pilot-scale operations have also used adsorbent full-flow oil filters. As an alternative, centrifugation systems can continuously separate WCO into pure oil, wastewater, and solids in one step.

**b) Deacidification** (C. G. Lopresto, 2024)

Waste cooking oil (WCO) contains free fatty acids (FFAs), which pose a significant challenge for alkaline transesterification. These FFAs react with alkaline catalysts to produce soap and water, both of which reduce biodiesel yield and make product separation more difficult. Additionally, the water formed can accelerate triglyceride hydrolysis, further increasing the FFA content.

Reducing FFAs is often the most costly pretreatment step, involving high energy consumption, material losses, waste generation, and substantial water use. When the FFA content exceeds about 1% (or 2.5% according to some sources), pretreatment is required before transesterification. Available methods can be grouped into chemical and physical processes:

***Neutralization*** : Addition of an alkaline solution (e.g., NaOH, KOH) to convert FFAs into soaps, which are then removed. Suitable for oils of any quality and energy-efficient, but produces wastewater, consumes large amounts of water, and reduces triglyceride content.

***Esterification :*** *c*onversion of FFAs into esters using an alcohol (commonly methanol) and an acid or enzymatic catalyst. Highly efficient and can be integrated with transesterification, but is costly, generates wastewater, and may corrode equipment.

***Biological treatment :*** Use of microorganisms or enzymes to degrade or transform FFAs. Environmentally friendly and can produce valuable biomass, but unsuitable for short-chain fatty acids and sensitive to inhibitory compounds.

***Distillation :*** Thermal separation of FFAs under vacuum or steam conditions. Produces high-purity FFAs and avoids by-products, but is energy-intensive and less effective for short-chain FFAs.

***Adsorption :*** Use of porous solids (e.g., activated carbon, silica) to trap FFAs. Low energy use and removes other impurities, but requires large adsorbent quantities, has limited capacity, and generates solid waste.

***Membrane separation*** : Physical separation based on molecular size differences. Chemical-free and efficient, but effectiveness can be limited by small molecular weight differences, and costs are high.

***Solvent extraction*** : Dissolution of FFAs in a selective solvent, followed by recovery. Produces good-quality FFAs and minimizes oil loss, but may not achieve full deacidification and requires strict solvent handling.

***Supercritical fluid extraction :*** Use of supercritical $CO_2$ or other fluids to extract FFAs. Avoids by-products and suits diverse oils, but requires extreme operating conditions and expensive equipment.

**c) De-watering** (Cárdenas et al., 2021)

Water in waste cooking oil (WCO) accelerates the hydrolysis of acylglycerols into free fatty acids (FFAs) and facilitates microbial and enzymatic degradation during storage and handling.For biodiesel production, water content should be below 0.05 wt% (500 ppm) to minimize side reactions and quality loss.

Water removal can be achieved through adsorption**,** thermal treatment**,** membrane separation, or centrifugation. Adsorbents such as silica gel, bentonite ,anhydrous sodium sulfate, and magnesium sulfate have been shown to effectively reduce moisture, often combined with vacuum filtration. Activated charcoal, derived from agricultural wastes, can simultaneously remove water, pigments, and other impurities.

Thermal drying is common, with pre-heating at 50-54 °C sufficient for most applications ,while higher temperatures (70-150 °C) under reduced pressure (≤ 40 mbar) can reduce residual water to below 200 ppm .Ultrafiltration and microfiltration can also separate water but face industrial limitations due to low permeation rates and high maintenance costs. Centrifugation is a promising alternative, especially for large-scale operations.

## 1.6 Biodiesel Production Methods

The direct use of neat vegetable oils or waste cooking oils in diesel engines is limited by their high viscosity (approximately 11 to 17 times greater than that of conventional diesel ) and eventually by other unfavourable physicochemical properties. These characteristics lead to poor atomization, incomplete combustion, and engine deposits. To address these issues, four main approaches have been used ( see figure 1.9) blending with petroleum diesel, microemulsification, pyrolysis, and transesterification.Among these, transesterification has become the dominant and most widely adopted method for biodiesel production, producing alkyl esters of vegetable oils or animal fats or waste oils that meet international fuel standards.

- **Blending** involves diluting vegetable oils with petrodiesel to reduce viscosity and improve combustion properties. Low-level blends (10–20%) have been shown to sustain engine performance without requiring major modifications, whereas higher blends (up to 50%) further reduce viscosity but increase the risk of incomplete combustion and carbon deposits (Ambat et al., 2018).
- **Microemulsification** forms stable, colloidal mixtures of oils and polar solvents with the aid of surfactants and co-surfactants (Jain & Sharma, 2010; Bora et al., 2016). To reduce viscosity, short-chain alcohols such as methanol, ethanol, or butanol are commonly added, and additional compounds can be included to improve the fuel's ignition properties (Attaphong et al., 2012). This approach can enhance fuel atomization and spray characteristics during injection, which may improve combustion efficiency. However, it also presents challenges, including lower cetane numbers, reduced cold-flow performance, incomplete combustion, and the potential for injector deposits, all of which can affect engine reliability and performance (Ziejewski et al., 1984; Jain & Sharma, 2010; Ambat et al., 2018). Overall, while microemulsification offers benefits for spray behavior, careful formulation is needed to balance its advantages and limitations for engine applications**.**
- **Pyrolysis** is a thermochemical process in which oils or biomass are decomposed at temperatures above 350 °C in the absence of oxygen, and sometimes in the presence of catalysts. This treatment generates a mixture of hydrocarbons, including alkanes, alkenes, aromatics, and carboxylic acids, along with char, gases, and water (Avhad & Marchetti, 2015). The process can be adjusted to favour char production through slow pyrolysis or maximize liquid fuel yields via fast pyrolysis, typically conducted at 400-

600 °C with short residence times. Using catalysts during pyrolysis can further improve fuel quality and increase aromatic content (Bwapwa et al., 2017). Despite producing diesel-like liquids, challenges such as high viscosity, poor cold-flow properties, and the loss of oxygenated functional groups limit the practical application of pyrolysis-derived fuels (Lee et al., 2017).

- **Transesterification** is now the most commonly used and effective method for producing biodiesel, to the point that the term "biodiesel" is largely associated with fuels made via this process. This reaction converts triglycerides into fatty acid esters using short-chain alcohols and was first reported in 1852. It later found practical applications in the soap and fat industries during the early 20th century. One of the earliest patents related to biodiesel described the production of palm oil ethyl esters in Belgium (Ramadhas, 2011).Since then, numerous reviews have examined technological progress in transesterification, highlighting its central role in both scientific research and industrial-scale biofuel production (Duran, 2019;Awogbemi et al., 2021;Ali Ijaz Malik et al., 2024;C. Chen et al., 2021).

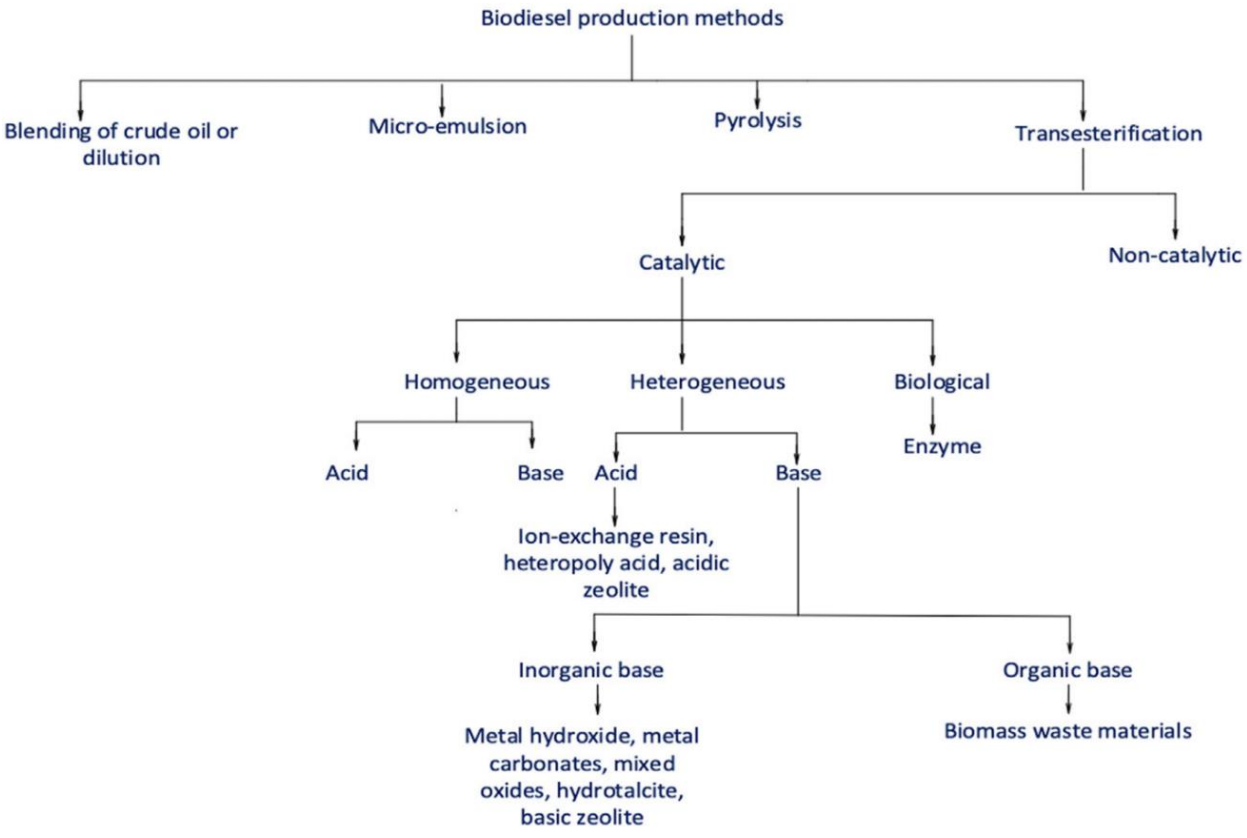


**Figure 1.9** Classification of biodiesel production process.

## 1.7 Basics of transesterification reaction

This process involves triglycerides and short-chain alcohols (typically methanol or ethanol) as the reactants and the fatty acid methyl or ethyl esters and glycerol as the products , all in the presence of a catalyst. The reaction is governed by chemical equilibrium and depends on effective mixing of the reactants. It occurs through three consecutive reversible stages: triglycerides are first transformed into diglycerides, then into monoglycerides, and ultimately into fatty acid monoesters and glycerol (Demirbas, 2009; Orege et al., 2022) as described in Figure 1.10.

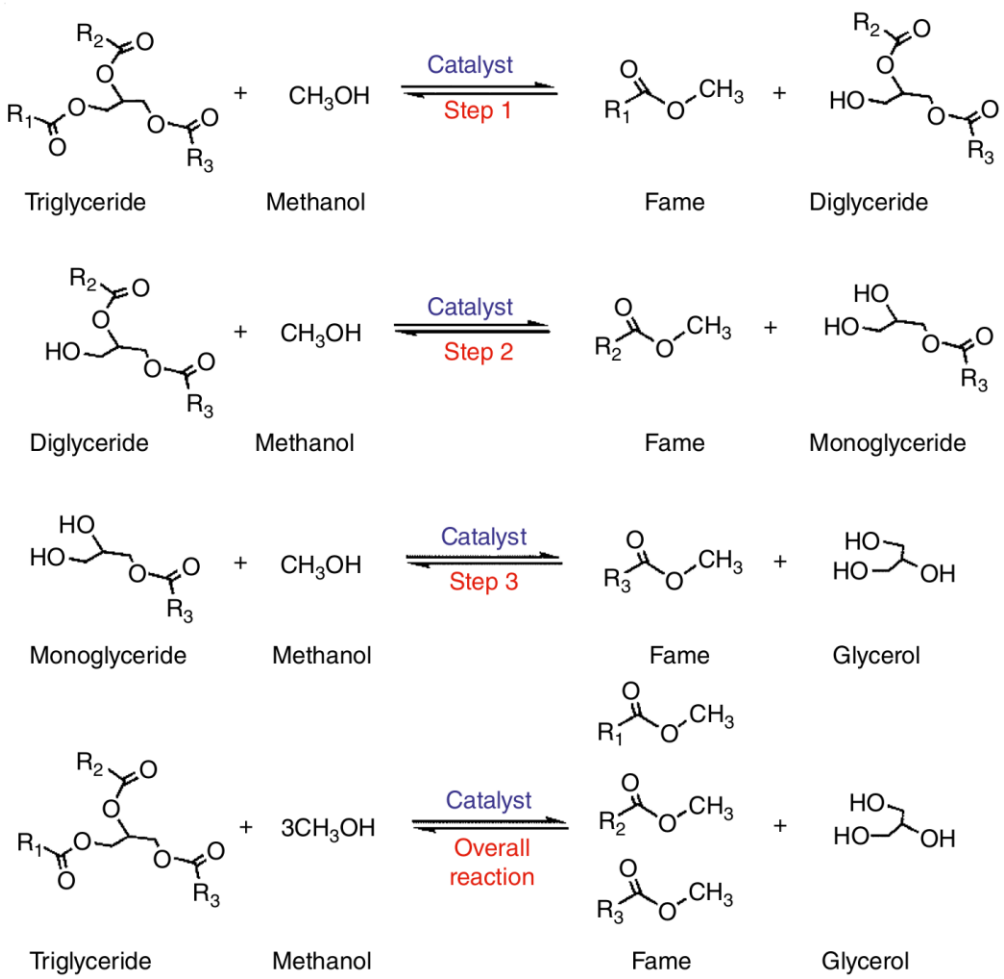


**Figure 1.10** Transesterification reaction.

### 1.7.1 Catalytic Transesterification

The immiscibility of alcohol and oil makes it difficult to form a homogeneous reaction mixture, which slows the transesterification process. To overcome this, factors such as vigorous stirring,

higher temperatures, and the addition of a catalyst are introduced, all of which improve solubility and reaction efficiency. The use of a catalyst at elevated temperatures significantly reduces the reaction time compared with reactions conducted under ambient conditions. Transesterification using catalysts is generally classified into three main categories: homogeneous (acidic and basic), heterogeneous (acidic and basic), and enzymatic catalysis (Figure 1.9).

Homogeneous catalysis, which commonly involves liquid-phase strong acids or bases, is extensively used in industrial-scale biodiesel production. Acid catalysts, including sulphuric, hydrochloric, and sulphonic acids, are capable of producing high ester yields; however, the reaction rate is comparatively slow and largely insensitive to the nature of the feedstock. Excess alcohol is typically required to facilitate phase separation after the reaction. In acid catalysis, the catalyst first activates the triglyceride molecule by making the carbonyl group more reactive. This allows the alcohol to easily attack the molecule and form an intermediate structure. The intermediate then breaks apart, producing fatty acid esters and glycerol, while the acid catalyst is released and reused in the reaction. Alkaline catalysts, such as sodium hydroxide and potassium carbonate, promote rapid transesterification and efficiently convert triglycerides into fatty acid esters when the feedstock contains low levels of free fatty acids (FFAs). Compared with acid-catalysed systems, base-catalysed reactions proceed at a much faster rate. However, when oils with high FFA content are used, soap formation may occur, leading to difficulties in product separation and purification. Despite their high catalytic activity, homogeneous catalysts present several significant limitations, including poor reusability, substantial wastewater production, and increased corrosion of processing equipment (Demirbas, 2009).

To address these issues, heterogeneous catalysis has gained attention. Heterogeneous catalysts, which are solid acids or bases, are easier to separate from the reaction mixture and create less waste. However, they usually work more slowly because the reaction involves three phases: oil, alcohol, and solid catalyst, and they can lose activity over time due to leaching or contamination. (Thangaraj et al., 2019). Solid acid catalysts are particularly effective for oils with high free fatty acid (FFA) content because they reduce soap formation. However, they are sensitive to temperature and usually require conditions above 170 °C to achieve high conversion rates. On the other hand, solid base catalysts; such as calcium oxide, magnesium oxide, and zinc oxide; typically exhibit higher catalytic activity because of their stronger basicity and better solubility in alcohols(Pydimalla et al., 2023). Recently, naturally derived catalysts from biomass, including eggshells, bones, and agricultural residues, have gained attention due to their

abundance, low cost, and stability after calcination. These catalysts offer high thermal stability, can be reused multiple times, and exhibit minimal leaching, making them promising for sustainable biodiesel production. (Erchamo et al., 2021).

Enzymes offer a third method for producing biodiesel. Lipases can catalyse both esterification and transesterification reactions under moderate conditions. Using immobilized enzymes allows them to be reused and makes it easier to separate biodiesel from glycerol. This approach works well even with oils that have high levels of free fatty acids and produces biodiesel with fewer impurities. However, the reaction is relatively slow, and glycerol can sometimes inhibit the enzymes, reducing their effectiveness. (Tabatabaei & Aghbashlo, 2019)

### 1.7.2 Non-Catalytic Transesterification

Non-catalytic transesterification, also known as supercritical alcohol transesterification, involves the reaction of alcohol with triglycerides at elevated temperatures (350 - 400 °C) and pressures (10 - 25 MPa) without requiring a catalyst. In this method, alcohol serves not only as a reactant but also as a medium that improves solubility and mass transfer between the reactants. Consequently, the reaction is usually completed in a shorter time than under conventional conditions (Karki et al., 2017).

This approach was developed as an alternative to catalytic transesterification to overcome operational issues such as sensitivity to moisture and high free fatty acid (FFA) content, difficulties in product separation, catalyst costs, and wastewater generation. Without a catalyst, the reaction between alcohol and oil proceeds very slowly due to limited solubility. However, by heating the mixture above the alcohol's critical temperature and pressure, transesterification can occur efficiently. For methanol, the critical conditions are 239 °C and 8.09 MPa, whereas for ethanol, they are 243 °C and 6.3 MPa (Bashir et al., 2022).

The non-catalytic supercritical process differs from catalytic methods in both its operating conditions and the by-products it produces. This approach typically prevents soap formation, eliminates wastewater associated with catalyst neutralisation, and enables simpler separation of biodiesel and glycerol. Additionally, it can process a wide variety of feedstocks, including those with high free fatty acid and water content, without the need for prior pretreatment. In this context, water, which is usually a limiting factor in catalytic reactions, may contribute positively by promoting ester formation in supercritical systems (Bashir et al., 2022)

**Table 1.1** Biodiesel production through various transesterification processes. (Dinesh Kumar, Kavitha, & Banu, 2020)

| Substrate | Catalyst/enzymes | Amount of catalyst used (wt.%) | Alcohol used | Alcohol:oil molar ratio | Reaction time (h) | Tempera-ture (°C) | Yield (%) |
|---|---|---|---|---|---|---|---|
| **Acid catalytic transesterification** | | | | | | | |
| Waste vegetable oil | Carbon-based acid | 0.2 | Methanol | 16.8 | 4.5 | 220 | 80.5 |
| Waste olive pomace | $H_2SO_4$ | 20 | Methanol | 35:1 | 1 | 40 | 97.8 |
| Fish waste | $SO_4^{2-}/SnO_2–ZrO_2$ | 5 | Ethanol | 6.5:1 | 6 | 78 | 82.58 |
| Waste cooking oil | Sulfamic acid | 1 | n-Butanol | 10:1 | 2 | 110 | 95.6 |
| **Alkaline or base catalytic transesterification** | | | | | | | |
| Waste vegetable oil | $CH_3ONa$ | 1.4 | Ethanol | 8:1 | 2 | 45 | 99.08 |
| Waste cooking oil | Activated carbon-CaO catalyst | 11 | Methanol | 40:1 | 7 | 120 | 96 |
| Waste cooking oil | KOH | 1 | Methanol | 1:3 | 50 | 60 | 94 |
| **Enzymatic or lipase transesterification** | | | | | | | |
| Waste cooking oil | Novozym-435 | 1 | Methanol | 6.2:1 | 10 | 50 | 90 |
| Waste cooking oil | Pseudomonas aeru-ginosa | 0.782 g | Methanol | 3.05:1 | 24 | 44.2 | 86 |
| Waste cooking oil | Rhizomucor miehei and Candida antarctica | – | Methanol | 3:1 | 10 | – | 91.5 |
| Fish waste | Novozym-435 | 50 | Ethanol | 4.66:1 | 8 | 35 | 82.91 |

## 1.8 Factors affecting the biodiesel production

The efficiency of transesterification is influenced by multiple factors, such as the type of feedstock, the molar ratio of alcohol to oil, the choice and concentration of catalyst, reaction temperature, intensity of mixing, and the purity of the reactants (Ramadhas, 2011). Optimizing these parameters ensures high yields and biodiesel that complies with fuel standards.

$$Yield(\%) = \frac{weight\ of\ biodiesel\ produced}{Weight\ of\ raw\ oil\ used} \times 100\% \quad \ldots\ldots\ldots (1.1)$$

### 1.8.1 Type of alcohols

Several alcohols, such as ethanol, propanol, butanol, and amyl alcohol, can be used to produce biodiesel through transesterification. Among them, methanol is preferred in industrial applications due to its low cost, high polarity, and short carbon chain, which simplify separation from the biodiesel product and enhance overall process efficiency. Conversely, ethanol is often preferred for its renewable origin from agricultural sources and its lower environmental impact. Studies on the effect of alcohol-to-oil ratios have shown that the highest biodiesel yield, around 99.5%, is achieved when the oil-to-methanol ratio is 1:6. In contrast, increasing the methanol ratio beyond this point continues to improve biodiesel production, indicating a positive correlation between methanol excess and yield (Gashaw & Teshita, 2014).

### 1.8.2 Alcohol-to-oil ratio

Transesterification theoretically requires three moles of alcohol per mole of triglyceride to produce one mole of alkyl ester (Thangaraj et al., 2019; Topare et al., 2022). Based on Le Chatelier's principle, increasing the concentration of reactants shifts the equilibrium toward product formation. Therefore, using a higher alcohol-to-oil ratio generally results in greater biodiesel yields (Musa, 2016). However, separating glycerol from unreacted methanol can be difficult, as their interaction in water may cause emulsion formation due to saponification. During biodiesel synthesis, two distinct phases are generated due to differences in density and polarity: the upper layer contains biodiesel, while the lower layer consists of crude glycerol. This crude glycerol mixture generally contains alcohol, glycerol, water, soaps, and other non-glycerol organic compounds, with the composition varying depending on feedstock quality (Ma & Hanna, 1999).

### 1.8.3 Catalyst type

Various types of catalysts, such as homogeneous, heterogeneous, and enzymatic systems, have been used for alkyl ester production. For the homogeneous basic transesterification, Vicente et al. (2004) conducted a comparative study of sodium hydroxide (NaOH) and potassium hydroxide (KOH) as catalysts to produce sunflower oil biodiesel. Under the same reaction conditions,it is found that ester yields reached 85.9 wt% with NaOH and 91.67 wt% with KOH. While increasing the catalyst concentration initially improved the conversion rate, no further gains were observed beyond a concentration of 1 % w/w.

Acid catalysts are less commonly employed in biodiesel synthesis than their basic counterparts, primarily due to slower reaction rates. Sulfuric acid, sulphonic acid, hydrochloric acid, and ferrous sulfate are the commonly used acids , with sulfuric and hydrochloric acids being the most frequently selected as reported by Bashir et al.(2022).

Vyas et al.(2010) investigated sulfuric acid as a catalyst for FAME production. It is effective but requires prolonged reaction times and harsh operating conditions; nevertheless, even a concentration of 1 mol% sulfuric acid can contribute to 99% yield. Both homogeneous and heterogeneous acid catalysts are especially effective for feedstocks containing high levels of free fatty acids (FFAs), as they are capable of catalysing esterification and transesterification reactions at the same time (Daramola et al., 2016). Homogeneous catalysts face drawbacks including the formation of soaps and difficulties in removing the catalyst from the final biodiesel product. To overcome these issues, heterogeneous catalysts have been increasingly investigated, as they are less sensitive to high free fatty acid content and moisture in the feedstock (Di Serio et al., 2007). Enzymatic catalysts, although significantly slower than chemical catalysts, can also be applied to both esterification and transesterification processes. Their use simplifies product separation, but the preparation and stabilization of enzyme catalysts remain a major challenge (Macario et al., 2010).

### 1.8.4 Catalyst concentration

Oils or fats can be converted into FAME at elevated temperatures without a catalyst; however, adding a catalyst significantly enhances both the reaction rate and overall yield (M. Agarwal et al., 2012). Generally, increasing the catalyst concentration improves product formation by providing more active sites, but using too much catalyst can raise solution viscosity and then reduce conversion efficiency (Zhang et al., 2012).

Researchers have investigated various catalyst types and concentrations to optimise biodiesel production and recovery as depicted in table 1.1. From an economic perspective, excessive catalyst use is not feasible due to cost implications. Thus, as with the oil-to-alcohol ratio, optimisation of catalyst concentration is crucial to ensure both efficiency and economic viability.

### 1.8.5 Reaction Temperature

The temperature at which transesterification is carried out has a major impact on both the reaction rate and the amount of biodiesel produced. Higher temperatures generally speed up the reaction and enhance yield, whereas lower temperatures below 50 °C) can result in increased viscosity of the biodiesel (Daramola et al., 2016). For WCO as biodiesel feedstock, it is preheated to around 120 °C and then cooled to 60 °C as the reaction temperature.

Enzymatic transesterification shows optimal conversion within the range of 30-55 °C. For instance, Shah and Gupta (2007) reported maximum conversion at 55 °C when using lipase with Jatropha oil, whereas 50 °C was most effective for cottonseed oil.

Similarly, Freedman et al. (1984) observed little difference in conversion between 45 °C and 60 °C, and at 32 °C, conversion was marginally lower. Interestingly, after four hours at 32 °C, conversion levels surpassed those obtained at higher temperatures, suggesting time-temperature interactions also influence yields.

### 1.8.6 Reaction Time

Transesterification efficiency relate to the availability of reactants within the reaction mixture, and poorly controlled parameters may encourage reverse reactions, thereby reducing overall yield. Longer durations contribute to achieve conversions of up to 99%.

For enzymatic processes, reaction time is particularly critical. Lipase-catalysed transesterification has been reported to require between 7 and 48 hours, depending on operating conditions (Silitonga et al., 2017). Reaction time also has economic implications, as extended durations increase production costs. Refaat et al. (2008) found a conversion efficiency of 96.1% after one hour, with only a negligible increase to 96.35% between one and three hours. These findings suggest that beyond a certain threshold, extending reaction time provides minimal improvements in yield while adding to process costs.

### 1.8.7 Stirrer speed

Proper mixing of reactants promotes complete reaction. The ideal stirring speed depends on the feedstock, since different substrates have unique physical properties (Abd Rabu et al., 2013). Agitation increases collisions and dispersion within catalysts , which reduces reaction time and

improves conversion. However, once a certain threshold of stirring speed is reached, increasing stirrer speed do not mark the biodiesel yield anymore (Khodadadi et al., 2020).

### 1.8.8 Moisture and FFA

High water content in the feedstock accelerates triglyceride hydrolysis, which lowers the ester yield (Felizardo et al., 2007). In enzymatic transesterification, a small amount of water is required to maintain lipase activity; however, excess moisture can deactivate the enzyme and decrease conversion efficiency (Norjannah et al., 2016).

Similarly, high FFA content promotes soap formation, reducing biodiesel recovery and complicating product separation. When the FFA concentration exceeds 3%, homogeneous base catalysts become ineffective; in such cases, acid or heterogeneous catalysts are preferred for esterification pretreatment to convert FFAs into esters (Adenuga et al., 2021).

## 1.9 Biodiesel Properties

Biodiesel is a biodegradable, sulfur-free, oxygen-containing fuel that serves as an environmentally friendly alternative to conventional diesel. The performance of biodiesel in diesel engines, as well as its environmental and economic impacts, is influenced by key physico-chemical characteristics, including stability, density, viscosity, bulk modulus, sound velocity, cetane number, cold-flow properties (cloud point, pour point, cold filter plugging point), flash point, chemical composition, and water content (Mahmudul et al., 2017).

Effective quality control is essential, with volatility parameters such as vapour pressure and boiling point serving as useful indicators (Awogbemi et al., 2019).

### 1.9.1 Density, Viscosity, Bulk Modulus, and Sound Velocity

Density refers to fuel mass per unit volume, while viscosity is its resistance to flow caused by internal friction. Bulk modulus describes fluid compressibility under pressure, and sound velocity is the speed of pressure-wave propagation within the fuel.

**Table 1.2** Density and viscosity of Biodiesel and Mineral Diesel fuels. (Kegl, Kegl, & Pehan, 2013)

| Fuel | Density [kg/m$^3$] | Kinematic viscosity [mm$^2$/s] |
|---|---|---|
| Mineral diesel | 835 | 2.8 |
| Canola (CaBIO) | 880–886 | 3.9–4.7 |
| Coconut (CoBIO) | 865–875 | 2.7–3.0 |
| Hazelnut (HaBIO) | 863–885 | 3.1–5.4 |
| Jatropha (JaBIO) | 873–875 | 4.2–4.3 |
| Karanja (KaBIO) | 871–883 | 4.2–4.3 |
| Olive (OlBIO) | 870 | 4.6 |
| Palm (PaBIO) | 870–880 | 4.3–5.7 |
| Rapeseed (RaBIO) | 877–893 | 4.2–5.1 |
| Soybean (SoBIO) | 880–885 | 3.9–4.6 |
| Sunflower (SuBIO) | 880–884 | 4.0–4.7 |
| Waste cooking oil (WcBIO) | 880–888 | 4.9 |

These properties strongly influence fuel injection performance. At low temperatures, increased density and viscosity raise pressure losses in filters and pumps and hinder atomization, promoting deposit formation. In mechanical injection systems, higher viscosity reduces leakage and advances injection timing, necessitating consideration of biodiesel's temperature-dependent viscosity when designing fuel supply components. Bulk modulus rises with injection pressure, enhancing pressure-wave transmission and advancing needle lift. Since viscosity and bulk modulus jointly determine sound velocity, they are critical for optimizing mechanically controlled injection systems (Kegl, Kegl, & Pehan, 2013).

### 1.9.2 Chemical Composition

Both biodiesel and mineral diesel primarily consist of carbon and hydrogen, with smaller amounts of oxygen and nitrogen. The higher oxygen content in biodiesel enhances combustion efficiency and typically results in lower soot emissions compared to mineral diesel (Zhang et al., 2018). Furthermore, while conventional diesel may contain up to 0.05 wt.% sulfur, biodiesel is essentially sulfur-free, providing an additional advantage by reducing the potential for acid rain formation (D. Agarwal et al., 2008) .

### 1.9.3 Cetane Number

The cetane number indicates the ignition quality of a diesel fuel and determines mostly engine performance. For biodiesel, it varies widely (48-67) depending on feedstock, climatic conditions, and production methods (Eevera et al., 2009) .This property influences engine startability, combustion noise, and exhaust emissions. Different biodiesels and their cetane number are presented in table 1.3 (Agarwal, 2007; Kegl, Kegl, & Pehan, 2013)

**Table 1.3** Cetane number of biodiesel and mineral diesel fuels**.**

| Fuel | Cetane number |
|---|---|
| Mineral diesel | 48–50 |
| Canola (CaBIO) | 52–55 |
| Coconut (CoBIO) | 60–65 |
| Hazelnut (HaBIO) | 52–55 |
| Jatropha (JaBIO) | 48–58 |
| Karanja (KaBIO) | 55–58 |
| Olive (OlBIO) | 61–62 |
| Palm (PaBIO) | 62–70 |
| Rapeseed (RaBIO) | 51–64 |
| Soybean (SoBIO) | 45–56 |
| Sunflower (SuBIO) | 49–52 |
| Waste cooking oil (WcBIO) | 51–53 |

### 1.9.4 Flash Point

The flash point is the minimum temperature at which fuel vapors ignite when mixed with air, making it an important parameter for storage and transport classification. Fuels with lower flash points require stricter safety measures, as this property is inversely related to volatility (Kaisan et al., 2020).

### 1.9.5 Cloud Point, Pour Point, and Cold Filter Plugging Point

Cloud point (CP), pour point (PP), and cold filter plugging point (CFPP) provide important information on cold weather behaviour of the fuel. Cold flow properties are critical for assessing diesel fuels in low-temperature environments. The cloud point marks the temperature at which wax crystals begin to form, while the pour point indicates the lowest temperature at which the fuel remains flowable; typically, occurs at a higher temperature than pour point. The cold filter plugging point measures the lowest temperature at which fuel can pass through a filter under standardized conditions. Elevated Cloud Point, Pour Point, and Cold Filter Plugging point values promote crystal growth, clogging of filters and fuel lines, and serious operability issues (Yuan, Chen, Chen, & Luo, 2017). To ensure reliable performance, especially in colder climates, fuels should exhibit a low cold filter plugging point.

### 1.9.6 Water Content and Corrosiveness

Excess water in biodiesel promotes microbial growth, which can block fuel injection systems, and must therefore be strictly controlled (Torres et al., 2010). It also lowers methyl ester yields

during production (Demirbas, 2009), reduces combustion efficiency with harder starts, more smoke, and power loss and accelerates gelling at sub-zero temperatures due to ice crystal formation. In addition, water induces corrosion in fuel tanks and injection components, posing risks to engine durability.

### 1.9.7 Fuel Stability

Fuel stability in biodiesel is influenced by degradation, phase separation, and oxidation. While biodiesel is environmentally favourable due to its high biodegradability, this property also accelerates microbial growth, leading to fuel degradation and storage challenges. Phase separation is another concern, particularly in biodiesel blends. Variations in temperature and storage time can cause fuel layers to separate, resulting in inconsistent injection and combustion performance; in some cases, remixed blending is required to maintain engine operation (Torres et al., 2010).Oxidative stability also poses risks, as biodiesel's susceptibility to oxidation depends on feedstock type, storage conditions, and fuel age. Poor stability can lead to compromised engine performance and reduced fuel reliability.

## 1.10 Biodiesel standards and characterization

The establishment of fuel quality regulations is essential to ensuring reliable engine performance. The characteristics of biodiesel are influenced by several factors, including the fatty acid ester composition of the feedstock, the presence of by-products, the degree of product purification, as well as post-production handling and storage conditions. Specific physicochemical attributes strongly influence biodiesel's quality and, in turn, its suitability as an alternative fuel capable of delivering efficient performance across diverse applications and climatic conditions worldwide. To ensure quality, biodiesel specifications focus on fatty alkyl esters and emphasize several critical factors: complete conversion of oils to esters, removal of free glycerides, elimination of catalyst residues through ash content analysis, reduction of excess alcohol via flash point measurement, and verification of the absence of free fatty acids (FFA) through acid number determination. Thus, defining biodiesel quality standards and developing corresponding testing methods are fundamental for its efficient application and commercial viability.

**ASTM and EN standards (Arumugam, 2022)**

Austria was the earliest country to establish quality specifications for biodiesel, introducing the Ö-NORM C-1190 standard in 1991, which was based on rapeseed oil methyl esters as an alternative to conventional diesel fuel. Germany subsequently adopted its own specification, DIN 51606. In the United States, standardization efforts began in 1994 when ASTM International

created a task force comprising researchers, producers, and manufacturers to define biodiesel fuel requirements. These efforts resulted in the provisional PS121 specification in 1999, followed by the publication of the first official ASTM biodiesel standard, ASTM D6751, in 2002. In Europe, the EN 14214 standard was introduced in 2003, largely derived from the German DIN 51606. Following these developments, numerous countries, including the Czech Republic, China, Argentina, Brazil, India, Italy, Japan, and South Africa, established national biodiesel standards adapted to their regulatory frameworks.

At present, ASTM D6751 and EN 14214 serve as the main international reference standards for biodiesel quality. The ASTM D6751 specification was initially established to regulate the properties of neat biodiesel (B100), primarily intended for use as a blending component rather than as a direct substitute for conventional automotive diesel fuel. In addition, ASTM fuel standards were later extended to include biodiesel–diesel mixtures, with ASTM D975 (2008) authorizing biodiesel contents of up to 5% (B5) in petroleum diesel, and ASTM D7467 defining quality requirements for blends ranging from B6 to B20.

In Europe, EN 14214 governs fatty acid methyl esters (FAME) for both pure biodiesel (B100) and blends. Diesel blends are regulated under EN 590, which initially allowed up to 5% FAME in 2004 and later 7% in 2009. EN 14214:2012 extended coverage to heating oil applications, permitting B10 blends, while EN 16709 (2015) introduced standards for B20 and B30 blends for fleet use.

Table 1.4 summarizes the specifications of neat biodiesel (B100) in comparison with conventional diesel fuel, along with the corresponding test methods specified in the ASTM D6751 and EN 14214 standards (Arumugam, 2022).

| | Diesel | | Biodiesel | | | |
|---|---|---|---|---|---|---|
| **Property** | **ASTM D975** | **Test Method** | **ASTM D6751-1B** | **Test Method** | **EN 14214** | **Test Method** |
| Water and sediment, % volume, max | 0.050 | D2709 | 0.050 | D2709 | 500 mg/kg | EN ISO 12937 |
| Water, max | — | — | — | — | — | EN ISO 2719 |
| Flash point (closed cup), °C, min | 60–80 | D93 | 93 | D93 | 101 | EN ISO 2719 |
| Distillation temperature (90% ), °C, max | 282–338 | D86 | 360 | D1160 | — | — |
| Density | — | — | — | — | 860–900 kg/m³ | EN ISO 12185 |
| Kinematic viscosity, mm²/s at 40°C | 1.9–4.1 | D445 | 1.9–6.0 | D445 | 3.5–5.0 | EN ISO 3104 |
| Ester content | 5% vol.max | EN 14078 | — | — | 96.5% min | EN 14103 |
| Copper strip corrosion, max | No. 3 | D130 | No. 3 | D130 | Class 1 | EN ISO 2160 / ISO 3987 |
| Sulfated ash, % mass, max | — | — | 0.020 | D874 | 0.02 | — |
| Ash, max | 0.01 wt % | D482 | — | — | — | — |
| Cetane number, min | 40 | D613 | 47 | D613 | 51.0 | EN ISO 5165 |
| Carbon residue, % mass, max | 0.35 | D524 | 0.050 | D4530 | — | — |
| Cloud point,°C | −35 to −5 | D2500 | Report | D2500 | Location and season | EN 23015 |
| Acid number, mg KOH/g, max | — | — | 0.50 | D664 | 0.50 | EN 14104 |
| Iodine value, max | — | — | — | — | 120 g/100 g | EN 14111 |
| Oxidation stability, h, min | — | — | 3 | EN 15751 | 8 | EN 15751 |
| Alcohol control – flash point °C (min) / methanol content mass % (max) | — | — | 130 / 0.2 | D93 / EN 14110 | −0.2 | −EN 14110 |

| | Diesel | | Biodiesel | | | |
|---|---|---|---|---|---|---|
| **Property** | **ASTM D975** | **Test Method** | **ASTM D6751-1B** | **Test Method** | **EN 14214** | **Test Method** |
| Sodium & potassium (Group I metals), ppm, max | — | — | 5 | — | 5 | EN 14538 |
| Calcium & magnesium (Group II metals), ppm, max | — | — | 5 | — | 5 | EN 14538 |
| Free glycerin, % mass, max | — | — | 0.020 | D6584 | 0.02 | EN 14105 |
| Total glycerin, % mass, max | — | — | 0.240 | D6584 | 0.25 | EN 14105 |
| Phosphorus content, max | — | — | 0.001 wt % | D4951 | 4.0 mg/kg | EN 14107 |
| Sulfur content, % mass, max | 0.0015 | D5453 | 0–0.0015 | D5453 | 10 mg/kg max | EN ISO 20846 |
| Monoglycerides, % mass, max | — | — | 0.4 | D6584 | 0.70 | EN 14105 |
| Diglycerides, % mass, max | — | — | — | — | 0.20 | EN 14105 |
| Triglycerides, % mass, max | — | — | — | — | 0.20 | EN 14105 |
| Cold soak filterability, max | — | — | 200 s | D7501 | — | — |

**Table 1.4** American and European biodiesel standards and associated test procedures

## 1.11 Methods of Improving Biodiesel Properties

The enhancement of biodiesel properties has been approached through blending, feedstock and product modification, and the use of chemical or metallic additives.

- **Blending with conventional diesel**

  Blending biodiesel with mineral diesel improves its low-temperature operability without altering its chemical structure. Effective blends typically contain up to 30% biodiesel, achieving cloud points of around –10 °C (A. K. Agarwal, 2007).

- **Modification of oil feedstock**

  Winterization, which separates oil fractions with different solidification points, enhances pour and handling qualities. This can be achieved through controlled refrigeration or by natural exposure to cold climates. Furthermore, genetic modification of oilseeds provides long-term potential for altering fatty acid profiles to improve cold-flow properties.

- **Modification of biodiesel product**

  Fractionation processes, including dry and solvent fractionation, reduce the proportion of saturated esters, improving low-temperature performance. Dry fractionation is cost-effective but less efficient, while solvent fractionation offers better yields but higher cost and safety concerns. An alternative approach involves electrophilic addition to unsaturated fatty acids, such as epoxidising isopropyl oleate, to form branched esters with improved cold properties.

- **Additives**

  The incorporation of additives is commonly employed to improve fuel performance. Conventional additives used in petroleum diesel, such as pour point depressants and wax crystal modifiers, enhance low-temperature behaviour by restricting crystal formation and altering crystallization mechanisms. In addition, several additives developed specifically for biodiesel have demonstrated a marked ability to reduce both pour point such as Tween-80, dihydroxy fatty acids, acrylated polyester pre-polymers, palm-derived polyols, and castor oil–based ricinoleate and cloud point temperatures.

- **Metal-Based Fuel Additives**

  Metallic additives act as combustion catalysts, promoting complete combustion and lowering the oxidation temperature. Common examples include cerium, platinum, iron, manganese, calcium, and copper. These not only enhance engine efficiency and

reduce emissions but also improve biodiesel's viscosity and pour point (Kannan et al. 2011).

- **Blending with Other Fuels (Bioethanol)**

Another approach is the addition of bioethanol to biodiesel. Torres et al. (2010) tested RaBIO-bioethanol blends (B95E05, B90E10, B85E15), finding that increasing bioethanol concentration reduces density and viscosity while slightly lowering lubricity. Importantly, bioethanol improves cold-flow properties (cloud point, pour point, CFPP) by altering paraffin crystallization. However, both biodiesel and bioethanol are hygroscopic, and higher ethanol concentrations increase water absorption risk during storage

## 1.12 Engine performance with biodiesel

Engine performance parameters, including power output, brake thermal efficiency (BTE), and brake specific fuel consumption (BSFC), are commonly used to assess engine compatibility with alternative fuels. Accordingly, this section reviews studies that examine BSFC, BTE, and power output for different engine configurations operating on biodiesel–diesel fuel blends.

### 1.12.1 Brake Specific Fuel Consumption (BSFC)

Brake specific fuel consumption (BSFC) is an indicator of an engine's fuel utilization efficiency during power generation. It represents the rate of fuel consumption relative to the effective power delivered by the engine over a given operating period and is commonly reported in units of grams per kilowatt-hour (g/kWh).

$$BSFC = \frac{fuel\ consumed\ in\ g/h}{brake\ power\ in\ kW}\, g/kWh \quad \text{.....(1.2)}$$

It is consistently reported that biodiesel and its blends tend to increase BSFC compared to conventional diesel. This effect is largely attributed to biodiesel's intrinsic physicochemical properties, such as lower calorific value, higher viscosity, and higher density, which alter combustion and fuel injection characteristics.

Gaur and Goyal (2025) experimentally evaluated the performance of a single-cylinder, four-stroke, water-cooled, multi-fuel diesel engine operating at a constant speed of 1500 rpm under load conditions ranging from 0 to 100% in steps of 20%. Biodiesel produced from a mixed oil feedstock comprising equal proportions of waste cooking oil and pongamia oil was blended with diesel at ratios varying from D95BWP5 to D75BWP25. The results indicated that brake specific energy consumption (BSEC) decreased as engine load increased; however, BSEC val-

ues for all biodiesel blends were consistently higher than those obtained with neat diesel. Moreover, the magnitude of BSEC increase was directly related to the biodiesel fraction in the blend. At 80% load, BSEC rose by 5.06%, 7.23%, 10.80%, 15.30%, and 21.15% for D95BWP5, D90BWP10, D85BWP15, D80BWP20, and D75BWP25, respectively, relative to diesel fuel.

**Table 1.5** Fuel properties for Gaur and Goyal (2025) experimental study

| **Fuel properties** | **Diesel** | **Mixed oil biodiesel** | **D95BWP5** | **D90BWP10** | **D85BWP15** | **D80BWP20** | **D75BWP25** |
|---|---|---|---|---|---|---|---|
| Viscosity (40°C) $mm^2/s$ | 2.63 | 4.8 | 2.75 | 2.86 | 3.0 | 3.12 | 3.2 |
| Density ($kg/m^3$) | 836 | 876 | 838 | 841 | 843 | 846 | 849 |
| Calorific value (MJ/kg) | 42.5 | 39.3 | 42.34 | 42.24 | 42.02 | 41.86 | 41.7 |

Similarly, Fareed et al. (2024) investigated the performance of biodiesel–diesel blends using a four-stroke, direct-injection diesel engine and observed that brake specific fuel consumption (BSFC) was consistently higher for biodiesel-fueled operation. This behavior was attributed to the lower calorific value, higher viscosity, and reduced volatility of biodiesel, which affected spray atomization and air–fuel mixing. As a result, a greater quantity of biodiesel was required to produce the same brake power output. Among the tested fuels, the WB10+CB10 blend demonstrated better performance, which was associated with its lower viscosity, reduced density, and higher heating value. At full load, the BSFC increased by 2%, 3.5%, 5.5%, 6%, and 8.5% for WB10, CB10, WB10+CB10, WB20, and CB20, respectively, relative to diesel fuel.

**Table 1.6** fuel properties of Fareed et al. (2024) investigations.

| Properties | Method | Diesel oil | WB100 | CB100 | WB20 | CB20 | WB10+CB10 |
|---|---|---|---|---|---|---|---|
| Density at 15.56 (°C), $kg/m^3$ | ASTM D-4052 | 827 | 873 | 890 | 840 | 855 | 835 |
| Calorific Value, kJ/kg | ASTM D-224 | 42100 | 39200 | 38400 | 41800 | 40700 | 42000 |
| Kinematic Viscosity at 40 (°C), cSt | ASTM D-445 | 2.4 | 4.2 | 6.5 | 3.0 | 3.4 | 2.8 |
| Cetane Number | ASTM D-13 | 44 | 51 | 53 | 47 | 49 | 46 |
| Flash Point (°C) | ASTM D-93 | 72 | 150 | 170 | 92 | 110 | 81 |

Complementary findings were reported by Chen et al. (2023). A numerical investigation was carried out using CONVERGE software on a four-cylinder, four-stroke, medium-speed inline diesel engine, typical of power generation applications. The study demonstrated that brake specific fuel consumption (BSFC) increased progressively as the biodiesel fraction in the fuel blend was raised.: at 50% load, D95B5, D90B10, D85B15, and D80B20 exhibited increases of 0.61%, 1.34%, 1.42%, and 2.17%, respectively, relative to diesel (D100). The trend was attributed to the lower heating value of biodiesel, necessitating higher fuel consumption to meet power demands.

**Table 1.7** Fuel properties of Chen et al. (2023) study.

| Fuel | Diesel | Biodiesel (RME) | D95B5 | D90B10 | D85B15 | D80B20 |
|---|---|---|---|---|---|---|
| Flash point temperature (°C) | 67 | 168 | 72.05 | 77.1 | 82.15 | 87.2 |
| Oxygen volume fraction (%) | 0.0 | 10.7 | 0.535 | 1.07 | 1.605 | 2.14 |
| Density (g/m³, at 20 °C) | 0.82–0.86 | 0.882 | 0.8231–0.8611 | 0.8262–0.8622 | 0.8293–0.8633 | 0.8324–0.8644 |
| Latent heat of vaporization (kJ·kg⁻¹) | 253.31 | 273.86 | 254.31 | 255.315 | 256.32 | 257.32 |
| Viscosity (MPa·s, at 20 °C) | 3.0–8.0 | 4.556 | 3.08 | 3.16 | 3.23 | 3.31 |
| Cetane number (CN) | 45–66 | 53.88 | 45.444 | 45.888 | 46.332 | 46.776 |
| Low heating value (MJ·kg⁻¹) | 42.5 | 39.53 | 42.3515 | 42.203 | 42.0545 | 41.906 |

Beyond blend ratio, engine speed and load conditions also influence BSFC. (Habibullah et al., 2014) investigated biodiesel blends deriverd from palm and coconut oil in a single-cylinder diesel engine under speeds between 1400 and 2400 rpm. They observed that the lowest BSFC occurred at 1800 rpm, with fuel consumption rising at higher speeds due to declining volumetric efficiency. At low load (105 Nm), BSFC increased with speed (800–2000 rpm), whereas at high load (420 Nm), it decreased as speed rose, indicating the strong interaction between speed, load, and fuel type.

Source dependency of biodiesel is another important factor,Ozsezen et al. (2009) compared diesel (D100) with palm biodiesel (PaBIO) and canola biodiesel (CaBIO) in a naturally aspirated DI engine under full load. While brake power differences were minor, BSFC values varied significantly across fuels. Both biodiesels showed higher BSFC than diesel, consistent with their lower heating values. Among them, PaBIO exhibited the highest BSFC, attributed to its lower energy content and shorter carbon chains. Other comparative studies similarly demonstrated that biodiesel feedstock strongly influences BSFC due to differences in density, viscosity, and energy content. Explanations for higher BSFC vary in the literature, with some attributing it to higher density leading to greater mass injection at constant volume and pressure (Buyukkaya, 2010;Qi et al., 2009), while others emphasize combined effects of higher viscosity, lower energy content, and density ;(Aydin & Bayindir, 2010). Finally, feedstock type, biodiesel concentration, blends properties, engine speed, and load collectively determine fuel consumption patterns.

### 1.12.2 Brake Power (BP)

Brake power (BP) refers to the effective power output measured at the engine crankshaft and is directly affected by both the characteristics of the fuel and the engine's operating conditions. Chen et al. (2023) reported that BP increased with load for both diesel and biodiesel blends, but diesel consistently delivered the highest BP. At full load, BP reductions of 0.64%, 1.31%, 1.88%, and 2.62% were observed for D95B5, D90B10, D85B15, and D80B20, respectively, relative to diesel. This decline was attributed to the lower calorific value of biodiesel.

Similar results were reported by Habibullah et al.( 2014) who found that PB30 had the lowest average BP, 3.92% less than diesel. Gaur and Goyal (2025) also noted reduced BP for mixed biodiesel blends, with diesel consistently outperforming all blends. These reductions in brake power reflect the inherent energy deficit of biodiesel compared to mineral diesel.

### 1.12.3 Brake Thermal Efficiency (BTE)

Brake thermal efficiency (BTE), indicates the proportion of the fuel's thermal energy that is converted into useful brake power. It is calculated as:

$$BTE = \frac{Brake\ Power\ (Kw)}{Fuel\ Energy\ input} \quad \ldots\ldots\ldots\ldots\ldots\ldots\ldots\ldots\ (1.3)$$

The fuel energy input is simply the mass flow rate of fuel multiplied by its lower heating value (LHV)

(Gaur & Goyal, 2025) reported that diesel fuel consistently delivered the highest BTE compared to mixed biodiesel blends (waste cooking oil + pongamia oil) Table 1.5. At 80% load, diesel reached a maximum BTE of 23.62%, while the lowest value, 19.56%, was recorded for D75BWP25. The percentage reduction in BTE relative to diesel was 5.0%, 7.75%, 10.47%, 12.57%, and 17.20% for blends D95BWP5, D90BWP10, D85BWP15, D80BWP20, and D75BWP25, respectively. This decline was attributed to the lower calorific value, higher viscosity, and higher density of biodiesel, which hinder vaporization and atomization, reducing combustion efficiency. Among the blends, D80BWP20 achieved better BTE than D75BWP25, suggesting that an optimal balance between oxygen content and energy density is needed for efficient combustion.

Chen et al. (2023) emphasized the dual aspects of performance, reporting both brake power and BTE for various biodiesel-diesel blends. Their results showed that BP rose with engine load, with D100 consistently achieving the highest BP, followed by D95B5, D90B10, D85B15, and D80B20. At full load, BP reductions of 0.64%, 1.31%, 1.88%, and 2.62% were observed for these blends relative to diesel. The decrease was also linked to the lower calorific value of biodiesel, which reduces in-cylinder pressure and temperature. In contrast, BTE improved with increasing load and higher biodiesel proportion, as the oxygen content in biodiesel promoted more complete combustion. At 50% load, D80B20 achieved the highest BTE, 3.82% greater than diesel, with a consistent increasing trend across blends.

(Fareed et al., 2024) further noted that BTE is strongly influenced by load and fuel composition. They observed that BTE initially increased with engine load but decreased beyond a certain point due to rising frictional and thermal losses. Biodiesel blends showed lower BTE than diesel, primarily due to higher viscosity, poor volatility, and atomization challenges, which compromise combustion quality. At maximum output power, the BTE of WB10, CB10, WB10+CB10, WB20, and CB20 were reduced by 2.5%, 4%, 5%, 6%, and 9.5%, respectively, compared to diesel. Among the blends, CB10+WB10 exhibited improved efficiency because of its lower viscosity, reduced density, and higher calorific value.

Several studies confirm that BTE of biodiesel is often slightly lower than diesel, though outcomes vary with feedstock and test conditions.(Gad et al., 2018) found that palm oil biodiesel blends (PO20, B20, and B100) showed reduced BTE compared to diesel across loads. At 4 kW, BTE values for diesel, B20, B100, and PO20 were 28.7%, 27.7%, 24.7%, and 26.8%, respectively. Habibullah et al. (2014) reported similar trends, where PB30 had the lowest average BP

(3.92% less than diesel) and biodiesel BTE values were 3.84-5.03% lower, consistent with their lower LHV. Conversely, some studies suggest biodiesel blends can achieve comparable or even higher BTE than diesel. (Muralidharan et al., 2011) demonstrated that waste cooking oil biodiesel blends (B20 and B40) achieved BTE values of 37.18% and 38.46%, surpassing diesel (34.45%). These improvements are attributed to biodiesel's oxygen content, which promotes better combustion phasing and increased peak pressures.

In summary, biodiesel generally reduces brake power compared to diesel because of its lower calorific value, but its higher oxygen content can enhance combustion efficiency, sometimes leading to comparable or even improved BTE under specific conditions. The combined influence of blend ratio, feedstock type, and engine load is critical in determining whether biodiesel will result in lower or higher thermal efficiency relative to diesel.

## 1.13 Engine Harmful Emissions

The primary harmful emissions from diesel engines include nitrogen oxides (NOx), particulate matter (PM) or smoke, carbon monoxide (CO), and unburned hydrocarbons (HC). The use of biodiesel as a substitute for conventional diesel can significantly affect the levels of these emissions.

Carbon monoxide (CO) is a key indicator of incomplete combustion in diesel engines .A consistent observation across studies is that biodiesel and its blends generally produce lower CO emissions than conventional diesel due to their higher oxygen content and lower carbon-to-hydrogen ratio (Agarwal, 2007; Enweremadu & Rutto, 2010)

Habibullah et al.( 2014) reported that palm biodiesel blends (PB30) reduced CO emissions by about 13.75% compared to diesel when tested on a single-cylinder engine operating between 1400 and 2400 rpm. They explained this reduction by the oxygenated nature of biodiesel, which promotes more complete combustion, particularly at higher engine speeds where cylinder temperatures increase and facilitate the conversion of CO to $CO_2$. Similarly, Buyukkaya (2010) observed a progressive decline in CO emissions with higher rapeseed biodiesel substitution: 12% for B5, 25% for B20, 31% for B70, and 35% for B100, with the trend more pronounced at increased engine speeds. Abed et al. (2018) also confirmed these findings using waste cooking oil biodiesel blends (B10-B30), showing that CO emissions decreased with increasing brake power at lower loads, again attributed to the higher oxygen availability in biodiesel compared to diesel.Chen et al. (2023) further emphasized that incomplete combustion is the main source of CO emissions, and that effective CO oxidation plays a central role in reducing them. Their

experiments demonstrated that CO emissions increased with engine load due to higher fuel consumption but decreased systematically as the biodiesel share in the blends rose. For instance, at full load, D80B20 produced 2.71% lower CO emissions than pure diesel (D100), reinforcing the role of biodiesel's inherent oxygen in promoting complete combustion.

Gaur and Goyal (2025) found that CO emissions were comparable to diesel at low and medium loads but rose progressively at high loads due to localized fuel-rich regions with limited oxygen. Nevertheless, the biodiesel blends consistently outperformed diesel, with average CO reductions of 3.57% (D95BWP5), 4.5% (D90BWP10), 17.53% (D85BWP15), 24.53% (D80BWP20), and 35.32% (D75BWP25). Among the tested blends, D80BWP20 exhibited the lowest CO emissions, beyond which no significant reduction was observed.Finally, higher oxygen concentration in biodiesel enhances CO oxidation to $CO_2$ and contributes to emission reduction (Loo et al., 2021; Abed et al., 2018; Chen et al., 2023).

### 1.13.1 NOx Emissions

Nitrogen oxides (NOx) are primarily formed in diesel engines due to the interaction between nitrogen and oxygen at elevated combustion temperatures. Their formation is strongly influenced by oxygen concentration, residence time, in-cylinder temperature, fuel composition, and ignition delay (Fareed et al., 2024; Chen et al., 2023). As engine load increases, fuel consumption and combustion temperature rise, which in turn elevates NOx emissions. During premixed combustion, the higher cylinder gas temperature enhances the reaction between dissociated nitrogen and oxygen, leading to the formation of thermal NOx.Fareed et al. (2024) observed that biodiesel blends typically produce higher NOx emissions than diesel, mainly due to their greater oxygen content and higher adiabatic flame temperature. At full load, blends such as WB10, CB10, WB10+CB10, WB20, and CB20 showed NOx increases of 1.5%, 2.5%, 3.5%, 5%, and 6.5% respectively, compared to diesel. Gaur and Goyal (2025) investigated mixed biodiesel blends (50% waste cooking oil + 50% pongamia oil) and reported that NOx emissions were consistently higher than those of neat diesel across different loads. Emissions rose gradually from low to medium load conditions due to increased in-cylinder temperature, but at full load, the limited oxygen availability slightly constrained NOx formation despite higher injection volumes. On average, NOx emissions increased by 7.40%, 10.89%, 17.94%, 24.24%, and 30.42% for D95BWP5, D90BWP10, D85BWP15, D80BWP20, and D75BWP25, respectively, compared to diesel. However, D80BWP20 showed lower NOx emissions than D75BWP25, indicating that excessive biodiesel content may not linearly increase NOx.Chen et al. (2023) further

confirmed that NOx emissions grow with biodiesel proportion and engine load. At 50% and 100% loads, blends with higher biodiesel content (e.g., D80B20) produced more NOx than diesel. This was attributed to the higher oxygen content of biodiesel, which prolongs combustion and raises in-cylinder temperatures. At very low loads, however, biodiesel blends tended to produce less NOx than diesel due to lower calorific value and higher evaporation heat, which reduced combustion temperature.Other investigations also demonstrated that biodiesel from soybean, palm, and waste frying oils increased NOx emissions as test loads rose, with the largest increase (92.6%) reported for POME20 at 75 kW(Vieira da Silva et al., 2017)). In general, biodiesel-diesel blends generate more NOx at partial and high loads due to the unsaturation level and inherent oxygen in biodiesel molecules, which promote higher flame temperatures.(Mueller & Martin, 2009) highlighted that the NOx rise is associated with stoichiometric conditions during premixed autoignition, which elevate in-cylinder temperatures and reduce radiative heat losses. Fuel properties also play a role; higher cetane numbers tend to suppress NOx emissions by shortening combustion duration, while lower cetane fuels can intensify them. Overall, NOx emissions from biodiesel blends are a complex outcome of engine operating conditions, combustion dynamics, and biodiesel characteristics such as oxygen content, degree of unsaturation, and cetane number.

### 1.13.2 Hydrocarbon (HC) Emissions

The emission of unburned hydrocarbons (HC) in diesel engines is closely related to fuel compo, cetane number, oxygen content, and combustion efficiency. Biodiesel blends generally exhibit lower HC emissions than neat diesel because of their intrinsic oxygen content and higher cetane number, which enhance fuel oxidation and shorten ignition delay (Habibullah et al., 2020). Gaur and Goyal (2025) reported that blends of waste cooking oil and pongamia oil biodiesel (BWP) consistently reduced HC emissions compared with diesel across different engine loads. At 80% load, the reductions were 11.69%, 16.87%, 25.63%, 34.32%, and 38.65% for D95BWP5, D90BWP10, D85BWP15, D80BWP20, and D75BWP25, respectively. The authors attributed these reductions to the higher oxygen availability and improved combustion efficiency of biodiesel blends.

Similar findings were presented by Fareed et al. (2024), who examined waste cooking oil methyl ester-diesel blends. HC emissions generally rose with increasing engine load due to richer fuel-air mixtures, but biodiesel blends still emitted lower HC than diesel at all loads. The reductions were explained by enhanced oxidation from biodiesel's oxygenated structure and the

improved ignition quality of blends with higher cetane number. Among the tested blends, WB10, CB10, WB10+CB10, WB20, and CB20 showed HC reductions of 6%, 7%, 10%, 12%, and 14% at full load, respectively, compared to diesel. Overall, the literature demon-strates that biodiesel-diesel blends substantially reduce HC emissions compared to diesel. This effect be-comes more pronounced at higher biodiesel proportions due to enhanced oxidation and com-bustion stability, though differences among biodiesel types reflect variations in oxy-gen con-tent, unsaturation level, and ignition characteristics.

### 1.13.3 Smoke Emissions

Smoke is a visible pollutant in diesel exhaust, primarily formed due to incomplete oxidation of fuel in oxygen-deficient regions of the combustion chamber. Conventional diesel combustion often produces high smoke levels because of the limited availability of oxygen during fuel ox-idation. In contrast, biodiesel contains intrinsic oxygen within its molecular structure, which promotes more complete combustion and reduces smoke formation (Gaur & Goyal, 2025).Ex-perimental findings consistently demonstrate this trend. For instance, Gaur and Goyal (2025) observed reductions in smoke opacity of approximately 15%, 20.09%, 24.9%, 35.48%, and 39.35% for blends D95BWP5, D90BWP10, D85BWP15, D80BWP20, and D75BWP25, re-spectively, compared with mineral diesel at 80% engine load. Fareed et al. (2024) similarly reported that neat diesel produced higher smoke concentrations than biodiesel blends, with re-ductions being more pronounced at elevated loads. The enhanced oxidation of carbonaceous particles during diffusion combustion, enabled by the oxygen content of biodiesel, was identi-fied as the primary mechanism for smoke reduction.Nonetheless, smoke emissions increase with engine load for all fuels, as richer mixtures pre-vail under higher fueling conditions. Raheman and Ghadge (2007) demonstrated that in a sin-gle-cylinder diesel engine, smoke lev-els rose sharply with load due to reduced air-fuel ratios, causing a greater fraction of unburned fuel to escape combustion. Furthermore, engine operat-ing conditions such as speed and tem-perature influence smoke behaviour.

### Particulate Matter (PM) Emissions

Particulate matter (PM) refers to microscopic solid or liquid particles emitted in engine exhaust, including soot, organic carbon, and sulfates. PM formation in diesel engines is strongly influ-enced by fuel composition, combustion conditions, and engine operating parameters. Compared with mineral diesel, biodiesel consistently produces lower PM emissions, a reduction largely

attributed to its higher oxygen content, lower aromatic fraction, and reduced stoichiometric air-fuel ratio.

Several studies have quantified this effect. Salamanca et al. (2012) found that 100% palm oil biodiesel reduced PM emissions by about 65% compared with diesel, with progressive reductions observed as biodiesel concentration in blends increased. These reductions are linked to improved oxidation during combustion and the absence of aromatic compounds, which limits soot nucleation and growth. The relationship between PM emissions and engine operating conditions is also well documented. PM levels generally increase with load due to richer combustion conditions, but decrease with rising engine speed (Kaplan et al., 2006; Buyukkaya, 2010). However, under low-temperature or cold-start conditions, biodiesel may exhibit elevated PM emissions.

## 1.14 Conclusion

In summary, the literature review underscores the critical role of biodiesel in addressing global energy and environmental challenges while identifying waste cooking oil as one of the most sustainable and scalable feedstocks. The analysis of production techniques and associated constraints has clarified the parameters influencing biodiesel yield and quality, particularly those related to feedstock composition and reaction optimization. This foundational understanding supports the experimental design of the present study, ensuring that the selected methodologies are both scientifically grounded and contextually relevant. Ultimately, the insights gained from this chapter form the conceptual bridge between the theoretical knowledge of biodiesel production and the practical investigations developed in the following chapters, including the case study, engine testing, and computational modelling.

# Chapter 2

# Biodiesel Production and Characterization

Following the theoretical background and literature insights outlined in the previous chapter. This chapter presents the experimental investigation of biodiesel production from waste cooking oil (WCO), emphasizing the upstream stages and their influence on fuel quality. The study begins with the collection, storage, and pretreatment of WCO, as these steps play a decisive role in determining the efficiency of the conversion process and the purity of the final product. The transesterification reaction is then optimized by adjusting key parameters to achieve maximum yield and fuel stability. Following production, the recovered biodiesel is characterized through a series of physicochemical analyses and compared with international standards (ASTM D6751 and EN 14214) to assess its compliance and suitability for engine applications. The outcomes of this chapter provide the experimental basis for the following stages of this research, where the produced biodiesel is evaluated in engine performance tests and computational simulations. The results presented in this section are partly derived from the author's previously published work (Medjahed et al., 2025).

## 2.1 Collection and storage

A comprehensive procedure was established for producing biodiesel from waste cooking oil (WCO), covering all stages from collection to conversion, as shown in the process diagram in Figure 2.1. The first stage involved selecting a suitable feedstock. For this study, WCO was obtained from the fish restaurant "LeVoilier 2 frères" in Oran, Algeria, chosen for its consistent frying operations and high oil turnover (Medjahed et al., 2025).

The oil used at this restaurant was originally soybean oil and was mainly employed for frying fish, following typical Mediterranean culinary practices. Frying was generally performed at moderate temperatures between 100 °C and 150 °C. Additionally, the oil was reused no more than seven times, which helped limit its degradation and the buildup of residues.

**Table 2.1** Conditions for storage and environment of WCO samples (Medjahed et al., 2025).

| Parameter | Sample 1 (May) | Sample 2 (November) |
|---|---|---|
| Collection Date | May | November |
| Weather Conditions | Warm and dry | Cool and humid |
| Estimated Ambient Temperature | ~28–32 °C (daytime) | ~15–20 °C (daytime) |
| Humidity Level | Low (~40–50%) | High (~70–80%) |
| Container Type | Transparent plastic | Opaque plastic |
| Light Exposure | Exposed to lab light (possibly sunlight) | Stored in dark conditions |
| Air Contact | Frequent exposure (opened occasionally) | Minimal exposure (remained sealed) |

Two samples of waste cooking oil (WCO) were obtained from the same restaurant at two separate time points, six months apart, in order to assess the impact of storage conditions on oil quality . Each sample was maintained under distinct environmental conditions, specifically temperature and relative humidity, using data provided by the Office Nationale de la Météorologie (ONM) for the Oran region, as summarized in Table 2.1. Before undergoing chemical conversion, both samples were subjected to the same pretreatment procedure.

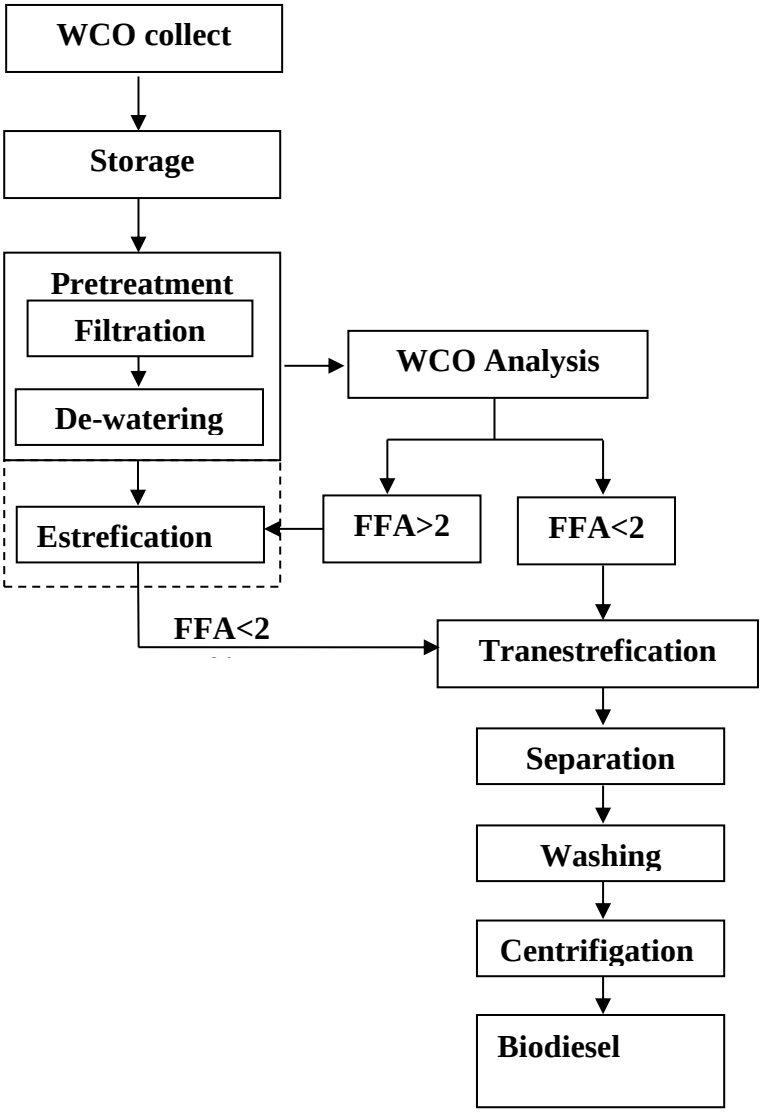


**Figure 2.1** Biodiesel production methodology (Medjahed et al., 2025).

## 2.2 Pretreatment

The pretreatment process for waste cooking oil (WCO) began with the separation of insoluble contaminants, primarily food particles, through gravity settling. This was followed by a sequential filtration procedure. In the initial stage, the oil underwent coarse filtration using a cotton fabric, after which it was passed through a stainless-steel sieve with a pore size ranging from 150 to 200 µm. Subsequently, the oil was heated to approximately 110-120 °C to liquefy any solidified fats, facilitate the release of trapped impurities, and lower the viscosity, thereby improving handling. A secondary filtration step was then carried out using stainless-steel meshes with apertures of 70–100 µm. This was followed by a tertiary filtration employing a 5 µm mesh to remove residual fine particulates. In the final stage, the treated oil was filtered through a

1 cm thick quartz bed composed of silicon dioxide ($SiO_2$), which functioned as an organic filtering medium to adsorb moisture and capture any remaining fine and ultrafine particles (as illustrated in Figures 2.2 and 2.3).

**Figure 2.2** Waste cooking oil sample pre-treatement

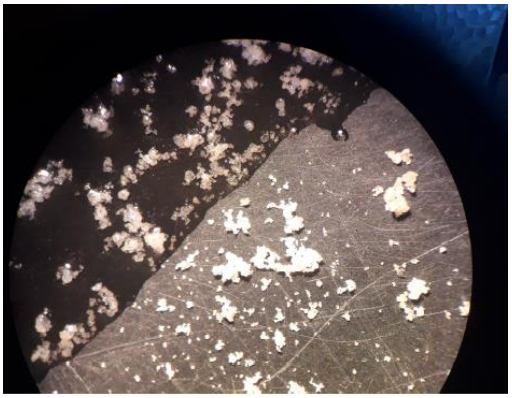

**Figure 2.3** quartz layer composed of silicon dioxide (SiO2)

## 2.3 Sample analysis

An initial characterization of the waste cooking oil (WCO) was conducted to determine the necessity of an esterification step for acid reduction during pretreatment. This analysis also determine the oil's quality for biodiesel production, particularly in preparation for the trans-esterification reaction.Potentiometric titration with a TitroLine automatic titrator is done to mesure free fatty acid (FFA) content. First, oil samples were dissolved in a solvent mixture of ethanol and diethyl ether. Then, the titration with a potassium hydroxide (KOH) solution prepared in isopropyl alcohol is conducted. The acid value is the milligrams of KOH needed to neutralize the acids in 1 g of oil and it is used then to calculate the FFA percentage using the following equation (assuming oleic acid as the predominant fatty acid):

$$FFA\ (\%) = \frac{(Acid\ Value \times Molecular\ Weight\ of\ Oleic\ Acid)}{(10 \times 1000)} \quad \ldots\ldots\ldots\ldots\ldots\ (2.1)$$

$$FFA(\%) = \frac{(Acid\ Value \times 282.47)}{10{,}000} = \text{Acid Value} \times 0.503 \ldots\ldots\ldots\ldots (2.2)$$

## 2.4 Feedstock Characterisation and Storage effects

To investigate how storage conditions affect waste cooking oil and its potential for biodiesel production, two samples were selected and analysed, with results summarised in Table 2.2

Both samples were collected from the same restaurant at different moments of the year and stored under environmental conditions distinct (see Table 2.1).

Sample 1, stored in a transparent plastic container exposed to light and air, exhibited a remarkable degradation seen as dark brown colour and strong odour. For Sample 2, stored in an opaque, airtight container, underwent a minimal deterioration because it maintained a lighter yellow colour and milder odour.These colour and odour changes are attributed to oxidation, which breaks down natural pigments and darkens the oil (Sikorska et al., 2007). The elevated free fatty acid (FFA) content in Sample 1 also contribute to this degradation. Topi (2020) classify darker oils with high FFA levels as "brown grease".Sample 1 had a high viscosity of 83.589 mm²/s at 40 °C, while Sample 2 measured 40.32 mm²/s. Increased viscosity is also associated to oxidation, which supports polymer formation (Gertz, 2000). According to Cordero-Ravelo and Schallenberg-Rodriguez (2018), oils with viscosities below 38.46 mm²/s at 40 °C can generally be converted to biodiesel in a single reaction stage, whereas oils within the 39.74-56.04 mm²/s range may yield lower-quality biodiesel (Alias et al., 2018).In addition, both samples revealed FFA levels below 2%, indicating that they could be directly subjected to base-catalysed transesterification without a prior esterification step. These results emphasise the importance of controlled storage conditions, particularly protection from light, heat, and air, in preserving WCO quality for biodiesel production (Adhikesavan et al., 2022; Bruun et al., 2021).

**Table 2.2** Waste cooking oil samples properties (Medjahed et al., 2025).

| Property | Sample 1 (May) | Sample 2 (November) |
|---|---|---|
| Color | Darkbrown to black | Light yellow and clear |
| Odor | Mild, less intense | Strong, pungent |
| FFA (%) | 1.25 | 0. 885 |
| Acid Value (mg KOH/g) | 2.50 | 1.77 |
| Density at 15 ◦C ( g/$cm^3$) | 0.9424 | 0.9393 |
| Kinematic Viscosity at 40◦C ($mm^2/s$) | 83.589 | 40.32 |

## 2.5 Transesterification

In this study of Medjahed et al.(2025) , biodiesel was synthesized from waste cooking oil through a homogeneous base-catalysed transesterification of triglycerides, using potassium hydroxide (KOH) as the catalyst and methanol as the alcohol. Potassium hydroxide was selected because of its high reactivity and cost-effectiveness, while methanol was preferred due to its availability, lower environmental impact, and economic feasibility (Topare et al., 2022;

Yaakob, Mohammad, Alherbawi, Alam, and Sopian, 2013). The reaction was conducted in a 300 mL flask placed on a hot plate equipped with a regulated magnetic stirrer and a temperature sensor.

The reaction parameters highly effect the chemical and physical properties of the resulting biodiesel, both. In this work (Medjahed et al., 2025) , the effects of key parameters on biodiesel production from WCO were systematically investigated. The selected values for each parameter were chosen based on ranges reported in the literature (Liazid et al., 2019; Duran, 2019; Saxena, Jawale, and Joshipura, 2013) as follows (see Table 2.3):

- Catalyst amount (mass of KOH /mass of WCO): 0.60, 0.8, 1.00, 1.20.
- Reaction temperatures: 40, 45, 50,55,60,65.
- Reaction times, minute: 30,45,60, 90.
- Oil to Methanol molar ratios: 1:6, 1:9 and 1:12.

Prior to initiating transesterification, the required amount of KOH was dissolved in a specific volume of methanol corresponding to the selected catalyst concentration. This methanolic solution was then introduced into the preheated waste cooking oil. The mixture was maintained at the target reaction temperature and stirred for the allotted time using a magnetic stirrer-hot plate setup (Table 2.3). A condenser was employed to minimize alcohol evaporation, and a thermometer was used to ensure the reaction temperature remained constant throughout the process.

### 2.5.1 Separation

After the transesterification reaction was complete, the mixture was gently transferred into a separating funnel. Within a few minutes, two distinct layers formed, as shown in Figure 2.4. The upper layer consisted of biodiesel (methyl esters), while the lower layer contained glycerol, residual methanol, unreacted catalyst, and soap. Due to its lower density, biodiesel remained on top. The mixture was allowed to settle for 24 hours to ensure complete separation, after which the layer in the bottom was removed from the funnel.

**Figure 2.4** Crude biodiesel and glycerol layers.

**Table 2.3** Experimental design of transesterification parameters with independent variable values (Medjahed et al., 2025).

| Reaction Temperature | | | | | Catalyst amount | | | | Molar ratio | | | Reaction time | | |
|---|---|---|---|---|---|---|---|---|---|---|---|---|---|---|
| 40 | 45 | 50 | 55 | 60 | 0.6 | 0.8 | 1 | 1.2 | 1 :6 | 1 :9 | 1 :12 | 30 | 45 | 60 |
| x | | | | | | | x | | x | | | | | x |
| | x | | | | | | x | | x | | | | | x |
| | | x | | | | | x | | x | | | | | x |
| | | | x | | | | x | | x | | | | | x |
| | | | | x | | | x | | x | | | | | x |
| | | | x | | x | | | | x | | | | | x |
| | | | x | | | x | | | x | | | | | x |
| | | | x | | | | x | | x | | | | | x |
| | | | x | | | | | x | x | | | | | x |
| | | | x | | | | x | | | x | | | | x |
| | | | x | | | | x | | | | x | | | x |
| | | | x | | | | x | | x | | | x | | |
| | | | x | | | | x | | x | | | | x | |

### 2.5.2 Washing

After gravity separation, the upper biodiesel layer was washed several times with warm distilled water (40-50 °C) to remove residual methanol, KOH, glycerol, and soap. This washing process is essential to improve fuel quality and prevent engine damage. Upon addition, another gravity

based separation is done; the water settled at the bottom of the separatory funnel, while biodiesel remained on top as depicted in Figure 2.5. During the initial washes, the water contained impurities because it appeared cloudy. The washing procedure was repeated for more cycles until the water turned clear (Figure 2.6). Finally, the biodiesel was heated to 110 °C to remove any remaining water and methanol, producing a dry, high-quality final product.

### 2.5.3 Centrifugation

To assure the biodiesel purity, the samples were transferred into centrifuge tubes and spun at high speed, causing the heavier impurities to settle at the bottom. This density based separation technique efficiently removed residual contaminants allowing the purified biodiesel in the upper layer to be collected as shown in Figure 2.7.

**Figure 2.5** First Wash Result

**Figure 2.6** washing Final Result

**Figure 2.7** Biodiesel centrifugation

## 2.6 Transesterification optimisation process

Since the FFA content of the waste cooking oil did not exceed 2%, direct transesterification was applied without prior esterification treatment. The current study, (Medjahed et al.,2025), began with experiments to determine the optimal catalyst concentration as part of a parametric analysis. Following the selection of an appropriate catalyst concentration, further experiments were performed to assess how reaction temperature, reaction time, and alcohol-to-oil molar ratio affect biodiesel yield and fuel quality.

### 2.6.1 Effect of Catalyst Concentration

An initial experiment performed in the absence of a catalyst at 60 °C for 90 min, using an oil-to-methanol molar ratio of 1:6, resulted in no biodiesel formation, underscoring the essential role of the catalyst in the transesterification reaction. To identify the optimum catalyst loading, potassium hydroxide (KOH) concentration was varied between 0.6% and 1.2% (w/w of oil), while all other reaction parameters were kept constant. An increase in biodiesel yield was observed as the catalyst concentration increased from 0.6% to 1.0% (Medjahed et al., 2025). However, further increasing the KOH concentration beyond 1.0% resulted in a decline in yield, which is mainly attributed to soap formation that impairs phase separation and limits conversion efficiency, in agreement with the observations of Agarwal et al. (2012). Consequently, a catalyst concentration of 1.0% KOH was selected as optimal, as it provided the highest ester yield.

### 2.6.2 Effect of Methanol to Oil Molar Ratio

The effect of the methanol-to-oil molar ratio was examined within the range of 1:3 to 1:12. Although the stoichiometric ratio for transesterification is 1:3, higher molar ratios are commonly employed to drive the reaction equilibrium toward ester formation. In this study, the highest biodiesel yield was obtained at a 1:6 molar ratio. Further increasing the methanol content beyond this point led to a reduction in yield, in agreement with the results reported by Topare et al. (2022).

This decline can be explained by two main factors: the reverse transesterification reaction, promoted by the solubility of glycerol in excess methanol, and challenges in separating the biodiesel and glycerol phases. Both factors negatively affect the yield and quality of the biodiesel. Similar trends have been documented by Sahar et al. (2018).

### 2.6.3 Effect of reaction temperature

At relatively low temperatures, the transesterification reaction proceeded slowly, resulting in incomplete conversion of the oil. Increasing the temperature accelerated the reaction, which improved biodiesel yield. However, temperatures near the methanol boiling point (64.7 °C) caused a decrease in yield, likely due to methanol evaporation and bubble formation that disrupted the reaction mixture. Therefore, 55 °C was chosen as the optimal temperature, providing efficient conversion while avoiding undesirable side reactions, in agreement with previous studies (Bilgin et al., 2015; Meng et al., 2008).

### 2.6.4 Effect of reaction time

The effect of reaction time was investigated by carrying out experiments for 30, 45, 60, and 90 minutes under the optimal conditions of 1.0% KOH, a methanol-to-oil ratio of 1:6, and a reaction temperature of 55 °C. At 90 minutes, the biodiesel yield increased progressively with time, reaching a maximum of 92%. Longer reaction times did not lead to a significant further increase, indicating that the reaction had essentially reached completion. Shorter durations produced incomplete conversion, while excessively long times are dissipating energy and could promote reverse reactions. Similar observations were reported by Eevera et al. (2009), where extending the reaction beyond 90 minutes did not improve conversion and in fact reduced yield. Consequently, 90 minutes was selected as the optimal reaction time for efficient biodiesel production.

The optimised transesterification conditions derived from these experiments are summarized in Table 2.4. Additionally, Table 2.5 presents the corresponding mass balance of the process, including the amounts of waste cooking oil used, the purified methyl esters obtained, the glycerol by-product, and the overall yield, confirming the effectiveness of the chosen reaction parameters.

**Table 2.4** Optimal reaction parameters (Medjahed et al.,2025)

| Parameter | Optimized Value |
|---|---|
| Catalyst Concentration | 1.0% (w/w KOH) |
| Methanol to Oil Ratio | 1:6 |
| Reaction Temperature | 55 °C |
| Reaction Time | 90 minutes |

**Table 2.5** The reactant, final products mass and yield of reaction (Medjahed et al.,2025)

| Parameter | Value |
|---|---|
| Waste cooking oil [g] | 200 |
| WCO Methyl Ester after washing [g] | 183 |
| Glycerol [g] | 130 |
| Yield [%] | 92 |

## 2.7 Blends preparation

At this stage of the experimental procedure, a range of biodiesel–diesel blends was formulated with different concentrations in order to evaluate the fuel characteristics. The blends (B5, B10, B20, B30, and B100) were prepared by mixing waste cooking oil (WCO) biodiesel with mineral diesel in specific volumetric proportions, according to the standard naming convention that indicates the biodiesel content in each blend. For example, B5 contained 5% biodiesel and 95% diesel, whereas B100 was composed entirely of biodiesel. Graduated cylinders are used to measure the required volumes, and then each blend was mixed thoroughly with a magnetic stirrer at room temperature to assure the fuel homogeneousness. Blends containing higher biodiesel volume were heated (up to 40 °C) to reduce viscosity differences and achieve a homogeneous mixture. The prepared blends are illustrated in Figure 2.8. Clean, airtight containers are used for storage until testing.


**Figure 2.8** Biodiesel-diesel blends

In the table 2.6, below a comprehensive list of instruments and equipment utilized during the experimental investigation on biodiesel production, indicating their technical specifications and specific purposes across the various stages of the research process. In addition to figures 2.9 – 2.12 of some of these equipments.

**Table 2.6** instruments and equipment utilized during our experimental study of the WCBIO production

| Phase / Parameter | Instrument / Equipment | Purpose |
|---|---|---|
| **Collection & Storage** | Plastic sealed bottles | Storage of collected WCO |
| | Cotton filter cloth | Removal of coarse impurities |
| | Stainless steel sieve (150–200 μm, 70–100 μm) | Filtration of solid particles |
| | Quartz layer (1 cm thick, $SiO_2$) | Fine purification/adsorption of impurities |
| **Pretreatment & Analysis** | TitroLine automatic titrator (potentiometric titration) | Acid value and FFA content determination |
| | Balance | Mass measurement of chemicals and catalysts |
| **Production (Transesterification)** | 300 mL flask, Erlenmeyer flask | Reaction vessels |
| | Hot plate with magnetic stirrer | Heating and agitation of reaction mixture |
| | Temperature sensor | Monitoring of reaction temperature |
| | Separating funnel | Phase separation of biodiesel and glycerol |
| | Centrifuge | Accelerated separation of phases |
| | Burette | Accurate liquid dispensing |
| **Blending** | Measuring cylinder | Preparation of biodiesel–diesel blends |
| | Mechanical stirrer | Homogeneous mixing of blends |

| Phase / Parameter | Instrument / Equipment | Purpose |
|---|---|---|
| **Characterization (ASTM Standards)** | Anton Paar DMA 35 density meter (ASTM D4052) | Density measurement |
| | Viscometer (ASTM D445) | Kinematic viscosity at 40 °C |
| | Potentiometric titration (ASTM D664) | Acid number and FFA content |
| | Cetane index method (ASTM D4737) | Cetane number |
| | Cooling bath (ASTM D2500, D97) | Cloud point and pour point |
| | Karl Fischer method (ASTM D2507) | Water content |
| | X-ray fluorescence analyzer (ASTM D4294) | Sulfur content |
| | Muffle furnace (ASTM D482) | Ash content |
| | Distillation apparatus (ASTM D6751) | Distillation temperature (T90) |
| | Bomb calorimeter | Lower heating value (LHV) |

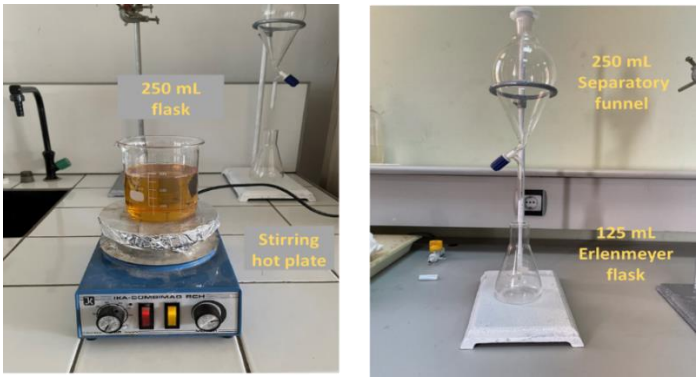


**Figure 2.9** some laboratory equipment used

**Figure 2.10** Bomb calorimeter

**Figure 2.11** viscosimeter RheolabQC

**Figure 2.12** Anton Paar DMA 35 density meter

## 2.8 Biodiesel characterisation

When using biodiesel, maintaining consistent quality is essential for achieving optimal engine performance. This requires careful evaluation of various fuel properties, such as density, viscosity, acid value, cloud and pour points, , ash content, distillation range, sediment, sulfur content, glycerol and water content, cetane number, and heating values. In this study (Medjahed et al.,2025), the produced biodiesel and its four blends were thoroughly characterised to ensure that they met the ASTM D6751 standards for all these critical parameters.

### 2.8.1 Fatty Acid Methyl Ester (FAME) Composition

The ester content composition of the produced biodiesel were determined following UNE-EN 14103:2011.The method is based on gas chromatography with flame ionization detection (GC-FID), using methyl nonadecanoate (C19) as an internal standard. Approximately 100 mg of biodiesel sample was dissolved in toluene with the internal standard and injected into a GC equipped with a Carbowax 20M capillary column. The total ester content and linolenic ester fraction were quantified from chromatographic peak areas and expressed as mass percentages, ensuring compliance with international biodiesel quality requirements. The analysis allowed identification and quantification of the main fatty acid methyl esters (FAME) present in the

biodiesel. Table 2.7 summarizes the relative proportions of saturated, monounsaturated, and polyunsaturated methyl esters, highlighting oleic, linoleic, and palmitic esters as the dominant components. The total ester content exceeded the minimum requirement of 90% (m/m), confirming the successful conversion of waste cooking oil into biodiesel of acceptable quality.

**Table 2.7** Fatty acid composition and corresponding methyl esters of waste cooking oil biodiesel.

| No. | Acid (GC label) | wt% | Methyl ester (name) | Methyl ester formula | Molecular weight ($g \cdot mol^{-1}$) |
|---|---|---|---|---|---|
| 1 | Palmitic acid ($C_{16:0}$) | 12.30 | Methyl palmitate | $C_{17}H_{34}O_2$ | 270.45496 |
| 2 | Stearic acid ($C_{18:0}$) | 4.00 | Methyl stearate | $C_{19}H_{38}O_2$ | 298.50872 |
| 3 | Oleic acid ($C_{18:1}$) | 27.50 | Methyl oleate | $C_{19}H_{36}O_2$ | 296.49284 |
| 4 | Linoleic acid ($C_{18:2}$) | 48.18 | Methyl linoleate | $C_{19}H_{34}O_2$ | 294.47696 |
| 5 | Linolenic acid ($C_{18:3}$) | 4.72 | Methyl linolenate | $C_{19}H_{32}O_2$ | 292.46108 |
| 6 | Arachidic acid ($C_{20:0}$) | 0.30 | Methyl arachidate | $C_{21}H_{42}O_2$ | 326.56248 |
| 7 | Gadoleic acid ($C_{20:1}$) | 0.43 | Methyl gadoleate | $C_{21}H_{40}O_2$ | 324.54660 |
| 8 | Eicosadienoic acid ($C_{20:2}$) | 0.40 | Methyl eicosadienoate | $C_{21}H_{38}O_2$ | 322.53072 |
| 9 | Behenic acid ($C_{22:0}$) | 0.61 | Methyl behenate | $C_{23}H_{46}O_2$ | 354.61624 |
| 10 | Erucic acid ($C_{22:1}$) | 0.50 | Methyl erucate | $C_{23}H_{44}O_2$ | 352.60036 |
| 11 | Lignoceric acid ($C_{24:0}$) | 0.41 | Methyl lignocerate | $C_{25}H_{50}O_2$ | 382.67000 |
| 12 | Nervonic acid ($C_{24:1}$) | 0.32 | Methyl nervonate | $C_{25}H_{48}O_2$ | 380.65412 |

### 2.8.2 Elemental composition

The elemental composition of the biodiesel was determined based on its FAME profile obtained using GC-FID. Gas chromatography is commonly employed for biodiesel analysis because of its high sensitivity in detecting minor components, enabling the quantification of methyl esters and identification of specific contaminants in alkyl esters. Each fatty acid methyl ester was treated in its free acid form (R–COOH), and its molecular formula was used to calculate the numbers of carbon, hydrogen, and oxygen atoms. The molecular weight of each ester was then calculated using the atomic weights of carbon (12.01 g/mol), hydrogen (1.008 g/mol), and oxygen (16.00 g/mol).The mass contributions of C, H, and O were then expressed as percentages relative to the total molecular weight. Finally, the weighted average across all esters, according to their relative abundance in the biodiesel, provided the overall elemental composition in Table 2.8. Nitrogen and sulfur are assumed negligible.

**Table 2.8** Elemental mass composition (mass %)

| **Element** | **Mass %** |
|---|---|
| Carbon (C) | 77.10 % |
| Hydrogen (H) | 11.98% |
| Oxygen (O) | 10.91% |

Based on the weighted fatty acid methyl ester (FAME) profile, the average molecular formula was estimated as $\mathbf{C_{18.82}H_{34.85}O_{2.00}}$, corresponding to an average molecular weight of about **293.2 g·mol$^{-1}$**.

### 2.8.3 Physicochemical characterization of biodiesel

The physicochemical characteristics of the synthesized biodiesel were evaluated to determine its compliance with ASTM D6751, the American Society for Testing and Materials standard for B100 biodiesel used as a blending component in middle distillate fuels. In this study, key parameters such as kinematic viscosity, density, acid value, ash content, sulfur content, and water content were measured, with the results summarized in Table 2.9. The properties of the produced biodiesel were then compared with the established ASTM biodiesel specifications.

**Table 2.9** Physicochemical properties of WCO-based biodiesel compared to ASTM D6751 standard specifications (Medjahed et al.,2025)

| Property | Unit | Method | Biodiesel from WCO | Biodiesel standard ASTM D6751 |
|---|---|---|---|---|
| **Density** | / | ASTM D 4052 | 0.8903 | ≤0.9000 |
| **Kinematic Viscosity at 40°C** | mm²/s | ASTM D445 | 4.88 | 1.9–6.0 |
| **Acid number** | mg KOH/g | ASTM D664 | <0.05 | ≤0.80 |
| **Cetane number** | / | ASTM D 4737 | 53.5 | ≥47 |
| **Cloud point** | °C | ASTM D 2500 | 5 | -3 to 12 |
| **Poor point** | °C | ASTM D97 | 0 | -15 to 10 |
| **Water content** | %v/v | ASTM D2507 | < 0.01 | ≤ 0.05 |
| **Sulfur content** | mass % | ASTM D4294 | < 0.01 | ≤0.01 |
| **Ash content** | mass % | ASTM D482 | Trace | ≤0.05 |
| **Distillation temperature T90** | °C | ASTM D 6751 | 351 | ≤360 |

The results obtained from this investigation were within the allowable limits prescribed by ASTM D6751. The biodiesel satisfied the density requirements specified by the standard, indicating its suitability for use in diesel engine fuel systems. Density plays a crucial role in determining fuel injection characteristics, spray formation, and air–fuel mixing in compression ignition engines (Tesfa, Mishra, Gu, and Powles, 2010). Excessively dense fuels can adversely affect fuel pumps and injectors, potentially resulting in incomplete combustion.

Kinematic viscosity is also a key parameter influencing biodiesel performance. The viscosity values recorded in this study fell within the recommended range, suggesting that the biodiesel would function effectively in standard diesel engines. Variations outside the optimal viscosity range can lead to engine-related issues: elevated viscosity may cause injector and pump damage, filter blockage, poor atomization, and higher emissions due to incomplete combustion, whereas low viscosity can reduce lubrication of injection system components, leading to increased wear, fuel leakage, and subsequent power loss (Ayetor et al., 2015).

After the transesterification and purification processes, the acid value of the biodiesel was lowered to less than 0.05 mg KOH/g, complying with ASTM D6751 requirements. Maintaining such a low acid value is important for reducing corrosion and preventing injector fouling associated with free fatty acids, as reported by Suzihaque, Alwi, Ibrahim, Abdullah, and Haron (2022).

The ash and sulfur contents were also found to be below their respective maximum allowable limits, suggesting a reduced likelihood of particulate emissions and engine component degradation. Additionally, the measured water content remained within the standard specification, which is critical for ensuring stable ignition and efficient combustion performance. Furthermore cloud and pour points serve as key parameters for evaluating the low-temperature flow properties of biodiesel. They have a direct impact on the performance of the fuel delivery system. A lower cloud point indicates superior cold-flow characteristics, enabling the fuel to function effectively at reduced ambient temperatures. This property is generally linked to enhanced fuel quality and greater applicability in cold-weather environments. In the present study, the biodiesel demonstrated a cloud point of 5 °C, which could restrict its use in extremely cold conditions.

The results demonstrate that waste cooking oil can be effectively converted into biodiesel meeting the required fuel quality standards under the applied experimental conditions. However, additional investigations focusing on long-term storage behaviour and practical engine operation are necessary to fully assess the fuel's durability and overall performance.

## 2.9 Blends characterisation

The fuel characteristics of biodiesel produced from waste cooking oil (WCO) via base-catalysed transesterification (B100), along with its blends with petroleum diesel (B5, B10, B20, and B30), were evaluated using ASTM standard testing procedures. The measured properties are presented in Table 2.10. The results indicate that the biodiesel achieved a cetane number of 53.5, which is higher than that of conventional diesel fuel, reflecting improved ignition quality. A higher cetane number promotes reduced ignition delay, enhanced combustion efficiency, and lower engine noise levels (Heywood, 1988).Minor variations in fuel density were observed; however, these differences remained within acceptable specification limits.

Fuel distillation characteristics play a critical role in determining evaporation behaviour, cold-start capability, susceptibility to vapour lock and flooding, ignition performance, emission profiles, and overall efficiency. A wide distillation range indicates the presence of fuel components

with varying boiling points, which can influence the formation of a uniform air–fuel mixture which is an important requirement for efficient combustion. In this investigation, the distillation ranges of the biodiesel blends were found to be comparable to those of conventional diesel fuel reported by Henein et al. (1985), suggesting satisfactory fuel quality. Nevertheless, biodiesel contains certain high-boiling compounds (above 360 °C) that may lead to increased particulate matter emissions during combustion, as reported by Chen et al. (2023) based on engine testing. The use of catalytic converters can help alleviate this issue and improve the environmental performance of biodiesel. Furthermore, all fuel blends exhibited low sulfur content, which contributes to reduced sulfur dioxide emissions and lower particulate matter formation, thereby decreasing overall atmospheric pollution.

Fuel viscosity plays a key role in engine performance. Figure 2.14 illustrates the temperature-dependent viscosity behaviour of different biodiesel-diesel blends. For all blends, viscosity decreases as temperature increases. Pure biodiesel (B100) shows the highest viscosity; however, a substantial reduction is observed at higher temperatures, reflecting enhanced flow properties. The results further indicate that incorporating diesel into biodiesel effectively lowers viscosity. A consistent downward trend is evident as the blend ratio shifts from B100 to B5, with viscosity progressively approaching that of conventional diesel fuel. This demonstrates that blend composition can be optimized to achieve viscosity levels compatible with existing engine and fuel system requirements while complying with established fuel standards.

As shown in Table 2.10 and figure 2.13, fuel density increased with a higher proportion of biodiesel in the blends. This trend is mainly associated with the higher molecular weight of biodiesel compared to conventional diesel, which leads to increases in density, viscosity, and pour point. In contrast, the heating value and cetane number showed a decreasing trend with increasing biodiesel content. Nevertheless, all fuel properties remained within the limits specified by ASTM D7467 and were consistent with findings reported in the literature (Saxena, Jawale, and Joshipura, 2013; Lahane and Subramanian, 2015). The heating value of the produced biodiesel was approximately 5% lower than that of conventional diesel fuel. An increase in heating value was observed as the proportion of diesel in the blend increased, as shown in Figure 2.13. The heating value represents the amount of energy released per unit mass of fuel during combustion. Due to its relatively lower energy content, biodiesel may result in reduced power output. Consequently, a higher fuel quantity is required to achieve comparable power levels. Therefore, for applications demanding sustained high performance, the use of neat diesel

or biodiesel blends with higher diesel content is preferable to ensure stable and efficient engine operation, in agreement with the observations of Bari et al. (2020).

**Table 2.10** Blends properties compared to conventional diesel (Medjahed et al.,2025)

| | **unit** | **Method** | **B5** | **B10** | **B20** | **B30** | **B100** | **Diesel** |
|---|---|---|---|---|---|---|---|---|
| **Density at 15°C** | - | ASTM D 4052 | 0.8231 | 0.8291 | 0.8333 | 0.845 | 0.8903 | 0.822 |
| **Viscosity at 40 °C** | mPa/s | / | 1.47 | 1.57 | 1.70 | 2.04 | 4.32 | 1.356 |
| **Distillation intial point** | °C | ASTM D 86 | 170 | 175 | 180 | 175 | 220 | 180–340 °C |
| **Distillation 10%** | | | 200 | 205 | 208 | 204 | 330 | |
| **Distillation 50%** | | | 263 | 272 | 280 | 299 | 340 | |
| **Distillation 90%** | | | 343 | 344 | 342 | 345 | 351 | |
| **Distillation final point** | | | 370 | 368 | 360 | 360 | 369 | |
| **Cetane index** | - | ASTM D 4737 | 55.6 | 55.3 | 55.5 | 54.5 | 53.5 | 47 - 50 |
| **Total Acid Number** | mg KOH/g | ASTM D 664 | <0.05 | <0.05 | <0.05 | <0.05 | <0.05 | - |
| **Poor point** | °C | ASTM D97 | -15 | -15 | -12 | -9 | 0 | -33 to -15 |
| **Cloud Point** | °C | ASTM D2500 | -4 | -4 | 0 | -1 | +5 | ≤ +5 |
| **LHV** | MJ/Kg | / | 43.055 | 43.011 | 42.923 | 42.831 | 42.279 | 45.20 |
| **HHV** | MJ/kg | / | 45.933 | 45.877 | 45.764 | 45.647 | 44.950 | 48.22 |
| **water** | %v/v | / | <0.01 | <0.01 | <0.01 | <0.01 | <0.01 | <0.05 |
| **sulfur** | mass % | / | <0.01 | <0.01 | <0.01 | <0.01 | <0.01 | ≤ 2 |

The elevated cloud and pour points observed adversely affect cold-start performance and may limit the applicability of biodiesel blends with high biodiesel content, such as B30 and B100. This observation is consistent with the findings reported by Yaakob, Mohammad, Alherbawi, Alam, and Sopian (2013).

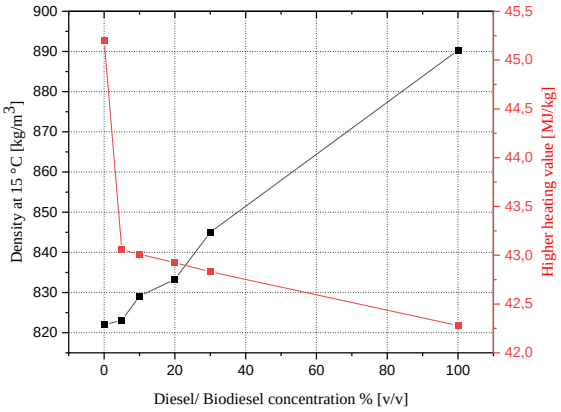


**Figure 2.13** Density and higher heating value for biodiesel and diesel mixtures

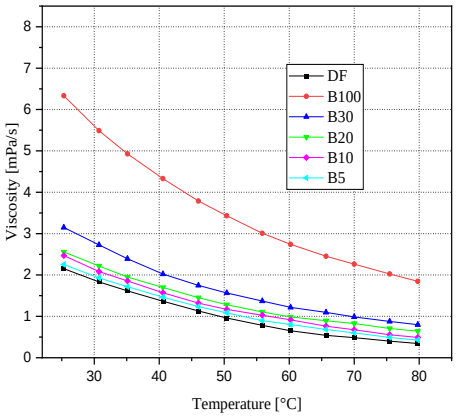


**Figure 2.14** Variation of viscosity the blends on fonction of temperature.

## 2.10 Conclusion

This chapter has demonstrated the waste cooking oil potential to be converted into a high-quality biodiesel when upstream handling and process optimisation are carefully addressed. The study underlines that the technical feasibility of WCO valorisation depends as much on collection, storage, and pretreatment practices as on the transesterification step itself.

- Improved collection and storage practices such as using sealed, opaque containers kept in cool, dark conditions, substantially increased the volume of feedstock that is suitable for processing and improving overall cost-effectiveness.
- Preliminary characterisation of WCO informed the choice of pretreatment and reaction route, and helped prevent common problems such as soap formation and catalyst deactivation.
- Transesterification was optimized with the dual aims of achieving high yield and keeping the process operationally simple and affordable. The reaction settings were selected (molar ratio of 6:1, 1% KOH catalyst, and 60 °C reaction temperature ) to increase yield

to be approximately 92% biodiesel. Downstream purification (washing and centrifugation) further improved fuel stability and removed residual contaminants.

- Quality assessment showed that the recovered biodiesel met the principal requirements of recognized international standards (ASTM D6751 and EN 14214) for the measured properties, confirming its suitability for blending and engine use.
- To improve key fuel properties and provides a practical approach for immediate use, we managed blending the produced WCBIO with conventional diesel. By combining the low sulfur and high oxygen content of biodiesel with the energy density and cold-flow advantages of petroleum diesel, the resulting fuel is well suited for existing engines without major modifications.

In conclusion, the chapter provides a complete and pragmatic account of WCO-to-biodiesel production under local conditions. These findings supply the experimental basis for the next stages of this research where combustion dynamics, performance metrics, and emissions are investigated.

# 3 Chapter 3

# Engine Testing of Biodiesel Blends

This chapter illustrates the experimental protocol and test-bench procedures used to evaluate the combustion behaviour, performance and emissions of biodiesel-diesel blends. Building on the production and quality assessment described in Chapter 2, the work reported here aims to quantify how progressively higher proportions of WCO-derived biodiesel influence in-cylinder combustion, engine output and exhaust pollutants in the laboratory environment.

Tests were performed on a compression-ignition engine test bench using five fuels: conventional petroleum diesel (baseline) and four biodiesel blends (B5, B10, B20 and B30). The test matrix was designed to capture representative operating conditions so that results are relevant for practical engine use; measurements were therefore taken across a range of engine loads and steady speeds typical of the target application. For each test point, key performance indicators (brake power, torque, specific fuel consumption), exhaust gases temperature and pollutant emissions (CO, $NO_x$).

Relevant, fuel properties reported in Chapter 2 (density, viscosity, calorific value, cetane index) were used to interpret performance differences and to normalise results.

By combining detailed combustion diagnostics with standard performance and emission metrics, this chapter provides the empirical basis for understanding the practical implications of using WCO-based biodiesel blends in compression-ignition engines. The experimental findings will be used in Chapter 4 to validate and inform the computational models and to support the broader assessment of biodiesel as a sustainable alternative to conventional fuels.

## 3.1 Experimental Test Bench

The experimental investigation was conducted on an academic test bench designed to evaluate the performance and pollutant emissions of diesel engines operating with biodiesel blends.
A schematic representation of the bench is provided in Figure 3.1, showing the arrangement of the engine, dynamometer, fuel system, exhaust analyser, and instrumentation.

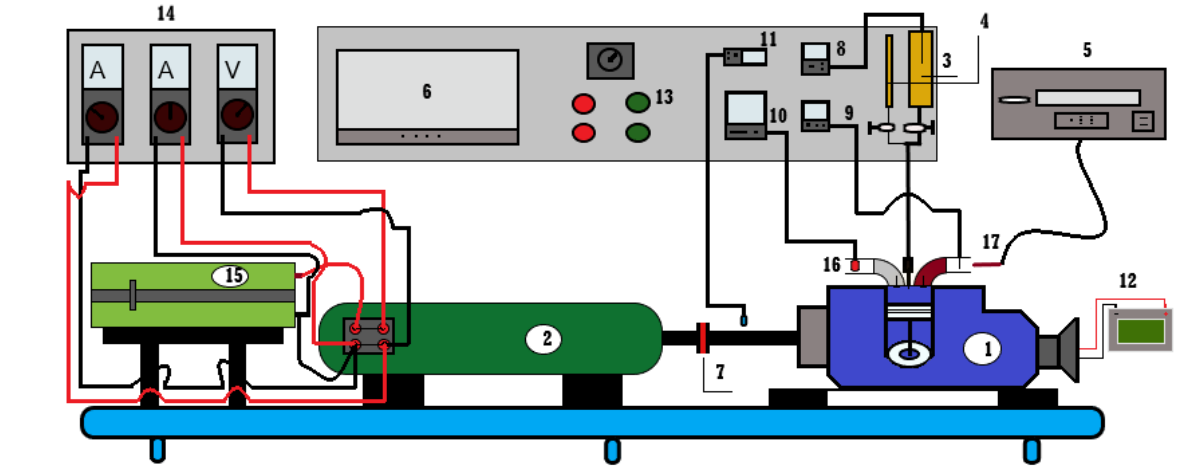


**Figure 3.1** Schematic representation of the diesel engine test bench exploited for testing biodiesel.
The setup includes the Deutz Z-MWM D302-1 single-cylinder diesel engine (1), load brake dynamometer (2), fuel supply system with tank (3) and burette for consumption me *measurement (4), exhaust gas analyzer (5), data acquisition computer (6), coupling (7), fuel and exhaust temperature sensors (8, 9), airflow meter (10), tachometer ( engine speed ) (11), starting battery (12), control system (13), electrical measurement unit (14), rheostat load (15), and intake (16) and exhaust (17) manifolds.*

The test rig consists of a single-cylinder diesel engine coupled to a dynamometer, with auxiliary systems for fuel supply, air intake, exhaust analysis, cooling, and power supply.

### 3.1.1 Test Engine

The engine used is a Deutz Z-MWM D302-1**,** a single-cylinder, four-stroke, direct-injection, air-cooled diesel engine manufactured by Motorenwerke Mannheim AG (MWM, Germany) (Figure 0.2). The engine delivers a maximum power of 8.5 kW (11.6 HP) at 3000 rpm, with a compression ratio of 17.5:1. The bore and stroke are 95 mm × 105 mm, giving a displacement of 744 $cm^3$**.** The injection system employs Bosch, Condiesel, or Delphy injectors with pressures ranging from 180 to 220 bar. The robust design, direct injection system, and moderate power output make it well suited for experimental biodiesel evaluation.
The principal technical specifications of the engine, including geometry, fuel injection characteristics, operating parameters, and valve timing, are summarized in Table 3.1.

**Figure 3.2** Deutz Z-MWM D302-1

**Table 3.1** Technical specifications of the Deutz Z-MWM D302-1

| Category | Parameter | Unit | Value |
|---|---|---|---|
| **General Information** | Model | — | D302-1 |
| | Number of cylinders | — | 1 |
| | Combustion system | — | Direct injection |
| | Cooling system | — | Air-cooled |
| | Rotation direction | — | Counter-clock-wise |
| | Fuel type | — | Diesel 2 |
| | Injection system | — | Direct injection |
| | Injection mode | — | Profile |
| **Engine Geometry** | Displacement | $cm^3$ | 744 |
| | Bore × Stroke | mm | 95 × 105 |
| | Compression ratio | — | 17.5:1 |
| | Valve clearance | mm | 0.2 |
| **Fuel Injection Characteris-tics** | Injection pressure | bar | Bosch: 180 ± 5; Condiesel: 220 ± 5; Delphy: 190 ± 8 |
| | Start of injection | °CA | 8° before TDC |
| | Injection duration | °CA | 20 |
| | Injection hole diameter | mm | 0.259 |
| | Number of nozzles | — | 4 |
| | Fuel temperature | K | 344 |
| **PerformanceData (Full Load)** | Maximum power | kW (HP) | 8.5 (11.6) |

| Category | Parameter | Unit | Value |
|---|---|---|---|
| | Maximum speed | rpm | 3000 |
| | Idle speed | rpm | 750–800 |
| | Ignition pressure | bar | 85 |
| | Fuel consumption | $dm^3/h$ | 3.54 |
| | Lubricating oil consumption | $cm^3/h$ | 10–20 |
| | Cooling air flow | $m^3/h$ | 420 |
| **Operating Temperatures** | Max. lubricating oil temperature | °C | 120 |
| | Max. exhaust manifold temperature | °C | 550 |
| **Filling Quantities** | Fuel tank capacity | $dm^3$ | 16 |
| | Lubricating oil capacity | $dm^3$ | 2.75 |
| | Net weight | kg | 165 |
| **Valve Timing** | Intake opening | °CA | 30° bBDC |
| | Intake closing | °CA | 0° aTDC |
| | Exhaust closing | °CA | 30° aBDC |
| | Admissible tolerance | °CA | ±3 |

### 3.1.2 Dynamometer and Coupling

Dynamometer system coupled to the engine shaft is employed to apply controlled loads during testing. As illustrated in the simplified electrical diagram (Figure 3.3), the dynamometer operates on the principle of a DC generator with shunt excitation, where the field winding is connected in parallel with the armature circuit carrying current *I*.

In this configuration, the field current is proportional to the terminal voltage, which maintains a stable magnetic field during operation. The electrical power generated by the armature is dissipated through a variable rheostat, allowing fine control of the load current and, consequently, the braking torque applied to the engine.

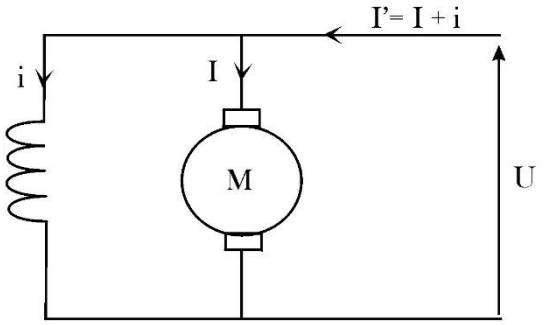


**Figure 3.3** Simplified electrical schematic of the dynamometer operating principle: the configuration of the DC generator with shunt excitation, where (i) the field current and (I) armature current, (I′ = I + i) the total current, (U) applied voltage

A precision coupling between the engine and the load machine ensured correct alignment, absorbed vibrations, and avoided resonance effects. Torque was determined from the electrical power absorbed by the generator, while brake power was calculated from torque and engine speed.

### 3.1.3 Starting and Power Supply

The test bench was equipped with a 12 V DC electrical system powered by a 75 Ah automotive battery for starting the engine. A medium-voltage 220 V AC line supplied the computing unit, sensors, and lighting systems. Indicators were installed to monitor power circuit status.

### 3.1.4 Air Intake System

The intake system was fitted with air filter connected to the manifold via a specially designed adapter. This ensured clean air supply, preventing dust and particles from entering the combustion chamber. An anemometer was installed for airflow measurement.

### 3.1.5 Fuel Supply and Measurement

A dual fuel supply arrangement was used to allow switching between diesel and biodiesel blends. Fuel consumption was measured using a burette system with a graduated scale and stopwatch method as illustrated in the Figure 3.4, allowing precise determination of volumetric consumption. The blends (B10, B20, B30, B100) were prepared by volume and stirred for homogeneity prior to testing.

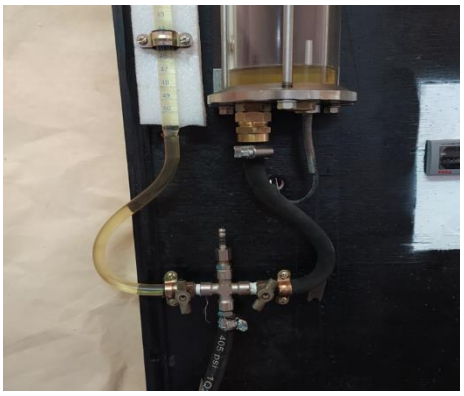

**Figure 3.4** Fuel supply system

### 3.1.6 Exhaust Gas Analysis

A gas analyser (HL 860 Exhaust gas analyser) measured the exhaust gas composition of O2, CO, CO2 and nitrogen oxides emissions. The analyser was connected directly to the exhaust manifold via sampling lines. Exhaust gas temperature was measured with thermocouples installed at the exhaust outlet.

### 3.1.7 Instrumentation and Control

The test bench was equipped with standard instrumentation to ensure accurate measurement of engine performance and emissions. Engine speed was monitored by a tachometer, while torque was determined through a load cell integrated into the dynamometer. Thermocouples were installed to record both fuel and exhaust gas temperatures. Airflow was determined using an anemometer. A real-time monitoring, recording, and subsequent processing of the experimental data was done using computer-based data acquisition system.

All the equipment were calibrated in agreement to the manufacturer's terms, before starting the experiments.

## 3.2 Experimental Protocol

The experimental operations was done on the test bench described in Section 3.1. The objective was to assess the performance and emissions of the Deutz Z-MWM D302-1 engine operating with commercial diesel and biodiesel blends derived from waste cooking oil (WCO).

### 3.2.1 Fuels

The fuels produced from waste cooking oil, along with the prepared diesel–biodiesel blends discussed in Chapter 2, were tested using the engine test bench. The reference diesel fuel was obtained from a local filling station in Oran, while the biodiesel blends were prepared volumetrically at concentrations of 5%, 10%, 20% and 30% , denoted as B5, B10, B20 and B30 respectively.The mineral diesel fuel was employed as the reference fuel to enable comparison of engine performance. Table 3.2 summarizes the main physical properties that impact the combustion behaviour of the fuels and, consequently, the engine performance.

**Table 3.2** Blends properties compared to conventional diesel properties.

| | unit | Method | B5 | B10 | B20 | B30 | B100 | Diesel |
|---|---|---|---|---|---|---|---|---|
| **Density at 15°C** | - | ASTM D 4052 | 0.8231 | 0.8291 | 0.8333 | 0.845 | 0.8903 | 0.822 |
| **Viscosity at 40 °C** | mPa/s | / | 1.47 | 1.57 | 1.70 | 2.04 | 4.32 | 1.356 |
| **Cetane Number** | - | ASTM D 4737 | 55.6 | 55.3 | 55.5 | 54.5 | 53.5 | 47 - 50 |
| **LHV** | MJ/Kg | / | 43.055 | 43.011 | 42.923 | 42.831 | 42.279 | 45.20 |

The test program was structured into three groups of experiments. The first group consisted of air mapping at no load (0% load) over a range of engine speeds, in order to characterize the airflow behaviour of the engine. The second group involved the load-speed matrix tests with commercial diesel, used as the baseline reference. The third group applied the same load-speed matrix to the biodiesel blends, allowing direct comparison with the diesel baseline.

For the load-speed matrix, four load levels were considered: 25%, 50%, 75% and 100% of full load. At each load level, the engine was operated at four speeds: 1500, 1800, 2000 and 2300 rpm. This resulted in a comprehensive set of operating points for performance and emissions evaluation.

At every test point, the following parameters were measured: brake torque, brake power (BP), brake specific fuel consumption (BSFC), exhaust gas temperature, and gaseous emissions of carbon monoxide (CO) and nitrogen oxides.

### 3.2.2 Fuel-switching procedure

To prevent cross-contamination between fuels, a strict switching protocol was applied. Baseline runs were first conducted using diesel until steady-state operating conditions were reached, after which measurements were taken across the full load-speed matrix. Before introducing a biodiesel blend, the engine was run on diesel until the remaining fuel from the previous test had been consumed. The supply was then switched to the biodiesel blend, and the engine was operated for approximately five minutes to purge residual diesel from the fuel line. Data acquisition then commenced under the same test conditions as with diesel. After completing the measurements for each biodiesel blend, the engine was again switched to diesel and run for sufficient time to flush the fuel line before the next blend was introduced.

### 3.2.3 Repetition and validation

All experimental points were repeated to ensure repeatability of the results. The mean values were used in the analysis, while clear anomalies were identified and discarded after verification. This approach ensured reliable comparison between the baseline diesel and biodiesel blends under all tested operating conditions.

### 3.2.4 Uncertainty and Limitations of Measurements

All experimental measurements are subject to a degree of uncertainty arising from both instrumentation limits and operating conditions.

During engine testing, measurement errors are inevitable and may arise from either systematic or random sources. Systematic errors generally originate from instrumental limits or calibration drift and can often be minimized through regular calibration and proper maintenance of the measurement devices. Random errors, by contrast, are caused by human factors or external disturbances such as temperature fluctuations or vibration, and they are usually evaluated through statistical analysis.

Manufacturers typically perform accuracy tests on their instruments to determine the precision limits and provide the corresponding uncertainty margins in their technical documentation. The uncertainties associated with the different measuring instruments used in the present experimental setup are summarized in Table 3.3.

**Table 3.3** Measurement uncertainties of the instruments used in the engine test bench.

| Parameter | Uncertainty |
|---|---|
| Engine torque (T) | ±0.1 N·m |
| Engine speed | ±3 rpm |
| Intake air flow rate | ±1% of the measured value |
| Fuel flow rate | ±0.5% of the measured value |
| Exhaust gas temperature | ±1.6 °C |
| Ambient air temperature | ±0.2 °C |
| Ambient relative humidity | ±2% |
| Nitrogen oxide emissions ($NO_x$) | ±100 ppm |
| CO concentration in exhaust gases | ±50 ppm |

In engine performance experiments, several parameters such as torque, engine speed, fuel consumption, and exhaust temperature are measured to evaluate the brake power, brake specific fuel consumption (BSFC. Each of these measured quantities carries an inherent uncertainty, which propagates into the final calculated parameters. To accurately quantify this effect, the Law of Propagation of Uncertainty (LPU) is applied, expressed by the following relation (Rishi, 2024):

According to this law, when a result F depends on several independent measured variables $x_1, x_2, x_3$, ...each with its own standard uncertainty, the combined uncertainty of F can be estimated using the following relation:

$$u(F) = \sqrt{\left(\frac{\partial F}{\partial x_1}u(x_1)\right)^2 + \left(\frac{\partial F}{\partial x_2}u(x_2)\right)^2 + \ldots + \left(\frac{\partial F}{\partial x_n}u(x_n)\right)^2} \quad \ldots\ldots\ldots\ldots(3.1)$$

where:

- *u(F)* is the combined standard uncertainty of the function *F*,
- $u(x_i)$is the standard uncertainty of the variable $x_i$ and
- $\frac{\partial F}{\partial x_i}$ represents the sensitivity coefficient, indicating how sensitive *F* is to changes in $x_i$

The analysis of the engine tests focused on brake power and brake specific fuel consumption (BSFC). The calculation methods for each parameter are summarized below,

### 3.2.4.1 Brake Power (BP)

Brake power is the effective mechanical power available at the engine shaft. In the present test bench configuration, where the engine is coupled to a DC generator dynamometer, the brake power is equal to the absorbed power (Pa) of the generator.

Brake power was obtained from the measured torque and engine speed according to:

$$BP = Pa = \omega \times T = \frac{2\pi N}{60} \times T \text{..... (3.2)}$$

Where

T = brake torque (N·m)

Pa= mechanical power absorbed by the generator (W)

ω = angular velocity (rad/s)

N = engine speed (rpm)

This represents the effective mechanical power available at the engine shaft.

And ,

The combined uncertainty of BP is given by: $U(BP) = \sqrt{[(\omega \times U(T))^2 + (T \times U(\omega))^2]}$

The relative uncertainty in brake power is: $Urel(BP) = \sqrt{[(\omega \times U(T))^2 + (T \times U(\omega))^2]} / (T \times \omega)$

### 3.2.4.2 Brake Specific Fuel Consumption (BSFC)

BSFC was determined as the ratio of fuel mass flow rate to brake power:

$$BSFC = \frac{\dot{m}_f}{BP} \text{ .....(03.3)}$$

Where $\dot{m}_f$ is the fuel mass flow rate (kg/s), obtained from volumetric fuel consumption and density. BP is the brake power (W)

And,

The combined uncertainty in BSFC is expressed as:

$$U(BSFC) = \sqrt{[(U(\dot{m}_f)/\dot{m}_f)^2 + (U(BP)/BP)^2]} \times BSFC$$

The relative uncertainty is therefore: $Urel(BSFC) = \sqrt{[(U(\dot{m}_f)/\dot{m}_f)^2 + (U(BP/BP)^2]}$

**Table 3.4** Relative uncertainties of the calculated parameters based on measured values

| Parameter | Relative Uncertainty Expression | Uncertainty Range (%) |
|---|---|---|
| Brake Power (BP) | $\sqrt{[(50\pi\times0.1)^2 + (T\times0.1\pi)^2]} / (50\pi\times T)$ | 0.4 – 1.9% |
| Brake Specific Fuel Consumption (BSFC) | $\sqrt{[(0.005)^2 + (U(BP)/BP)^2]}$ | 0.6 – 2% |

## 3.3 Results and discussions

### 3.3.1 First group of experiments: Air-Fuel Ratio Mapping at No Load

A first series of experiments was conducted at no load (0% load) with the aim of establishing the engine air-fuel ratio (richness) map**.** Such a mapping serves as a reference tool for regulating engine operation, since in automotive applications similar calibration maps are stored in the engine control unit (ECU). Optimizing or reprogramming these maps is a key method to improve engine performance and emissions behaviour.

In this study, the richness measurements were performed at different engine speeds ranging from 800 to 2600 rpm**,** under ambient temperature conditions and with no external load applied to the engine. The results obtained provide the baseline richness characteristics of the engine across its operating range, and serve as input for analysing the impact of biodiesel blends in subsequent tests.

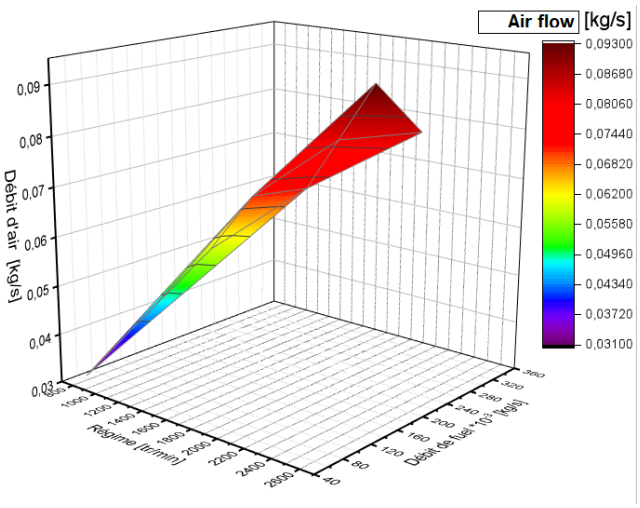


**Figure 3.5** the variation of the air mass flow rate as a function of engine speed and fuel mass flow under no-load conditions.

The results show a nearly linear increase in air flow rate with engine speed. At low speeds (≈1000 rpm), the air flow rate remains close to 0.03-0.04 kg/s, while at higher speeds (≈2500 rpm) the flow rate exceeds 0.08 kg/s, representing more than a threefold increase. From a thermodynamic perspective, this behaviour is expected, since the volumetric air intake per cycle increases proportionally with engine speed, while the intake system ensures nearly constant volumetric efficiency under no-load conditions. The absence of external load means that the fuel injection quantity is relatively small, which explains the lean mixture formation observed

at low and medium speeds. At higher speeds, although the mixture remains globally lean, the relative increase in injected fuel contributes to a progressive enrichment of the air–fuel ratio.

### 3.3.2 Second group of experiments

At 25% load, the variations of brake power, torque and brake specific fuel consumption (BSFC) with engine speed are shown in figure 3.6

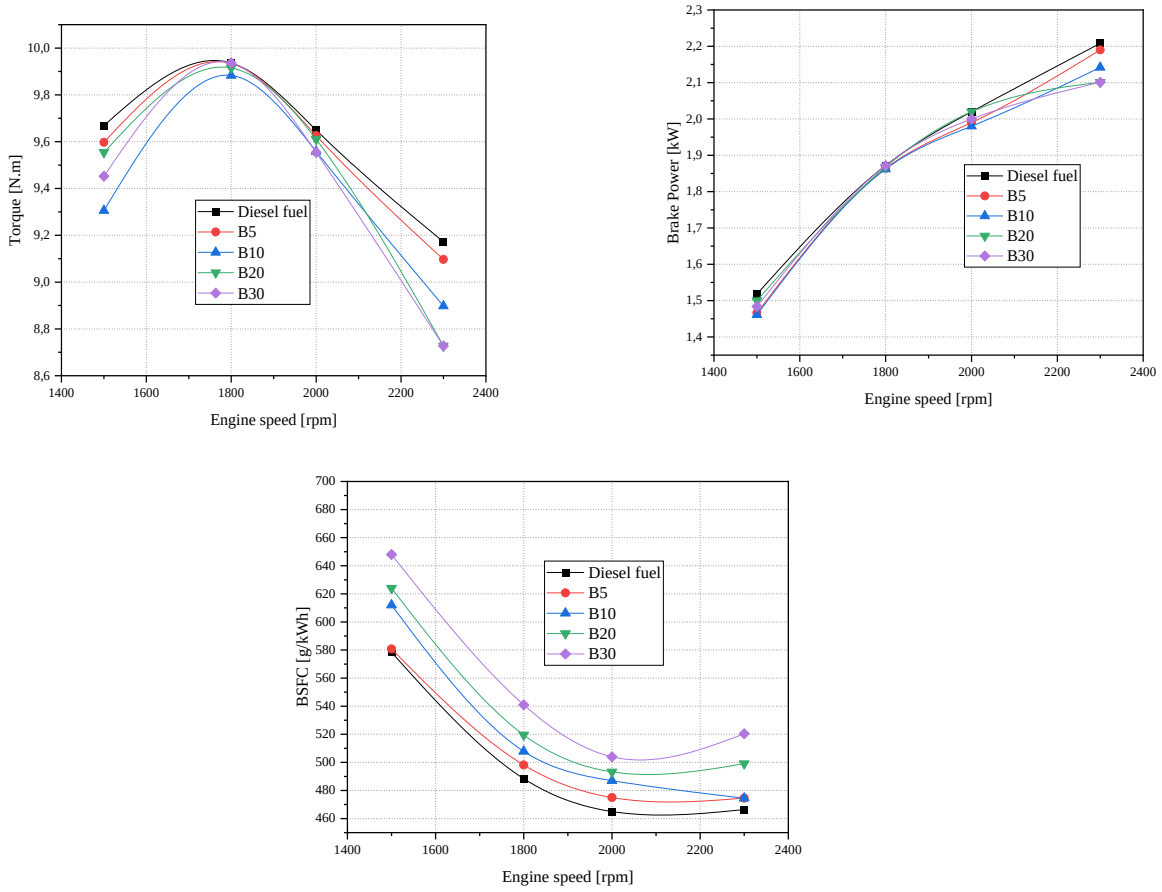


**Figure 3.6** Engine Performance with engine speed under 25% load conditions for diesel and biodiesel blends

Torque as shown in figure 3.6 rose with increasing speed, peaking around 1700–1900 rpm before declining at higher speeds. This trend was observed for both diesel and biodiesel blends, reflecting the typical torque curve of a compression ignition engine (Heywood, 2018).This profile reflects the balance between improved combustion phasing at mid-range speeds and rising mechanical and pumping losses beyond 2000 rpm. Biodiesel blends delivered slightly lower torque than diesel, with the difference more visible beyond 2000 rpm. Primarily due to their lower lower heating value (LHV), which limits the energy released per cycle under identical fuelling conditions.

Brake power trend in figure 3.6 increased steadily with engine speed. This continuous rise occurred despite the decline in torque beyond 2000 rpm, due to the strong dependence of brake power on rotational speed as the brake power of an engine is directly proportional to torque and engine speed (Habibullah et al., 2014)

The absolute differences between fuels remained modest at this low load, but diesel consistently provided higher output. This is linked to its superior LHV and more favourable volatility, which support more efficient combustion compared to biodiesel blends.

For all fuels, BSFC decreased with increasing engine speed up to around 2000 rpms. As speed increased, BSFC decreased and stabilized, consistent with improved combustion efficiency at higher air-fuel throughput which is consistent with Heywood (2018, Chapter 2.15) findings. Biodiesel blends exhibited consistently higher BSFC than diesel across the speed range. This is due to the combined effects of their higher density and lower heating value, which require a greater mass of fuel to achieve the same brake power output (Bhuiya et al., 2019; Qi et al., 2009).

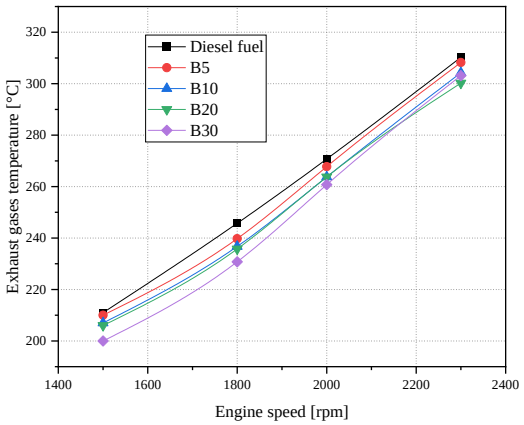


**Figure 3.7** EGT variations with engine speed at 25 % load

At 25% load, exhaust gas temperature increased monotonically with engine speed (Figure 3.7).The trend reflects the higher rate of combustion events and greater cumulative heat release as engine cycles accelerate. Diesel consistently produced slightly higher EGT than biodiesel blends which is not the expected trend from litterature (Cihan, 2021;Agarwal et al., 2008)

This behaviour can be explained by the lower calorific value of biodiesel, which releases less heat per unit mass of fuel. In addition, at low load, the in-cylinder temperature and pressure are relatively low, leading to slower evaporation and less efficient air–fuel mixing for biodiesel due

to its higher viscosity. As a result, part of the combustion energy is consumed in fuel vaporization rather than raising the gas temperature, which reduces the overall exhaust temperature.

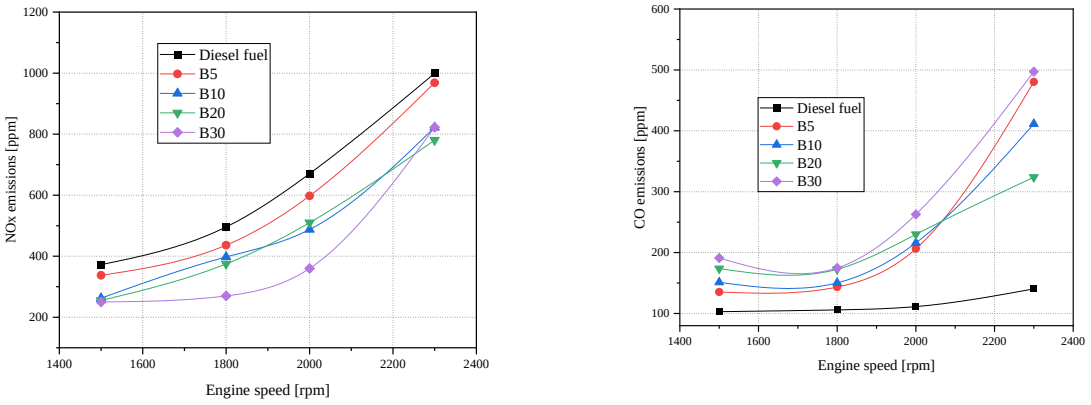


(a) (b)

**Figure 03.8** harmful emissions variations with engine speed for 25% load

At 25% load Figure 3.8.a illustrates the Nox emissions evolution with engine speed,it increased progressively with engine speed. This trend reflects the direct dependence of thermal NOx formation on in-cylinder temperature and residence time. As speed rises, the higher frequency of combustion events and greater cumulative heat release elevate the bulk gas temperature, favoring the Zeldovich mechanism of NOx formation

In diesel engines, the majority of nitrogen oxides (NOx) are produced through the thermal pathway, which means their formation primarily depends on the combustion temperature and the availability of oxygen in the combustion gases. Thermal NO is generated from the dissociation of atmospheric nitrogen ($N_2$) in the presence of oxygen and reactive oxygen radicals such as –O and –OH.

The most widely used model to describe thermal NO formation is the Zeldovich mechanism**,** represented by the following reactions (Maroa & Inambao, 2020):

$$\begin{aligned} N_2 + O &\longleftrightarrow NO + N \\ N + O_2 &\longleftrightarrow NO + O \\ N + OH &\longleftrightarrow NO + H \end{aligned} \qquad \text{.....(3.4)}$$

This mechanism highlights that NOx formation is highly sensitive to the peak flame temperature and the oxygen concentration in the combustion zone.

In this case, diesel consistently produced higher NOx emissions compared to biodiesel blends. The difference arises from biodiesel's intrinsic oxygen content, which promotes more complete

combustion but simultaneously lowers peak flame temperatures, thereby suppressing NOx formation. Among the blends, higher biodiesel fractions yielded progressively lower NOx levels, with B30 exhibiting the most pronounced reduction. This confirms the moderating effect of biodiesel on thermal NOx despite the global rise with engine speed.

Figure 3.8.b highlights CO emissions. Carbon monoxide is an intermediate product of the combustion process, which can be further oxidized in the presence of hydroxyl radicals (–OH) and oxygen ($O_2$). Its formation is therefore primarily dependent on the fuel-air equivalence ratio (richness) within the combustion chamber. According to Sunggyu & Shah (2012) oxygenated fuels generally promote CO oxidation but the present low-load tests show higher CO emissions for biodiesel blends relative to diesel.

The higher CO emissions observed with biodiesel blends may result from poorer atomization due to higher viscosity and density, shorter ignition delay leading to altered combustion phasing, and lower peak temperatures caused by the reduced heating value. Moreover, the small naturally aspirated engine's characteristics and measurement sensitivity may contribute to deviations from typical literature trends, leading to locally rich zones and incomplete oxidation despite the fuel's oxygen content.

At 50% load, the torque vs speed curves in figure 3.9a exhibit the typical bell-shaped profile: torque rises with increasing engine speed, reaches a maximum around 2000 rpm, and then declines. Diesel achieved the highest torque peak at 2000 rpm, while all biodiesel blends produced lower values. Among the blends, B30 consistently showed the lowest torque, reflecting the combined effect of higher viscosity and lower heating value, whereas B5, B10 reached the maximum earlier, near 1800 rpm, and B20 peaked closer to 2000 rpm. These variations are attributable to differences in ignition delay, spray atomization, and combustion phasing induced by blend properties. Minor differences between blends, however, remain within the expected range of experimental variability (Mahmudul et al., 2017).

At 50% load, brake power increased steadily with engine speed, showing an exponential-like rise rather than the bell-shaped profile observed for torque (Figure 3.9b).This behaviour is consistent with the brake power equation because of the effect of rising rotational speed. Diesel achieved the highest brake power across the entire speed range, reaching about 4.45 kW at 2300 rpm. Among the biodiesel blends, B5 was closest to diesel, followed by B10 and B20, while B30 consistently gave the lowest output, with approximately 4.28 kW at 2300 rpm.

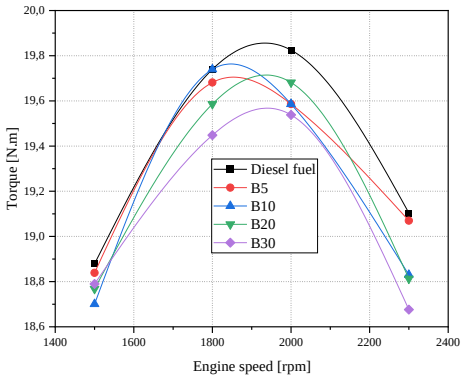


(a)

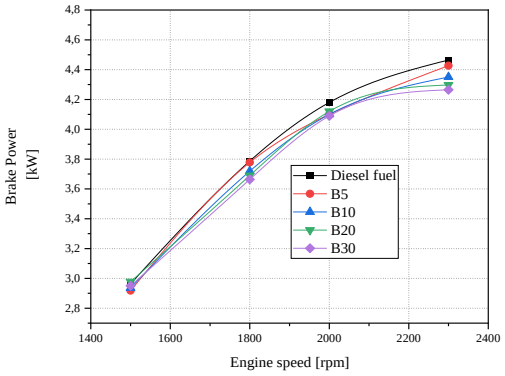


(b)

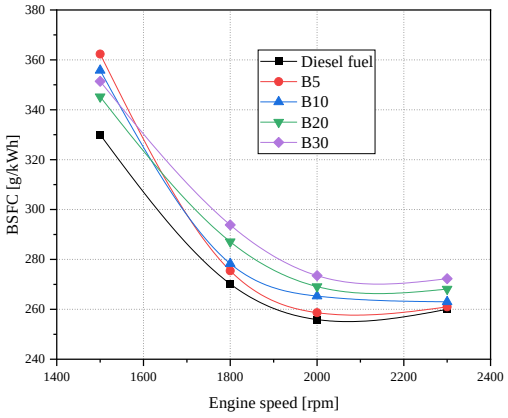


(c)

**Figure 3.9** Engine performance evolution with engine speed at medium load

Although the absolute differences between fuels are modest, the relative order (Diesel > B5 > B10 > B20 > B30) was preserved throughout the tests, confirming that increasing biodiesel substitution produces a gradual but measurable reduction in brake power due to the lower heating value and higher viscosity of the blends. This findings are in agreement with Habibullah et al.(2014) study results.

BSFC decreased progressively as engine speed increased from 1200 to 2300 rpm reduced (Figure 3.9c). At higher speeds , combustion efficiency was improved and relative frictional losses were. Diesel and B5 recorded the lowest BSFC values across the range, with B5 closely approximating diesel. Higher biodiesel content resulted in consistently greater BSFC, the effect being most pronounced for B30. At 1200 rpm, B30 consumed 360 g/kWh compared to 330 g/kWh for diesel, a penalty of about +9.1%**.**At 1800 rpm, the difference narrowed to +7.4%, while at 2300 rpm it was still measurable at +3.9%**.** These differences exceed the estimated

BSFC measurement uncertainty (≈±2.8%), confirming a genuine impact of biodiesel substitution. The increase arises from biodiesel's lower heating value and higher density, which involve a greater mass of fuel to produce the same brake output which is consistent to How et al.( 2018) findings . The blending effect is clear: B5 remains nearly indistinguishable from diesel, whereas higher fractions (B20, B30) progressively increase same as (Y. Chen et al., 2023).

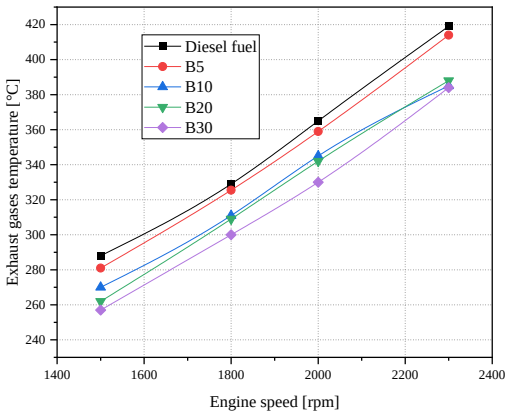


**Figure 03.10** Exhaust gases temperature variations with engine speed at medium load

Exhaust gas temperature increased steadily with engine speed, reaching a maximum of about 420 °C for diesel at 2300 rpm (Figure 3.10) The B5 blend followed the diesel curve closely, with negligible difference across the speed range. The intermediate blends (B10 and B20) showed nearly overlapping curves, consistently about 20 °C lower than diesel, while B30 ehibited the lowest exhaust temperatures among the tested fuels.

This trend reflects the combined influence of fuel heating value and combustion characteristics. Diesel and B5, with higher calorific content, released more energy per unit mass, leading to higher in-cylinder temperatures and thus higher exhaust gas temperatures. As biodiesel content increased, the lower heating value reduced the overall combustion temperature, resulting in progressively lower exhaust gas temperatures. The near-superposition of B10 and B20 suggests that modest variations in biodiesel fraction within this range do not strongly influence EGT, whereas B30 produces a clear cooling effect in line with its higher oxygen content and reduced energy density.

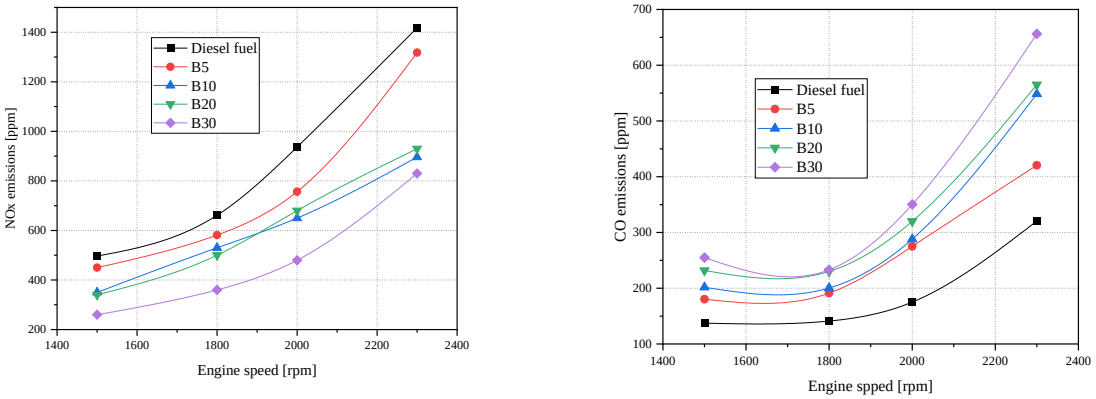


**Figure 3.11** Emissions evolution of NOx and CO with engine speed at medium load

For all fuels, NOx emissions increased progressively with engine speed, with a sharper rise at higher rpm (Figure 3.11a). Diesel consistently produced the highest NOx levels across the speed range, while biodiesel blends showed lower emissions, decreasing further with increasing biodiesel fraction. Among the blends, B30 yielded the lowest NOx values, followed by B20 and B10, whereas B5 remained close to diesel.

This behaviour is linked to in-cylinder combustion temperature and oxygen availability. Diesel, with the highest heating value, generated higher peak temperatures, which favoured thermal NOx formation. Biodiesel blends, on the other hand, released less heat per unit mass and showed slightly cooler combustion, reducing NOx production. Although biodiesel's inherent oxygen content would normally promote NOx formation, in this case the dominant effect of reduced heating value and lower combustion temperature outweighed the oxygen effect, resulting in an overall NOx reduction with increasing biodiesel content.

CO emissions at 50% load showed a generally increasing trend with rising engine speed **(**Figure 3.11b).Biodiesel blends produced higher levels while Diesel consistently exhibited the lowest CO values across the range. Among the blends, B5 maintained relatively moderate emissions, whereas B10 and B20 displayed higher CO outputs, and B30 reached the maximum values, exceeding 600 ppm at 2300 rpm.

The higher CO emissions observed with biodiesel blends contrast with the general expectation that biodiesel's inherent oxygen promotes more complete combustion (Attia & Hassaneen, 2016). In this study, the increase is likely due to biodiesel's lower heating value, higher viscosity, and reduced volatility, which can hinder atomization and air-fuel mixing, especially at

higher engine speeds where injection time is limited. These factors may slow down CO oxidation to $CO_2$, even with oxygen present in the fuel. The gradual rise in CO emissions with increasing biodiesel content therefore reflects the interplay between improved oxygen availability and reduced combustion efficiency, with the latter having a stronger influence under the tested conditions.

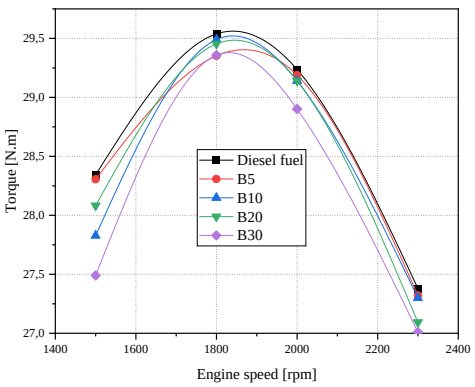


(a)

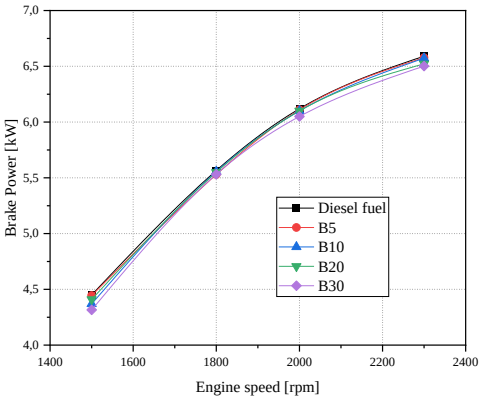


(b)

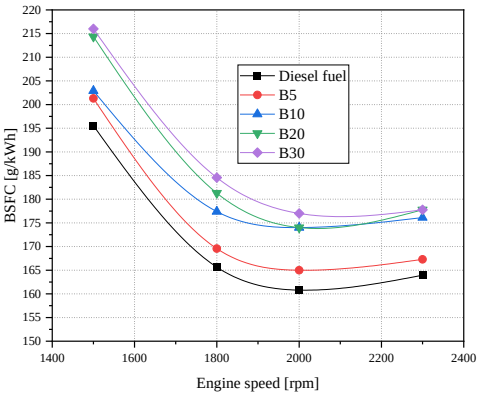


(c)

**Figure 03.12** Torque , Brake Power, BSFC variations with engine speed at mid-high load

At 75% load, all fuels exhibited the characteristic bell-shaped torque profile with increasing engine speed (Figure 03.2a). Torque rose steadily from low rpm, reached a maximum between 1800–2000 rpm, and then declined at higher speeds, in line with the typical behaviour of diesel engines (Heywood, 2018) .Diesel delivered the highest peak torque, closely followed by B10, while B20 and B30 showed slightly lower values across the operating range.

An exception was observed for the B5 blend at low engine speed (~1500 rpm), where its torque was slightly lower than that of diesel and closer to the higher biodiesel blends. However, as the

engine speed increased, the B5 torque curve gradually converged with that of diesel, ultimately reaching a comparable peak torque around 1900 rpm. This deviation may result from subtle variations in injected fuel mass, injection timing, or combustion phasing under light-fueling conditions. Minor differences in density and compressibility can affect injector dynamics and mixture preparation at low speed, leading to a temporary reduction in torque output (Kegl, Kegl, & Pehan, 2014).

At 75% load, the brake power curves of diesel and all biodiesel blends are almost perfectly superimposed across the full engine speed range (Figure 3.12b). No significant deviations are observed between fuels. This indicates that, under mid-high load conditions, biodiesel substitution up to 30% has no meaningful impact on brake power output, and the engine delivers essentially the same shaft performance regardless of the blend.

At 75% load, BSFC trends for all fuel types show a typical U-shaped curve, decreasing with engine speed up to ~2000 rpm, then slightly increasing due to rising frictional and thermal losses at higher speeds. Blends with increasing biodiesel content (B5 to B30) showed a gradual rise in BSFC Figure 3.12. This is attributed to biodiesel's lower energy content and higher viscosity, which slightly compromise atomization and combustion efficiency. Among the blends, B5 and B10 closely approached diesel performance, while B20 and B30 showed more pronounced increases in fuel consumption, particularly at lower engine speeds.

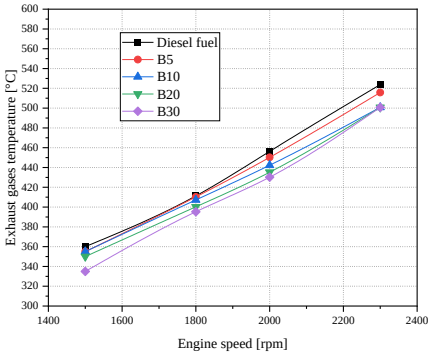


**Figure 03.13** Variation of EGT versus engine speed at mid-high load

Exhaust gas temperature increased steadily with engine speed for all fuel types, reflecting the expected rise in combustion intensity and heat release rate. Biodiesel blends showed slightly lower temperature values than diesel across the speed range. Among the blends, B5 and B10 closely tracked diesel, whereas B20 and B30 exhibited marginally cooler exhaust streams, especially above 2000 rpm.

The results confirm that biodiesel blends burn more cleanly but release less thermal energy, slightly reducing exhaust temperatures. This trend has positive implications for thermal loading on engine components and may contribute to lower NOx formation.

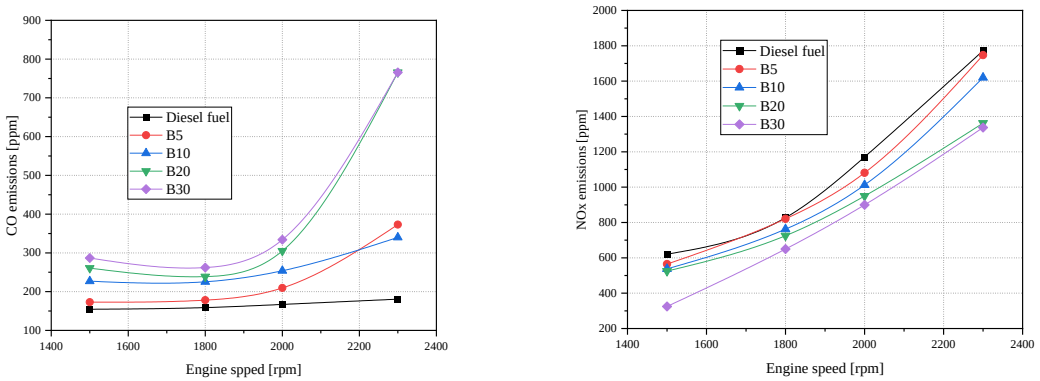


**Figure 3.14** variation of CO and NOx emissions with engine speed at 75% load.

At 75% load, CO emissions from diesel remained nearly constant at around 150 ppm across the entire speed range (Figure 3.14a). In contrast, biodiesel blends displayed a gradual rise in CO levels with increasing engine speed, reaching nearly 780 ppm for B20 and B30 at 2300 rpm. This increase is mainly associated with the reduced heating value and less favourable spray characteristics of biodiesel, which can limit air-fuel mixing and oxidation efficiency at high speeds where injection and combustion occur rapidly. As the biodiesel proportion increases, these effects become more evident, resulting in higher CO formation despite the additional oxygen present in the fuel.

At 75% load, NOx emissions for biodiesel blends rose steadily with engine speed but remained consistently below those of diesel (Figure 3.14b). The reduction became more evident as the biodiesel proportion increased, with B30 exhibiting the lowest values. This behaviour follows the same trend observed at low and mid loads, confirming that the lower heating value of biodiesel consistently leads to reduced in-cylinder temperatures and suppressed thermal NOx formation. Although biodiesel provides additional oxygen that could favour NOx generation, the cooling effect associated with its lower energy content remains dominant, resulting in a systematic decrease in NOx emissions with increasing biodiesel fraction.

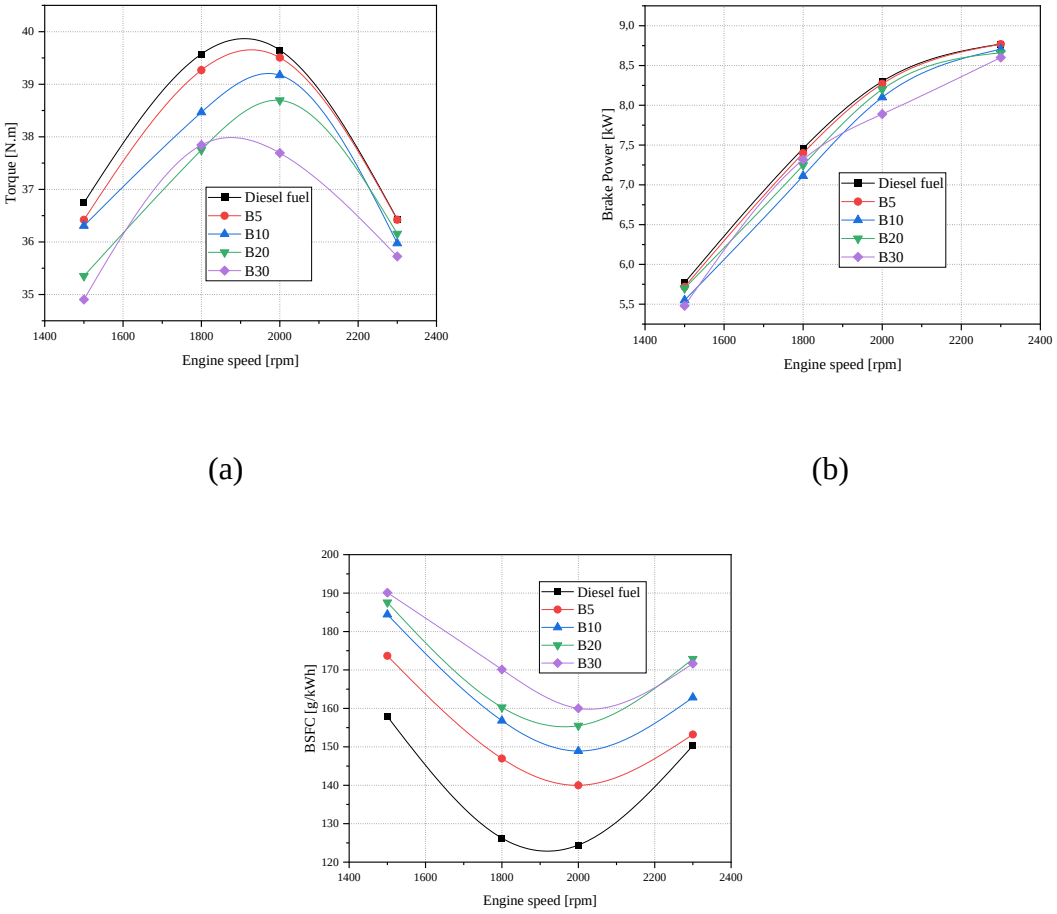


**Figure 03.15** Evolution of engine torque, BP and BSFC with engine speed at full load

At full load, all fuels exhibited the typical bell-shaped torque profile with speed, reaching maximum values between 1800 and 2000 rpm (Figure 3.15a). B5 closely followed diesel trend across the operating range, particularly at higher speeds above 2000 rpm, where its curve nearly overlapped with diesel. The intermediate blends (B10 and B20) showed slightly reduced torque, and B30 produced the lowest values, in line with its higher biodiesel content.

The observed ranking reflects the direct influence of fuel heating value on torque generation. Moreover, the close alignment of B5 with diesel demonstrates the blending benefit at low substitution ratios, where performance penalties remain negligible (Sodhi et al., 2017). At full load, brake power increased almost exponentially with engine speed for all tested fuels (Figure 3.15b). The curves for diesel and the biodiesel blends were largely overlapping across most of the operating range, indicating that substitution with biodiesel does not significantly

alter shaft output under full-load conditions. A slight divergence was observed beyond 1800 rpm, where B30 delivered the lowest brake power compared with the other fuels.

This reduction for B30 is consistent with its lower heating value and higher viscosity, which limit the net energy release and can marginally impair mixture formation at high injection rates. Nevertheless, the difference remains modest, and the overall trend confirms that biodiesel blends up to 20% maintain comparable brake power to diesel even under maximum load.

BSFC at full load, as shown in Figure 3.15c, decreases with increasing engine speed, reaching a minimum around 2000 rpm for all tested fuels. Among the blends, B5 and B10 demonstrated BSFC performance closest to diesel, indicating that these fuels are ready to be used in conventional diesel engines without significant efficiency penalties. In contrast, B20 and B30 showed noticeably higher BSFC, suggesting that higher blend ratios may necessitate engine calibration to optimize performance.

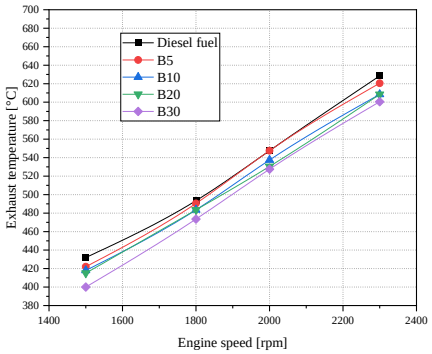


**Figure 3.16** Variation of exhaust gases temperatures with engine speed at full load

At full load, exhaust gas temperature increased with engine speed (Figure 3.16). Diesel and B5 showed similar values, while higher biodiesel blends recorded lower temperatures, with B30 being the coolest. This trend, consistent with lower-load results, is mainly due to biodiesel's lower heating value and slower evaporation, which reduce combustion temperature despite its oxygen content.

In addition, at full load, NOx emissions increased steadily with engine speed for all fuels, reaching maximum values near 2300 rpm (Figure 3.17a). Diesel consistently exhibited the highest NOx levels across the entire range, followed closely by B5, while emissions decreased progressively with higher biodiesel fractions, with B30 recording the lowest values.

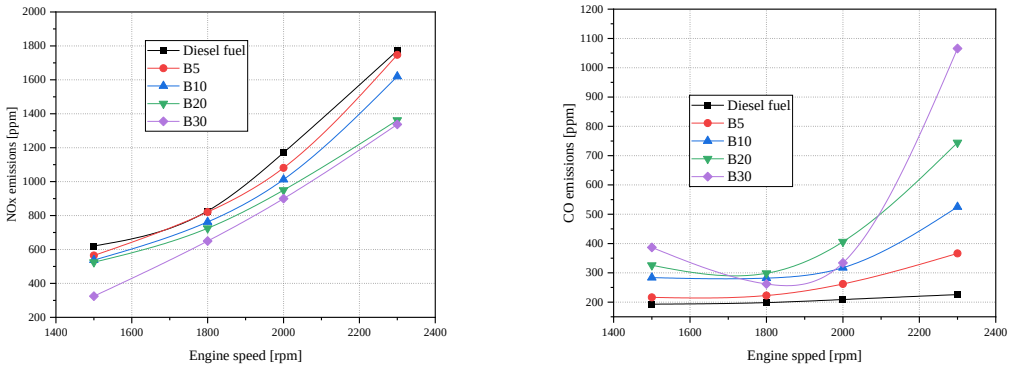


**Figure 3.17** NOx and CO emissions evolutions at full load across engine speed variation

This behaviour is governed mainly by in-cylinder temperature dynamics. At full load, fuel delivery is high, leading to elevated combustion temperatures that favour thermal NOx formation. Diesel and B5, with their higher heating value, generate more energy per unit mass and thus sustain higher peak temperatures, which enhances NOx formation. In contrast, blends with higher biodiesel content (B10–B30) release less heat due to their lower calorific value, resulting in slightly cooler combustion and reduced NOx emissions.

At full load, diesel fuel emitted the lowest CO emissions, remaining nearly constant around 150 ppm across all speeds (Figure 3.17b). In contrast, biodiesel blends emitted higher CO levels, especially at high speeds. While CO emissions were moderate at 1500-1800 rpm, they increased sharply beyond 2000 rpm, reaching over 1000 ppm for B30, followed by B20 and B10, with B5 closest to diesel.

The rise in CO with higher biodiesel content is attributed to increased viscosity and lower volatility, which impair fuel atomisation and evaporation. At high speeds, the short injection duration and high fuelling rate restrict air-fuel mixing and limit CO oxidation, outweighing the oxygen content benefit of biodiesel and resulting in higher CO emissions for blends with larger biodiesel fractions.

### 3.3.3 Third group of experiments: Load-Dependent Tests at 1800 rpm

A third series of results is presented at a constant engine speed of 1800 rpm, which corresponds to the peak torque region of the test engine. This operating point was chosen because it represents a stable and efficient combustion condition, widely considered representative of typical diesel engine operation. At this speed, the influence of load variation (25%, 50%, 75%, and 100%) on performance, thermal, and emission parameters (torque, brake power, BSFC, exhaust

gas temperature, CO and NOx emissions) can be assessed and compared for diesel and biodiesel blends.

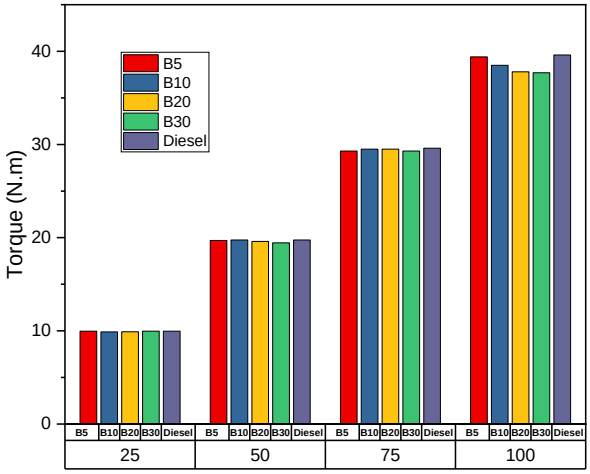


**Figure 3.18** Variation of torque with engine load at 1800 rpm for different biodiesel blends and diesel.

As depicted in Figure 3.18, torque increased progressively with load for all fuels, reaching its maximum value at full load. This behaviour reflects the direct relationship between load and the quantity of fuel injected per cycle, which enhances the rate of energy release and consequently the torque output. Across all operating conditions, the torque values for biodiesel blends were very close to those of diesel, indicating that the substitution of diesel with up to 30% biodiesel did not significantly affect engine torque

Figure 3.19 illustrates the brake power evolution with load for diesel and biodiesel blends at 1800 rpm. Brake power increased almost linearly with load for all fuels due to higher fuel input and heat release at elevated loads. Biodiesel blends showed slightly lower power than diesel, mainly because of their lower calorific value. However, B5 and B10 performed nearly identically to diesel, while B20 and B30 showed only minor reductions. Overall, blends up to B30 maintained comparable performance at this speed.

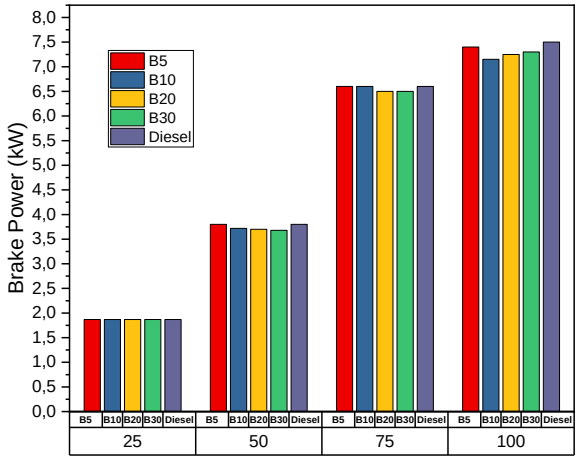


**Figure 3.19** Variation of brake power with engine load at 1800 rpm for different fuels.

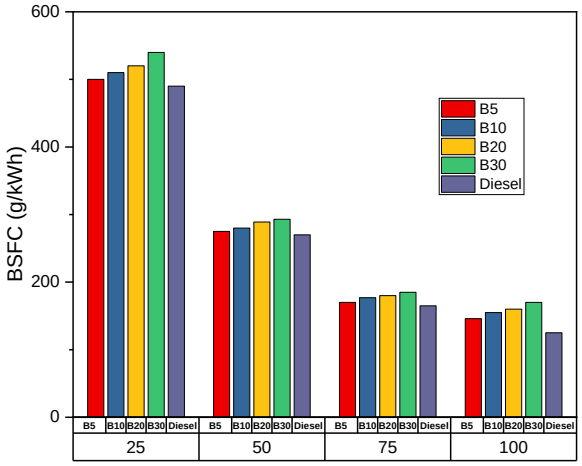


**Figure 3.20** Variation of brake specific fuel consumption (BSFC) with engine load at 1800 rpm for different biodiesel-diesel fuels.

Figure 3.20 exhibits the variation of BSFC with load for different biodiesel blends and diesel. A general decreasing trend in BSFC is observed as the load increases from low to high. At low load, BSFC is highest for all fuels due to incomplete combustion and greater relative frictional losses. As the load increases to medium and high levels, BSFC decreases markedly, indicating more efficient fuel utilization and better energy conversion.

Across all loads, biodiesel blends exhibit slightly higher BSFC compared to diesel. This behaviour is mainly attributed to their lower heating value and higher density, which require a greater volume of fuel to deliver equivalent power. However, the difference becomes less pronounced

at higher loads, where improved combustion temperature and oxygenated nature of biodiesel enhance combustion efficiency. Among the blends, B5 and B10 perform most comparably to diesel, while B20 and B30 show marginally higher consumption.

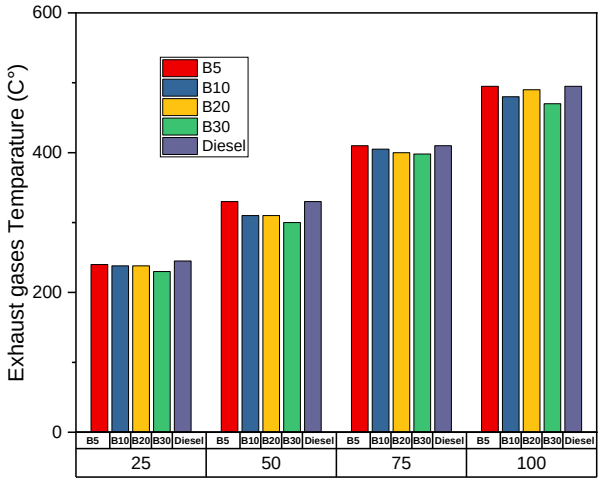


**Figure 3.21** Variation of exhaust gas temperature (EGT) with engine load at 1800 rpm for biodiesel blends and diesel fuel.

The variation of exhaust gas temperature with engine load for diesel and its biodiesel blends is displayed in Figure 3.21. A clear increase in temperature is observed as the load increases from low to high, reflecting higher fuel input and combustion intensity. However, the overall behaviour among the tested fuels remains similar, indicating comparable combustion characteristics.Diesel and B5 exhibit nearly identical temperature profiles, while the biodiesel blends show slightly lower EGT values. This minor reduction is attributed to the lower heating value of biodiesel, which results in reduced peak combustion temperature. Among the blends, the EGT follows the order B30 > B20 > B10, suggesting a marginal effect of biodiesel proportion on thermal release during combustion.

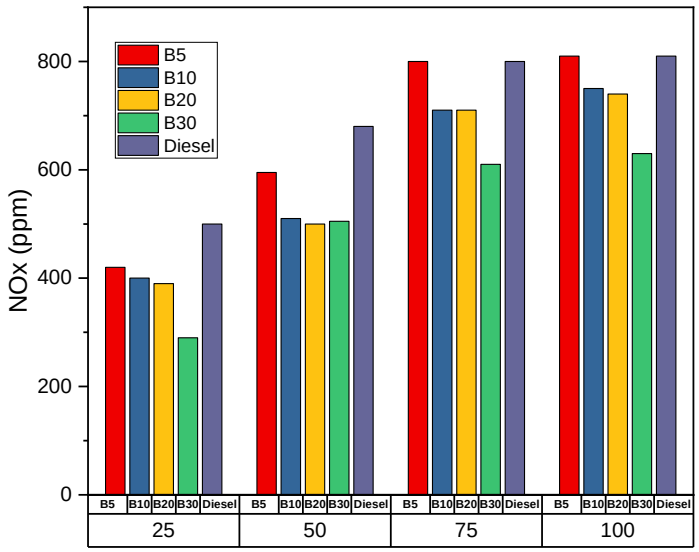


**Figure 3.22** Variation of $NO_x$ emissions with engine load at 1800 rpm for diesel and biodiesel fuels.

As shown in Figure 3.22, NOx emissions increase consistently with engine load for all fuels, primarily due to higher combustion temperatures and greater oxygen availability at elevated loads. Despite this general trend, the emission profiles of all fuels are similar across the load range.

Diesel and B5 produce the highest NOx emissions, though the difference between them is minimal. B10 and B20 exhibit nearly identical NOx levels, slightly lower than diesel, while B30 records the lowest emissions among all tested fuels. The reduction observed with increasing biodiesel proportion can be attributed to the lower combustion temperature and reduced premixed burning rate, which limit thermal NOx formation despite biodiesel's inherent oxygen content.

We constated that the variation of CO emissions with load is not particularly pronounced. As shown in Figure 3.23.Across all loads, diesel consistently exhibits the lowest CO levels, while higher biodiesel fractions show progressively higher emissions. At low and mid loads, B5 behaves similarly to the biodiesel blends, displaying slightly elevated CO levels. However, at mid-high and full loads, B5 aligns closely with diesel, showing almost identical emissions.

This behaviour suggests that at lower loads, incomplete combustion associated with cooler temperatures and lower in-cylinder pressures affects biodiesel blends more strongly. At higher

loads, enhanced combustion efficiency and increased temperature reduce these differences, making B5's performance comparable to diesel.

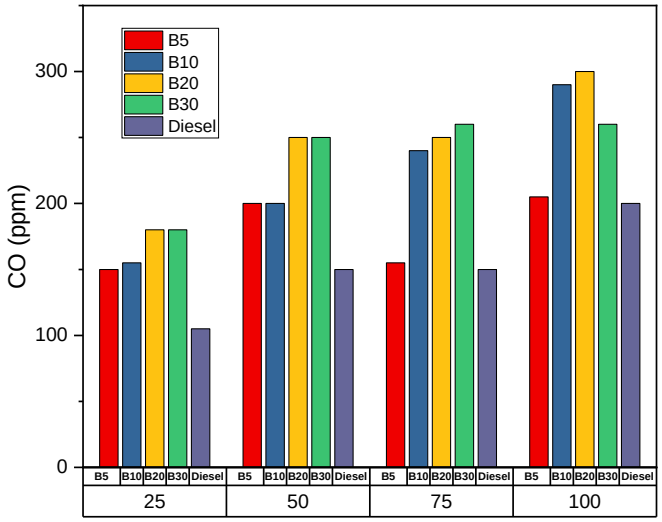


**Figure 03.23** Variation of carbon monoxide (CO) emissions with engine load at 1800 rpm for tested fuels.

## 3.4 Conclusion

The experimental investigation conducted in this chapter confirms many of the trends reported in the literature regarding the use of biodiesel-diesel blends in compression-ignition engines. As expected, increasing the proportion of WCO-derived biodiesel generally led to slight reductions in engine power and torque, attributable to the lower heating value of biodiesel compared to conventional diesel (Loo et al., 2021). Similarly, the fuel consumption behavior aligned with observations reported in earlier studies (Kukana & Jakhar, 2022; Seraç et al., 2020), showing a consistent increase as the biodiesel proportion rose. This trend highlights the combined influence of fuel characteristics, combustion kinetics, and engine operating conditions.

Some deviations from widely reported trends were observed in this case study. Notably, nitrogen oxide ($NO_x$) emissions decreased with increasing biodiesel proportion, contrary to the common finding that biodiesel increases $NO_x$ due to higher combustion temperatures (Can, 2014). In addition, carbon monoxide (CO) emissions increased slightly, whereas most studies suggest a decrease because of biodiesel's higher oxygen content (Senthur Prabu et al., 2017). These differences may be attributed to the specific properties of the locally sourced WCO, the optimized transesterification process, and the engine's response to the fuel's physical characteristics, including viscosity and density (Kegl, Kegl, & Pehan, 2013).

Overall, the results demonstrate that WCO-based biodiesel blends can be used as practical alternatives to conventional diesel with minimal impact on engine performance and potential improvements in emission profiles. The findings of this chapter provide an essential experimental reference for the next stage of the research, where combustion characteristics and emissions will be further analysed and validated through computational modelling in Chapter 4.

# Chapter 4

# Computational Modelling of Biodiesel-Diesel Combustion Using CONVERGE

This chapter presents the computational investigation of WCO-derived biodiesel blends using the CONVERGE CFD software. Computational modelling offers a cost-effective and versatile approach to analyze in-cylinder combustion, spray dynamics, and emissions, complementing the experimental work described in Chapter 3. By simulating different operating conditions and fuel blends, CFD enables detailed insight into processes that are difficult or expensive to measure experimentally.

Compared to general-purpose CFD tools, CONVERGE is particularly suited for engine studies due to its built-in modules for fuel injection, multi-component combustion, and emission prediction. Its features include automated mesh generation, adaptive mesh refinement (AMR), and robust coupling of spray, combustion, and turbulence models that represent accurately transient complex phenomena like fuel injection, vaporisation, and in-cylinder chemical reactions, while minimising computational cost.

The workflow in CONVERGE typically begins with defining the engine geometry, boundary conditions, and initial operating parameters. Fuel properties and injection profiles are specified based on experimental characterization from chapter 2, while appropriate models for turbulence, spray breakup, evaporation, and chemical kinetics are selected.

By integrating detailed physical modelling with experimental data from chapter 3, this chapter presents a general understanding of the combustion characteristics and emission behaviour of WCO biodiesel blends under varying operating conditions. Furthermore, parametric studies that are impractical to perform on the test bench will be done after the validation of the models by comparing the outcomes with experiments results.

## 4.1 Introduction to CONVERGE CFD

### 4.1.1 Computational Fluid Dynamics (CFD) and CONVERGE Software

Computational Fluid Dynamics (CFD) is a numerical technique adopted to study different fluid motion and related transport phenomena (gaseous, liquid, or multiphase) by solving the governing conservation equations of mass, momentum, and energy. These equations, known as the Navier-Stokes equations, are inherently nonlinear and coupled, making analytical solutions possible only for simplified cases. Therefore, numerical simulation has become an indispensable approach for investigating complex fluid and thermal systems across a wide range of engineering applications.

CFD provides the capability to analyse detailed flow structures, heat and mass transfer, turbulence, and chemical reactions in geometrically complex domains. Its accuracy depends on the quality of the discretization, the robustness of the numerical schemes, and the physical models employed. Vis-à-vis internal combustion engines, CFD has emerged as a vital tool for investigating in-cylinder phenomena, including fuel injection, air–fuel mixing, evaporation, ignition, combustion, and pollutant formation. Since these processes are inherently transient and strongly interrelated, accurate modeling is essential for optimizing engine performance and minimizing emissions.

Modern engines present additional challenges that further justify the use of CFD, including:

- Direct fuel injection and atomization processes within the combustion chamber;
- Stratification of mixture composition and temperature due to exhaust gas recirculation;
- Increasingly stringent emission regulations requiring predictive modeling of pollutant formation;
- The use of alternative fuels, such as biodiesel, natural gas, and hydrogen, introduces unique physical and chemical characteristics that significantly affect combustion behaviour.CFD thus offers a detailed and time-resolved understanding of in-cylinder processes, complementing experimental observations and enabling virtual prototyping with reduced cost and time.

### 4.1.2 Justification for the Use of CONVERGE in Computational Modelling

In this study, CONVERGE CFD (version 2.4.0) was employed to model diesel engine combustion fuelled with mineral diesel and biodiesel blends . CONVERGE is a specialized CFD software package developed to simplify and accelerate the simulation of complex, transient, and chemically reactive flows particularly in internal combustion engines.

The computational mesh is constructed directly from the imported surface geometry (typically in STL format) and dynamically adapts during the simulation. This eliminates the need for manual meshing and ensures high grid quality throughout the calculation.

CONVERGE further incorporates an Adaptive Mesh Refinement (AMR) algorithm that locally refines the grid in regions exhibiting steep gradients, such as near spray fronts, ignition zones, or flame fronts. This feature enhances numerical accuracy while maintaining computational efficiency. The automatic handling of moving boundaries, such as piston motion and valve dynamics, makes the code especially suitable for internal combustion engine studies, avoiding the mesh distortion issues common in traditional CFD approaches.

Beyond its meshing capabilities, CONVERGE includes a comprehensive suite of physical and chemical models. It can simulate three-dimensional, transient or steady-state, compressible or incompressible flows, including turbulence, sprays, evaporation, combustion, cavitation, and conjugate heat transfer. The software solves the conservation equations for mass, momentum, energy, and species concentration at each time step, providing detailed 4D resolution of various processes that occur in the cylinder.

Turbulence can be modelled using RANS or LES formulations, while combustion chemistry is treated through both detailed and reduced chemical kinetic mechanisms. These features allow accurate representation of fuel oxidation, ignition delay, and pollutant formation essential for studying alternative fuels such as biodiesel.

Finally, CONVERGE's proven reliability in both academic and industrial research, combined with its efficient pre- and post-processing environment, makes it a powerful tool for combustion modelling. Its integration of automated meshing, advanced physical modelling, and high computational efficiency provides a strong foundation for this study's simulations and for the comparison between numerical predictions and experimental data.

### 4.1.3 CONVERGE simulation workflow

The workflow of a CONVERGE simulation can be broadly divided into three stages: pre-processing, solver execution, and post-processing**.**

**1.Pre-processing**

In this phase of pre-processing, the computational domain is prepared. The geometry is imported as a triangulated surface, typically in STL format from a CAD application. Any geometric inconsistencies (gaps, misaligned surfaces, or incorrect triangle orientations) are corrected to ensure a closed and valid surface. Boundary identifiers are then assigned to different regions

of the geometry and linked to entries in the boundary specification file. Once processed, the geometry and boundary definitions are saved for use in the simulation.

Beyond preparing the geometry, ASCII-formatted input (.in) and data (.dat) files are essential. The input files specify the numerical setup, physical models, and initial and boundary conditions, while the thermodynamic properties, the detailed or reduced chemical reaction mechanisms, and surface geometry information are given in the data files . These files can either be made manually using a text editor or generated through the CONVERGE Studio graphical interface, which provides a guided process for case setup.

**2.Solver execution**

At this stage, CONVERGE discretizes and solves the governing equations of mass, momentum, energy, and species transport, together with any additional sub-models (e.g., turbulence, spray, combustion). The solver operates on the automatically generated mesh, adapting it as required during runtime to capture gradients and moving boundaries.

**3.Post-processing**

Following execution, the results are processed and visualized. Output data can be displayed in the form of scalar and vector fields, time histories, or contour maps of key variables such as pressure, temperature, heat release rate, or pollutant formation. CONVERGE includes basic visualization tools, and results can also be exported in formats compatible with third-party software (e.g., Tecplot, ParaView) for more detailed analysis and graphical representation.

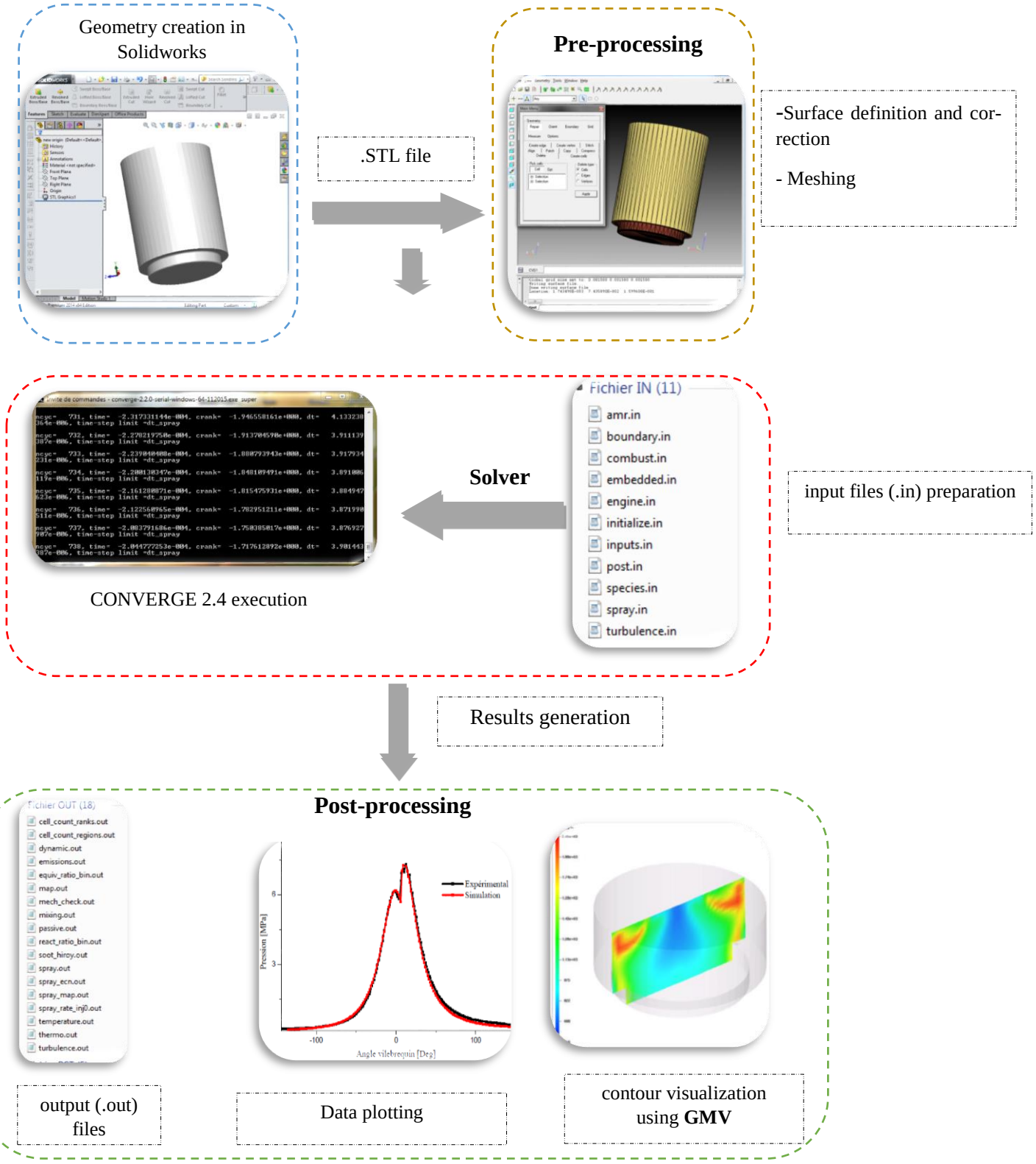


**Figure 4.1** CONVERGE workflow and file types.

### 4.1.4 CONVERGE Data Files

#### Input and Data Files

Prior to running a CONVERGE simulation, a set of ASCII-formatted files must be prepared, including input files (.in) and data files (.dat). The input files specify numerical settings, model parameters, and boundary and initial conditions, whereas the data files provide thermodynamic properties, chemical reaction information, and surface geometry details.

These files can be created or edited using a standard text editor; however, it is recommended to use the CONVERGE Studio graphical interface, which helps ensure proper formatting and consistency. All input and data files must be placed in the case directory from which CONVERGE is executed. If any required file is missing, the program will halt and indicate the missing file. At a minimum, the case directory must contain:

- **inputs.in** – general simulation settings
- **boundary.in** – boundary condition definitions
- **initialize.in** – initial conditions
- **mech.dat** – list of species and combustion reaction mechanisms
- **therm.dat** – thermodynamic properties of gaseous species
- **liquid.dat** – temperature-dependent liquid fuel properties such as viscosity, density, surface tension, thermal conductivity, and specific heat, latent heat, vapour pressure.
- **surface.dat** – surface geometry file

#### Output Files

CONVERGE generates four main types of output files: echo (*.echo)**,** restart (*.rst)**,** cell-averaged (*.out), and *cell-based post-processing (post.out)** files.

1. **Echo files (*.echo) :**

   For each input file (*.in), CONVERGE produces a corresponding echo file (e.g., *combust.in → combust.echo*). These files record all recognized input parameters and help verify case setup. If a parameter does not appear in the echo file, it was entered incorrectly and was not read by CONVERGE.

2. **Restart files (*.rst) :**

   Restart files are periodically generated to the case directory during the simulation . These files allow the simulation to be restarted from a specific point without repeating previous calculations.

3. **Averaged output files (*.out) :**

   These files are created only when the corresponding physical model is activated

(e.g., *spray.out* is generated only if a spray model is used). Each line of data represents values for a given time step or cycle.

The first column indicates time (in transient simulations) or cycles (in steady-state simulations). Depending on the setup, time may be expressed in seconds or as crank angle degrees for engine simulations.

4. ***Post-processing files (post.out) :***

   These files contain cell-by-cell quantities across the computational domain, written at user-defined intervals. They are formatted for visualization in post-processing software such as EnSight**,** GMV, Tecplot, or FieldView

### 4.1.5 Meshing Techniques

Mesh generation techniques are commonly employed in numerous engineering fields thanks to their ability to provide high computational performance and modeling flexibility. Several studies have demonstrated that mesh-based approaches offer reliable numerical accuracy and control over spatial resolution.

CONVERGE allows the creation of a structured mesh capable of representing complex engine geometries, including vertical valves, flat or bowl-shaped pistons (ω-type), and other configurations. In addition, several mesh refinement strategies are implemented in the code, among which the base grid refinement and the Adaptive Mesh Refinement (AMR) techniques are the most important.

#### 4.1.5.1 Base Grid Refinement

In CONVERGE, the base grid defines the initial spatial resolution of the computational domain using uniformly sized cubic cells. Refining this grid increases numerical accuracy by better capturing gradients in flow, temperature, and species concentration. However, finer grids also raise computational cost.

In order to balance accuracy and efficiency, several base grid sizes are often tested, and mesh independence is verified by comparing key simulation results.

#### 4.1.5.2 Adaptive Mesh Refinement (AMR)

The Adaptive Mesh Refinement (AMR) technique is an advanced method that automatically refines the mesh during the simulation according to specified physical conditions such as temperature**,** pressure**,** species concentration**,** or velocity gradients**.**

This adaptive refinement enables the accurate and efficient resolution of complex phenomena, including flame propagation**,** spray evolution, and pollutant formation, without excessively increasing computational cost.

### 4.1.6 Boundary and Initial Conditions

In CONVERGE, boundary and initial conditions define the thermodynamic and flow states at the domain limits and at the start of the simulation.

For engine modeling, pressure**,** temperature**,** velocity, and species composition are specified at the inlet, outlet, and wall boundaries. Intake and exhaust valves operate as time-dependent openings linked to the crank angle, while piston and cylinder walls are treated as moving or stationary surfaces with defined thermal properties.

The initial conditions describe the in-cylinder gas state before injection, including temperature, pressure, and mixture composition. Proper initialization ensures numerical stability and realistic prediction of ignition, combustion, and emissions.

### 4.1.7 Solver Setup

The numerical solution in CONVERGE is established by the conservation equations of mass**,** momentum, and energy, coupled with turbulence and combustion models. The solver employs a finite-volume method with adaptive time-stepping to ensure both accuracy and stability throughout the engine cycle.

For turbulence modelling, the RANS-based RNG k–ε model is adopted, providing a balance between computational efficiency and predictive accuracy for internal combustion engine simulations. Combustion is handled through the SAGE detailed chemistry solver, which can incorporate detailed or reduced kinetic mechanisms to calculate ignition delay, heat release rate, and pollutant formation.

### 4.1.8 Pressure-Velocity Coupling (PISO Algorithm)

To solve the nonlinear and highly coupled partial differential equations governing in-cylinder fluid flow, CONVERGE applies the PISO (Pressure-Implicit with Splitting of Operators) algorithm for pressure-velocity coupling in the RANS equations. The PISO scheme begins with a prediction step, in which the momentum equation is solved to estimate the velocity field. From this prediction, a pressure correction equation is derived and solved, and the resulting correction is applied to the momentum equation.

This correction-prediction series may be iterate for numerous times to achieve the desired level of accuracy. After pressure and velocity fields are updated, the energy and species transport equations are solved sequentially.

The PISO algorithm was originally developed for non-iterative transient flow problems and later adapted for iterative steady-state calculations. Compared to the SIMPLE algorithm, PISO

performs two successive corrections instead of one, improving convergence and accuracy for compressible and unsteady flows.

The main iterative steps are recapped here :

1. Pressure prediction $P^p$
2. Solution of the momentum (velocity) equation
3. Solution of the energy equation
4. Pressure correction $P^c$, and combined transport equation,
5. Convergence test $\|P^p - P^c\| < TOL$.

This algorithm ensures consistent coupling between pressure and velocity, enhancing solution stability in complex transient engine simulations

## 4.2 Numerical model of diesel engine

### 4.2.1 Governing Equations

The behavior of fluid flow in CONVERGE is described through the fundamental conservation laws of mass, momentum, and energy.These equations form the basis of the numerical solver and are supplemented, when required, by transport equations for turbulence quantities, passive scalars, and chemical species.

**1. Transport equations of chemical species m**

The conservation equation for species m can be written as follows:

$$\frac{\partial \rho_m}{\partial t} + \frac{\partial \rho_m u_j}{\partial x_j} = \frac{\partial}{\partial x_j}\left(\rho D \frac{Y_m}{\partial x_j}\right) + S_m \text{.....(4.1)}$$

With

$$Y_m = \frac{M_m}{M_{tot}} = \frac{\rho_m}{\rho} \text{.....(4.2)}$$

And

$$\rho_m = Y_m \rho \text{..... (4.3)}$$

Where $\rho_m$ is the density of species $m$, $\rho$ is the total density, and $u_j$ is the fluid velocity. $S_m$ represents the source term due to chemical reactions and species spray.

Supposing all species have the same diffusivities, given by $D = \frac{\mu}{\rho\, S_C}$ where $\mu$ is the dynamic viscosity and $Sc$ is the Schmidt number. The Schmidt number compares the effects of viscosity and molecular diffusion in the fluid and is defined as: $S_C = \frac{v}{D}$.

**2. mass transport and momentum transport**

The compressible equations for mass transport and momentum transport are given by

$$\frac{\partial \rho}{\partial t} + \frac{\partial \rho u_i}{\partial x_i} = S \text{…….(4.4)}$$

And

$$\frac{\partial \rho u_i}{\partial t} + \frac{\partial \rho u_i u_j}{\partial x_j} = -\frac{\partial P}{\partial x_i} + \frac{\partial \sigma_{ij}}{\partial x_j} + S_i \text{ …….(4.5)}$$

where the viscous stress tensor is given by

$$\sigma_{ij} = \mu\left(\frac{\partial u_i}{\partial t} + \frac{\partial u_j}{\partial x_i}\right) + \left(\mu' - \frac{2}{3}\mu\right)\left(\frac{\partial u_k}{\partial x_k}\delta_{ij}\right) \text{ ….. (4.6)}$$

In the previous equations: $u$ is velocity, $\rho$ is the density, $S$ is the source term, $P$ is pressure, μ is viscosity, μ' is the dilatational viscosity (set to zero), and δij is the Kronecker delta.

By summing Equation (4.1) over all species, equation 4.4 is obtained

If a turbulence model is activated, the viscosity is substituted by the total viscosity,

$$\mu_{tot} = \mu_{mol} + C_\mu \rho \frac{k^2}{\varepsilon} \text{ …….. (4.7)}$$

where $\mu_{mol}$ is the molecular viscosity, $C_\mu$ is a turbulence model constant, $k$ is the turbulent kinetic energy, and $\varepsilon$ is the turbulent dissipation.

**3. Energy conservation equation**

The compressible form of the energy equation is given by

$$\frac{\partial \rho e}{\partial t} + \frac{\partial u_j \rho e}{\partial x_j} = -P\frac{\partial u_j}{\partial x_j} + \sigma_{ij}\frac{\partial u_i}{\partial x_j} + \frac{\partial}{\partial x_j}\left(K\frac{\partial T}{\partial x_j}\right) + \frac{\partial}{\partial x_j}\left(\rho D \sum_m h_m \frac{\partial Y_m}{\partial x_j}\right) + S \text{ …….. (04.8)}$$

Here, ρ is density, D is the mass diffusion coefficient,

$S$ is the source term, $P$ is the pressure, $e$ is the specific internal energy, $K$ is the conductivity, $T$ is temperature, $h_m$ is the species enthalpy, $Y_m$ is the mass fraction of species m and $\sigma_{ij}$ is the stress tensor.

The conductivity is also changed by the turbulent conductivity once the turbulence model is activated, which is given by

$$K_t = K + c_p \frac{\mu_t}{\mathrm{Pr}_t} \text{ ……..…(4.9)}$$

The energy equation now incorporates four supplementary terms further to the conventional convection and diffusion terms,. The first is a source term introduced to account for user-defined energy inputs, chemical heat release, and turbulent dissipation effects. In the case of compressible flows, the $P\frac{\partial u_j}{\partial x_j}$ represents the work associated with pressure forces, whereas for incompressible flows, this term vanishes due to the zero divergence of the velocity field.

**4. Equation of state**

For compressible flows, an equation of state is needed to relate density, pressure, and temperature. CONVERGE offers several options, including the ideal gas, Redlich-Kwong, and Redlich equations of state.

In this study, the fluid is assumed to be a homogeneous mixture of ideal gases, allowing the following relationships to be applied in 4.10 equations:

$$p = R_0 \, T \sum_m ( \rho / W_m )$$

$$I(T) = \sum_m ( \rho_m / \rho ) \, I_m(T) \quad \text{.....(4.10)}$$

$$Cp(T) = \sum_m ( \rho_m / \rho ) \, C_{pm}(T)$$

$$h_m(T) = I_m(T) + R_0 \, T / W_m$$

Where $R_0$ is the universal gas constant, $W_m$ is the molar mass of species $m$, and $I_m(T)$ denotes its specific internal energy. The specific heat capacities of the species are obtained from the thermodynamic data in the JANAF tables.

### 4.2.2 RANS Approach

The first approach to turbulence modeling is the RANS method (Reynolds-Averaged Navier–Stokes equations), in which the Navier-Stokes equations are averaged according to Reynolds decomposition. In this framework, the instantaneous flow variables are expressed as the sum of a mean component and a fluctuating component. The resulting averaged equations contain additional terms that represent the production of velocity fluctuations and the convective transfer of momentum due to these fluctuations. These additional terms are referred to as Reynolds stresses.

The appearance of these stresses introduces a closure problem in the governing equations, which is typically addressed through turbulence models. Such models involve solving transport equations for turbulence quantities, most commonly the model *(k-ε)*, to evaluate the turbulent viscosity.

Within the CONVERGE framework, three categories of turbulence models are available. Under Reynolds decomposition, all fluctuating quantities are separated into their mean and fluctuating components.

$$u_i = \bar{u}_\iota + \acute{u}_\iota \text{ .....(4.11)}$$

In compressible flows the Favre average is often, it is defined as a density-weighted average

$$u_i = \tilde{u}_i + \acute{u}_\iota \text{ .....(4.12)}$$

Avec

$$\tilde{u} = \frac{\overline{\rho u_1}}{\bar{\rho}} \text{ .....(4.13)}$$

The Favre decomposition applied to equations (4.1), (4.4), (4.5), and (4.8) yields a new system of equations that is similar to the original one.

Transport Equation for Chemical Species

$$\frac{\partial \bar{\rho}\,\tilde{Y}_m}{\partial t} + \frac{\partial \bar{\rho}\,\widetilde{u_j}\tilde{Y}_m}{\partial x_j} = \frac{\partial}{\partial x_j}\left(\bar{\rho} D_t \frac{\partial \tilde{Y}_m}{\partial x_j}\right) + \widetilde{\dot{S}_m} \quad \text{..... (4.14)}$$

Mass Conservation Equation

$$\frac{\partial \bar{\rho}}{\partial t} + \frac{\partial \overline{\rho u_j}}{\partial x_j} = \bar{\dot{\rho}}^s \text{ ..... (4.15)}$$

Momentum Conservation Equation

$$\frac{\partial \overline{\rho}\widetilde{u_i}}{\partial_t} + \frac{\partial \overline{\rho}\widetilde{u_i}\widetilde{u_j}}{\partial x_j} = -\frac{\partial \bar{p}}{\partial x_i} + \frac{\partial}{\partial x_j}\left[\mu\left(\frac{\partial \widetilde{u_i}}{\partial x_j} + \frac{\partial \widetilde{u_j}}{\partial x_i}\right) - \frac{2}{3}\mu \frac{\partial \widetilde{u_k}}{\partial x_k}\delta_{ij}\right] \text{ ..... (4.16)}$$

The Reynolds stress $\sigma_{ij}$ is given by:

$$\sigma_{ij} = -\bar{\rho}\widetilde{u'_\iota u'_j} \text{ .....(4.17)}$$

Energy Transport Equation

$$\frac{\partial \overline{\rho}\tilde{e}}{\partial_t} + \frac{\partial \overline{\rho}\widetilde{u_j}\tilde{e}}{\partial x_j} = -P\frac{\partial \widetilde{u_j}}{\partial x_j} + \widetilde{\sigma_{ij}}\frac{\partial \widetilde{u_i}}{\partial x_j} + \frac{\partial}{\partial x_j}\left(K_t \frac{\partial \tilde{T}}{\partial x_j} + \tilde{\rho} D_t \sum_m \tilde{h}_m \frac{\partial \tilde{Y}_m}{\partial x_j}\right) + S \text{ ..... (4.18)}$$

### 4.2.3 Physical Models

The terms that appear in the averaged equations represent the interaction between the mean flow and turbulent fluctuations. These additional terms give rise to a closure problem in the system of equations, as the number of unknowns becomes greater than the number of available equations. Therefore, turbulence models are required to close the system and enable the solution of the governing equations.

#### *4.2.3.1 RNG k–ε Turbulence Model*

For determining the turbulent viscosity, a turbulence model is fundamental. the RNG *k–ε* model is expressed by Equation (4.19). This approach solves two transport equations: the turbulent kinetic energy (*k*) and the dissipation rate of turbulent kinetic energy (*ε*).

The transport equation for the turbulent kinetic energy is given by:

$$\frac{\partial \bar{\rho}\tilde{k}}{\partial t}+\frac{\partial \bar{\rho}\tilde{u}_i\tilde{k}}{\partial x_i}=-\frac{2}{3}\bar{\rho}\tilde{k}\frac{\partial \tilde{u}_i}{\partial x_j}+\sigma_{ij}\frac{\partial \tilde{u}_i}{\partial x_j}+\frac{\partial}{\partial x_j}\frac{\mu}{Pr_k}\frac{\partial \tilde{k}}{\partial x_j}-\bar{\rho}\tilde{\varepsilon}+\bar{S_s} \quad \ldots\ldots\ldots\ldots\ldots (4.19)$$

The transport equation for the turbulent dissipation rate is given by:

$$\frac{\partial \bar{\rho}\tilde{\varepsilon}}{\partial t}+\frac{\partial(\bar{\rho}\tilde{u}_i\tilde{\varepsilon})}{\partial x_i}=\frac{\partial}{\partial x_j}\left(\frac{\mu}{Pr_t}\frac{\partial \varepsilon}{\partial x_j}\right)-\left[\frac{2}{3}c_{\varepsilon 2}-c_{\varepsilon 3}-\frac{2}{3}c_\mu c_\eta\frac{\tilde{k}}{\tilde{\varepsilon}}\frac{\partial \tilde{u}_i}{\partial x_i}\right]\bar{\rho}\tilde{\varepsilon}\frac{\partial \tilde{u}_i}{\partial x_i}+\left(\left(c_{\varepsilon 1}-c_\eta\right)\frac{\partial \tilde{u}_i}{\partial x_j}\sigma_{ij}-c_{\varepsilon 2}\bar{\rho}\tilde{\varepsilon}+c_s\bar{S_s}\right)\frac{\tilde{\varepsilon}}{\tilde{k}} \quad \ldots\ldots\ldots\ldots\ldots\ldots (4.20)$$

And

$$\sigma_{ij}=-\bar{\rho}\widetilde{u'_\iota u'_J}=2\mu_t S_{ij}-\frac{2}{3}\delta_{ij}\left(\rho k+\mu_t\frac{\partial \tilde{u_\iota}}{\partial x_i}\right) \quad \ldots\ldots\ldots\ldots\ldots (4.21)$$

The turbulent viscosity $\mu_t$ is given by

$$\mu_t=C_\mu\rho\frac{k^2}{\varepsilon} \quad \ldots\ldots\ldots (4.22)$$

The turbulent kinetic energy *k* is defined as one-half of the trace of the Reynolds stress tensor.

$$k=\frac{1}{2}\widetilde{u'_\iota u'_\iota} \ldots\ldots\ldots\ldots (4.23)$$

$C_\mu$ is a model constant matches the specific flow and the dissipation of turbulent kinetic energy.

$S_{ij}$ is mean strain rate tensor and it is given by:

$$S_{ij}=\frac{1}{2}\left(\frac{\partial \tilde{u_\iota}}{\partial x_j}+\frac{\partial \tilde{u_J}}{\partial x_i}\right) \ldots\ldots\ldots\ldots (4.24)$$

$$c_\eta=\frac{\eta\left(1-{}^{\eta}/_{\eta_0}\right)}{1+\beta\eta^3} \quad \ldots\ldots\ldots\ldots\ldots\ldots (4.25)$$

Where

$$\eta=\frac{S\,k}{\varepsilon} \quad \ldots\ldots\ldots\ldots\ldots\ldots (4.26)$$

The terms $D_t$ and $K_t$ are introduced to describe the turbulence impact on mass and energy transport,. They are defined as:

$$D_t = \left(\frac{1}{Sc_t}\right)\mu_t \quad \text{..... (4.267)}$$

and

$$K_t = \left(\frac{1}{Pr_c}\right)\mu_t\, C_{p'} \quad \text{..... (4.28)}$$

Here, $Sc_t$ is the turbulent Schmidt number, $Pr_t$ is the turbulent Prandtl number, $D_t$ represents the turbulent diffusivity, and $K_t$ denotes the turbulent thermal conductivity. The source term $\overline{S_s}$ arises from spray-flow interactions, and the values of the model constants are determined based on experimental studies.

**Table 4.1** Values of the constants used in the RNG k–ε turbulence model

| Constant | $c_{\varepsilon 1}$ | $c_{\varepsilon 2}$ | $c_{\varepsilon 3}$ | $c_s$ | $c_{ps}$ | $\mathrm{Pr}_k$ | $\mathrm{Pr}_\varepsilon$ | $\eta_0$ | $\beta$ | $c_\mu$ |
|---|---|---|---|---|---|---|---|---|---|---|
| RGN k-ε | 1.42 | 1.68 | -1.0 | 1.5 | 0.164 | 0.71 | 0.719 | 4.38 | 0.012 | 0.084 |

### 4.2.4 Liquid Phase Equations

In diesel engines with direct injection system, the fuel is introduced into the combustion chamber through an injector. The liquid jet emerging from the injector orifice atomizes and breaks up into fine droplets that can evaporate easily, thereby promoting efficient air-fuel mixing and combustion. The transformation of the liquid jet into a spray (a cloud of droplets) is known as atomisation**.**

Atomisation follows two phases. The primary breakup of the jet produces droplets directly from the liquid column, while the secondary breakup further divides these primary droplets into smaller ones. Once injected into the cylinder, the droplets may undergo several processes, including atomisation, collision, and evaporation. Consequently, it is necessary to employ models that designate the fuel injection phenomena, namely atomisation, collision, and evaporation.

The evolution of the spray over time is obtained by solving the following equation:

$$\frac{\partial f}{\partial t} + div_{\vec{x}}(f\vec{v}) + div_{\vec{v}}(f\vec{F}) + \frac{\partial}{\partial r}(fR) + \frac{\partial}{\partial T_d}(f\dot{T_d}) + \frac{\partial}{\partial y}(f\dot{y}) + \frac{\partial}{\partial \dot{y}}(f\ddot{y}) = \dot{f}_{coll} + \dot{f}_{bu}$$

..... (4.29)

In this equation, $f$ represents the probability density function. The quantities $F$, $R$,$\dot{T_d}$ $\ddot{y}$ denote the time rates of change of an individual droplet's velocity, radius, temperature, and oscillation velocity, respectively. The source terms $\dot{f}_{coll}$ and $\dot{f}_{bu}$correspond to the effects of droplet collisions and breakup.

The breakup source term $\dot{f}_{bu}$ takes the following form:

$$\dot{f}_{bu} = \int f(\vec{x},\vec{v}_1,r_1,T_{d1},\dot{y}_1,t)\dot{y}_1 B(\vec{v}_1,r,T_d,\dot{y}_1,\vec{x},t)d\vec{v}_1\, d_{r1}\, dT_{d1}\, d\dot{y}_1 \quad \text{.....(4.30)}$$

The collision source term $\dot{f}_{coll}$ is expressed as:

$$\dot{f}_{coll} = \frac{1}{2}\iint f(\vec{x},\vec{v}_1,r_1,T_{d1},\dot{y}_1,t) f(\vec{x},\vec{v}_2,r_2,T_{d2},\dot{y}_2,t)\pi(r_1-r_2)^2\left|\vec{v}_1-\vec{v}_2\right|$$
$$\left[(\sigma(\vec{v},r,T_d,y,\dot{y},\vec{v}_1,r_1,T_{d1},y_1,\dot{y}_1,\vec{v}_2,r_2,T_{d2},y_2,\dot{y}_2))(-\delta(\vec{v}-\vec{v}_1)\delta(r-r_1)\right.$$
$$\left.\delta(T_d-T_{d1})\delta(y-y_1)\delta(\dot{y}-\dot{y}_1))\right]-\delta(\vec{v}-\vec{v}_2)\delta(r-r_2)\delta(T_d-T_{d2})\delta(y-y_2)$$
$$\delta(\dot{y}-\dot{y}_2)\times(d\vec{v}_1 dr_1 dT_{d1} dy_1 d\dot{y}_1 d\vec{v}_2 dr_2 dT_{d2} dy_2 d\dot{y}_2) \quad \text{……(4.31)}$$

### 4.2.4.1 Atomisation Models

In CONVERGE v2.3, several models are available to describe jet atomization. These include models based on the growth of disturbance waves generated at the injector outlet, such as the Kelvin–Helmholtz (KH) and Rayleigh–Taylor (RT) models, as well as those based on the amplification of droplet oscillation or deformation caused by aerodynamic effects. Although these models primarily address secondary droplet breakup, they are also employed in CONVERGE to simulate primary jet atomization.

Among these, the KH–RT (Kelvin–Helmholtz/Rayleigh–Taylor) model provides the initial conditions for atomization by accounting for both KH and RT instabilities.

In the present study, the KH–RT model was adopted due to the high Weber number conditions and its ability to simulate the two breakup mechanisms independently. Moreover, this model is widely used in the literature for modelling diesel spray atomisation.

- **KH Model**

The physics of atomization at high Weber numbers is highly complex. According to Reitz (1987) , this primary breakup model assumes that atomization results from the development of Kelvin–Helmholtz (KH) type surface instabilities at the injector exit. Based on the linear instability theory, Reitz derived expressions for the wavelength $\Lambda_{KH}$ and growth rate $\Omega_{KH}$ of the fastest-growing wave. As functions of the dimensionless parameters of the problem, these correlations are given as follows:

$$\frac{\Lambda_{KH}}{r_0} = 9.02\frac{(1+0.45Z_l^{0.5})(1+0.4T^{0.7})}{(1+0.87We_g^{1.67})^{0.6}} \quad \text{……(4.32)}$$

$$\Omega_{KH}\left[\frac{\rho_l r_0^3}{\sigma}\right]^{0.5} = \frac{(0.34+0.38We_g^{1.5})}{(1+Z_l)(1+1.4T^{0.6})} \quad \text{……..(4.33)}$$

where

$$T = Z_l\sqrt{We_g}\text{ (Taylor number)},\ Z_l = \sqrt{\frac{We_l}{Re_l}}\text{ (Ohnesorge number)}$$

$$We_g = \frac{\rho_g U^2 r_0}{\sigma}\text{ (Gas Weber number)},\ We_l = \frac{\rho_l U^2 r_0}{\sigma}\text{ (liquid Weber number)}$$

$$Re_l = \frac{U r_0}{v_l}\text{ (Liquid Reynolds number).}$$

In the KH model, the droplet radius *r* obtained after a breakup time $\tau_{KH}$ is given by:

$$r = B_0\Lambda_{KH} \quad \ldots\ldots\ldots\ldots\ldots(4.34)$$

And

$$\tau_{KH} = \frac{3.726\,B_1 r_0}{\Lambda_{KH}\Omega_{KH}} \quad \ldots\ldots\ldots\ldots..(4.35)$$

Here, $B_0$ is a constant taken as 0.61, while $B_1$ depends on the level of initial perturbations in the liquid jet and varies from one injector to another. Reitz fixed this constant, which depends on the injector geometry, at 10, while in CONVERGE, typical values range between 5 and 100. During the breakup process, the droplet radius (initially equal $r_0$) decreases until it reaches the stable radius $r_1$, according to the following relation:

$$\frac{dr_0}{dt} = -\frac{(r_0 - r)}{\tau_{KH}},\ r \leq r_0$$

- **RT Model**

The Rayleigh-Taylor (RT) model operates in a slightly different manner. The wavelength $\Lambda_{RT}$ and growth rate $\Omega_{RT}$ of the instability wave, as functions of the dimensionless parameters:

$$\Lambda_{RT} = 2\pi\sqrt{\frac{3\sigma}{a(\rho_l - \rho_g)}} \quad \ldots\ldots\ldots\ldots\ldots\ldots(4.36)$$

$$\Omega_{RT} = \sqrt{\frac{2}{3\sqrt{3\sigma}}\frac{[a(\rho_l - \rho_g)]^{3/2}}{\rho_l + \rho_g}} \quad \ldots\ldots\ldots\ldots(4.37)$$

When the hybrid KH–RT model is activated, the breakup length $L_b$ can be expressed as:

$$L_b = C_{bl}\sqrt{\frac{\rho_l}{\rho_g}}d_0 \quad \ldots\ldots\ldots\ldots\ldots(4.38)$$

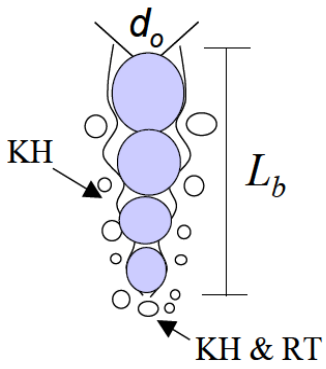


**Figure 4.2** Schematic of the KH–RT spray breakup model.

### 4.2.4.2 Evaporation

For droplet evaporation modelling, the energy flux at the droplet surface, with droplet temperature as the variable, can be expressed as:

$$4\pi r^2 \dot{Q}_d = \rho_d \frac{4}{3}\pi r^3 C_{p,l} \dot{T}_d - \rho_d 4\pi r^2 RL(T_d) \quad \text{..... (4.39)}$$

$\dot{Q}_d$ The rate of heat conduction is given by the Ranz–Marshall correlation:

$$\dot{Q}_d = \frac{K_{air}(\hat{T})(T - T_d)}{2r} Nu_d \quad \text{.....(4.40)} \qquad \text{with} \qquad \hat{T} = \frac{2}{3}T_d + \frac{1}{3}T \quad \text{.....(4.41)}$$

The convective heat transfer from the droplet is represented by the Nusselt number:

$$Nu_d = \left(2 + 0.6\,\mathrm{Re}_d^{1/2}\,\mathrm{Pr}_d^{1/3}\right)\frac{\ln(1+B_d)}{B_d} \quad \text{..... (4.42)}$$

where *Re* and *Pr* are the Reynolds and Prandtl numbers, respectively, *L* is the latent heat of vaporization**,** and the Spalding mass transfer number is defined as:

$$B_d = \frac{Y_1^* - Y_1}{1 - Y_1^*} \quad \text{.....(4.43)}$$

$Y_1^*$ denotes the mass fraction of vapor at the droplet surface, and $Y_1$ represents the vapor mass fraction in the surrounding gas.

In CONVERGE, the time rate of change of droplet radius due to vaporization is calculated using the Frössling correlation (Amsden et al., 1989)

$$\frac{dr}{dt} = -\frac{\rho_g D}{2\rho_L r} B_d Sh_d \quad \text{.....(4.44)}$$

where *D* is the diffusion coefficient of the vaporized liquid in air.

The Sherwood number, $Sh_D$ is defined as:

$$Sh_d = \left(2.0 + 0.6\, Re_d^{1/2} Sc^{1/3}\right) \frac{ln(1+B_d)}{B_d} \quad \text{.....(4.45)}$$

The $Y_1^*$ vapor mass fraction at the droplet surface, is given by:

$$Y_1^* = \frac{M_{C_n H_{2m}}}{M_{C_n H_{2m}} + M_{mix}\left(\frac{P_{gas}}{P_v} - 1\right)} \quad \text{.....(4.46)}$$

where $M_{mix}$ is the molar mass of the gas mixture, $P_{gas}$ is the ambient gas pressure, and $P_v$ is the vapor pressure at the droplet temperature.

And $Sc = \frac{\mu_{air}}{\rho_{air} D}$

Finally, R represents the rate of change of droplet radius, defined using the Frössling correlation (Amsden et al., 1989):

$$R = -\frac{(\rho D)_{air}(\hat{T})}{2\rho_d r} B_d Sh_d \quad \text{.....(4.47)}$$

### 4.2.5 Turbulent Combustion Modelling

Turbulent combustion involves complex interactions between turbulence and chemical reactions. Classical turbulence equations for statistical moments are not closed, requiring closure assumptions to relate higher-order moments to lower-order ones. These assumptions, often empirical, allow modelling of mean reaction rates while accounting for turbulence effects on chemical kinetics.

CONVERGE 2.4 offers several turbulent combustion models that express mean reaction rates based on averaged variables (temperature, species mass fractions) and turbulence properties. Source terms in species transport equations are usually evaluated using Arrhenius expressions, with predefined reaction mechanisms.

**Table 4.2** Turbulent combustion models in CONVERGE CFD

| Model | Solver | Applicable Combustion Type | Key Features |
|---|---|---|---|
| **SAGE** | Detailed Chemical Kinetics | Premixed & Non-Premixed | Solves full chemical mechanisms; high accuracy for complex fuels like biodiesel; computationally expensive. |
| **CEQ** | Chemical Equilibrium Solver | Premixed & Non-Premixed | Assumes local chemical equilibrium; simple and computationally efficient; not suitable for transient kinetics. |
| **FGM** | Flamelet Generated Manifold | Premixed & Non-Premixed | Uses precomputed flamelets to reduce computational cost; captures turbulence–chemistry interactions efficiently. |
| **G-Equation** | Level-Set Flame Front Solver | Premixed | Tracks flame front propagation using turbulence deformation; efficient for premixed flames. |
| **ECFM** | Extended Coherent Flamelet Model | Premixed | Models partially turbulent premixed flames; considers coherent flame structures; balances accuracy and cost. |
| **ECFM3Z** | 3-Zone Extended Coherent Flamelet | Non-Premixed | Subdivides domain into three zones; suitable for non-premixed flames; improves accuracy while managing computational cost. |
| **CTC** | Shell + Characteristic Time Combustion | Non-Premixed | Relates reaction rate to characteristic time; widely used for diesel and biodiesel combustion; good accuracy vs. cost. |
| **RIF** | Representative Interactive Flamelet | Non-Premixed | Treats turbulent diffusion flames as ensembles of thin laminar flamelets; captures fine-scale turbulence-chemistry effects. |

To simulate the combustion process of the fuel SAGE Model is adopted here .

The SAGE approach models combustion using detailed chemical kinetics, where a set of elementary chemical reactions, called a reaction mechanism, describes the combustion process in detail rather than as a single global reaction. The SAGE predicts the reaction rates for each elementary reaction, while the CFD solver simultaneously resolves the transport equations.

The general form of an elementary reaction is:

$$\sum_{m=1}^{M} \nu'_{m,r} X_m \Leftrightarrow \sum_{m=1}^{M} \nu''_{m,r} X_m \quad , r = 1,2, \dots R \quad \text{.....(4.48)}$$

where:

- $\nu'_{m,r}$ and $\nu''_{m,r}$ are the stoichiometric coefficients of reactants and products,
- *m* represents the species index,
- *r* represents the reaction index,
- *R* is the total number of reactions, and
- $X_m$is the chemical symbol of species *m*.

The net production rate of species m is given by:

$$\dot{\omega}_m = \sum_{r=1}^{R} \nu_{m,r} q_r \quad , m = 1,2, \dots M \quad \text{.....(4.49)}$$

where *M* is the total number of species,

$$\nu_{m,r} = \nu''_{m,r} - \nu'_{m,r} \quad \text{.....(4.50)}$$

And The reaction progress variable $q_r$for reaction r is:

$$q_r = k_{fr} \prod_{m=1}^{M} [X_m]^{\nu'_{m,r}} - \nu k_{rr} \prod_{m=1}^{M} [X_m]^{\nu''_{m,r}} \quad \text{.....(4.51)}$$

where $[X_m]$ is the molar concentration of species *m*, and $k_{fr}$ and $k_{rr}$ are the forward and reverse reaction rate coefficients, respectively.

The forward reaction rate follows an Arrhenius form:

$$K_{fr} = A_r T^{b_r} e^{\left(-\frac{E_r}{R_u T}\right)} \quad \text{.....(4.52)}$$

where:

- $A_r$is the pre-exponential factor,
- $b_r$ is the temperature exponent,
- $E_r$ is the activation energy, and
- *Ru* is the universal gas constant.

The reverse reaction rate can be specified similarly or calculated from the equilibrium constant $K_{cr}$ :

$$K_{rr} = \frac{k_{fr}}{K_{cr}} \quad \text{.....(4.53)}$$

Where $K_{cr}$ is determined from thermodynamic properties**.**

With these definitions, the mass and energy conservation equations for each computational cell can be solved:

$$\frac{d[X]}{dt} = \dot{\omega}_m \quad \text{..... (4.54)}$$

This formulation allows SAGE to capture detailed species evolution and reaction kinetics in both premixed and non-premixed flames, providing high-fidelity combustion modelling for complex fuels such as biodiesel.

In this study, we used a reduced mechanism that contains 69 species and 192 reactions developed by Brakora et al.,( 2012)

### 4.2.6 Heat transfer model

Heat transfer occurs continuously during engine operation.To model this process in CONVERGE, the O′Rourke and Amsden model was employed. The heat transfer behaviour can be described using these expressions:

$$k(dT/dx_i) = \begin{cases} \mu c_p (T_b - T_a) n_i / y Pr_t & , \ y^+ < 11.05 \\ \left[\rho c_p \mu_\tau T_b \ln(T_b/T_a) n_i\right] / [2.1 \cdot \ln(y^+) + 2.513] & , \ y^+ > 11.05 \end{cases} \quad \text{..... (4.55)}$$

Where *k* is the coefficient of conductivity of the molecule, $T_b$ (K) is the temperature of the wall, Pr is the Prandtl number of the molecule, $T_a$ (K) is the temperature of the liquid, $\mu_\tau$ is the shear speed, $y^+$ is the dimensionless distance.

### 4.2.7 Pollutant Formation Models

- **NOx Formation Model**

Heywood (1988) described the extended Zel'dovich mechanism. It is used to model the formation of NO during high-temperature combustion. Nitrogen oxides ($NO_x$, primarily NO and $NO_2$) are generated in engines under these conditions. The mechanism involves the following reactions (4.56):

$$N + NO \longleftrightarrow N2 + O$$

$$O + NO \xleftrightarrow{k_2} O2 + N \quad \text{.....(4.56)}$$

$$N + OH \xleftrightarrow{k_3} NO + H$$

$k_1$, $k_2$ et $k_3$ are the forward and reverse reaction rate constants given by:

$$k_{1f} = 7.6 * 10^{13} \exp[-38000/T] \quad \ldots\ldots\ldots\ldots(4.57)$$

$$k_{1b} = 1.6 * 10^{13} \quad \ldots\ldots\ldots\ldots\ldots\ldots(4.58)$$

$$k_{1f} = 6.4 * 10^{9} T * \exp[-3150/T] \quad \ldots\ldots\ldots\ldots(4.59)$$

$$k_{1b} = 1.5 * 10^{9} T * \exp[-19500/T] \quad \ldots\ldots\ldots\ldots\ldots (4.60)$$

$$k_{1f} = 4.1 * 10^{13} \ldots\ldots\ldots\ldots\ldots\ldots (4.61)$$

$$k_{1b} = 2.0 * 10^{14} * \exp[-23650/T] \quad (4.62)$$

$$\frac{d[NO]}{dt} = \frac{2R\left\{1-\left([NO]/[NO]_e\right)^2\right\}}{1+\left([NO]/[NO]_e\right)R_1/(R_2+R_3)} \quad (4.63)$$

Equilibrium concentrations are denoted by $[\,]_e$

$$R_1 = K_1^f [O]_e [N_2]_e = K_1^r [NO]_e [N]_e$$

$$R_2 = K_2^f [N]_e [O_2]_e = K_2^r [NO]_e [O]_e$$

$$R_3 = K_3^f [NO]_e [H]_e = K_3^r [OH]_e [N]_e$$

- **Soot Formation Model (Hiroyasu-NSC)**

The soot concentration at the exhaust is governed by soot formation and oxidation**,** expressed as:

$$\frac{dm_s}{dt} = \frac{dm_{sf}}{dt} - \frac{dm_{so}}{dt} \quad \ldots\ldots\ldots(04.64)$$

The rates of soot formation and oxidation have been the subject of various models. The Hiroyasu model often used in multi-zone simulations, defines these rates as:

$$\frac{dm_{sf}}{dt} = A_f m_{fg} P^{0.5} \exp\left(\frac{-E_{sf}}{\bar{R}T}\right), \quad \text{Rate of formation}\ldots\ldots\ldots\ldots(4.65)$$

$$\frac{dm_{so}}{dt} = A_o m_s \frac{P_{ox}}{p} p^{1.8} \exp\left(\frac{-E_{so}}{\bar{R}T}\right), \text{ Rate of oxidation}\ldots\ldots\ldots\ldots(4.66)$$

where:

- $E_{sf} = 1.25 \times 10^4 \ Kcal \ / Kmol$ , $E_{so} = 1.40 \times 10^4 \ Kcal \ / \ Kmol$ are activation energies,
- $A_f$ et $A_0$ are constants determined experimentally,
- $m_{fg}$ is the mass of vaporized fuel,
- $m_s$ is the soot mass emitted at the exhaust.

For this work, we used the models outlined in the following table to simulate combustion within the combustion chamber of our diesel engine.

**Table 4.3** Model Selection

| Process | Model |
|---|---|
| Turbulence | RNG-ε |
| Combustion | SAGE |
| Spray | KH-RT |
| Heat transfer | O′Rourke and Amsden |
| NOx | Zeldovich |
| Soot | Hiroyasu |

## 4.3 Experimental scheme and verification

Main parameters and boundary conditions of diesel engine

### 4.3.1 Geometric specifications of the engine

To begin our numerical analysis in CONVERGE, initially, we focused on designing the combustion chamber with an asymmetric bowl (See Figure 4.3). This design process was executed in SOLIDWORKS , a CAD software. The geometric specifications of the engine are provided in the following table .

**Table 4.4** Geometric specifications of the modelled engine

| | | | |
|---|---|---|---|
| **Engine Geometry** | Displacement | cm³ | 744 |
| | Bore × Stroke | mm | 95 × 105 |
| | Compression ratio | — | 17.5:1 |

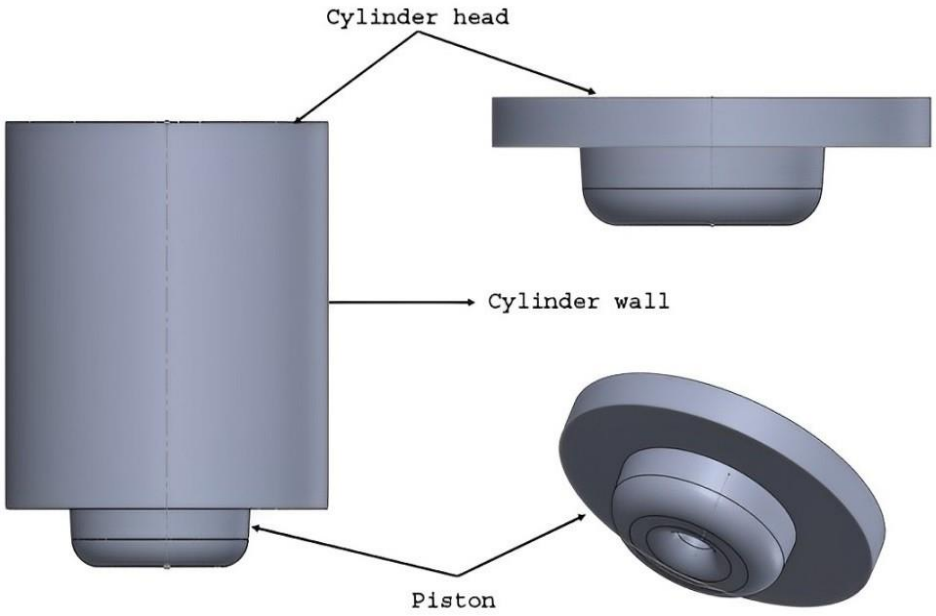


**Figure 4.3** 2D and 3D Views of the engine's combustion chamber

### 4.3.2 Injection System Specifications

In this simulation work, injection parameters were carefully defined, as the injection system plays a crucial role in governing fuel delivery and combustion efficiency. The injector position, nozzle geometry, and spray orientation significantly affect fuel atomization, mixing, and overall combustion characteristics.

The present setup in CONVERGE was configured to ensure accurate representation of the injection process. All relevant parameters, including injector location, nozzle direction, injection

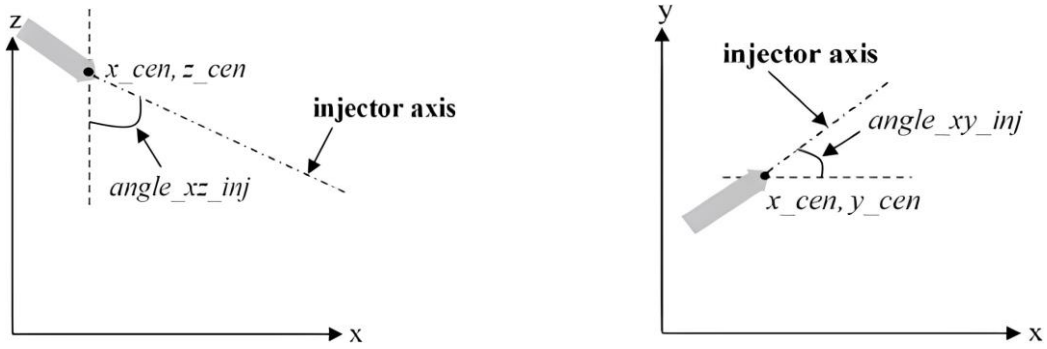


**Figure 4.4** Parameters for placement and orientation of injectors

profile, fuel quantity, and temperature, were precisely specified. Figures 4.4 and 4.5 illustrate the geometric configuration of the injection system, enabling accurate jet positioning and calibration within the computational domain.

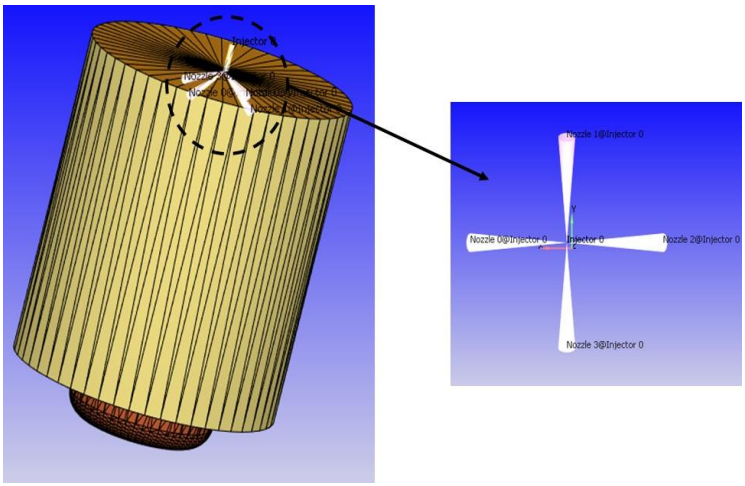


**Figure 4.5** Localization of Injector and Nozzles in CONVERGE.

### 4.3.3 Initial conditions and boundary conditions

In the initial conditions, the combustion chamber was assigned an initial pressure of 117,000 Pa and an initial temperature of 350 K.

We specified empirically the temperature boundary conditions, with the piston, cylinder head, and cylinder walls set at 543 K, 423 K, and 533 K, respectively.

The velocity boundary condition corresponds to the piston motion, defined by the actual piston speed during operation.

### 4.3.4 Fuel characteristics

In this modelling case the waste cooking oil biodiesel blended with diesel was considered as the engine fuel. Notably, the neat biodiesel (B100) is primarily composed of five major components, with their chemical formulas and volume fractions presented in Table 4.5. In addition, diesel (D100) and biodiesel–diesel blend containing 30% biodiesel (denoted as B30) was used. Further details on the preparation and composition of these blends are provided in Chapter 2. The key fuel properties are summarized in Table 4.6.

**Table 4.5** Chemical formula and mass fraction of the five components of WCBio (B100)

| Components | Chemical formula | wt% |
|---|---|---|
| Methyl palmitate | $C_{17}H_{34}O_2$ | 12.72 |
| Methyl stearate | $C_{19}H_{38}O_2$ | 4.14 |
| Methyl oleate | $C_{19}H_{36}O_2$ | 28.44 |
| Methyl linoleate | $C_{19}H_{34}O_2$ | 49.82 |
| Methyl linolenate | $C_{19}H_{32}O_2$ | 4.88 |

**Table 4.6** Blends properties compared to conventional diesel.

| | unit | B30 | Diesel |
|---|---|---|---|
| **Density at 15°C** | - | 0.845 | 0.822 |
| **Viscosity at 40 °C** | mPa/s | 2.04 | 1.356 |
| **Cetane index** | - | 54.5 | 47 - 50 |
| **LHV** | MJ/Kg | 42.831 | 45.20 |

### 4.3.5 Mesh Generation and Grid Strategy

Grid resolution is a key factor in accurately capturing spray development, evaporation, and combustion in CFD simulations of internal combustion engines. In this study, simulations were performed using CONVERGE CFD, which utilizes an orthogonal Cartesian mesh combined with Adaptive Mesh Refinement (AMR) to dynamically increase resolution in regions with complex flow features.

A base grid of 4 mm was applied across the computational domain. Due to piston motion, the total number of computational cells varied throughout the engine cycle, reaching approximately 449,121 cells at bottom dead center (BDC, 180 CAD) and decreasing to around 8,156 cells at top dead center (TDC, 0 CAD).

Instead of a conventional static grid-independence study, numerical accuracy was maintained via the AMR strategy. As illustrated in Figure 4.6, the mesh was automatically refined in the injector nozzle, active combustion zones, the piston-head clearance region, and close to the

cylinder walls. These regions with excessive gradients of velocity, temperature, and species concentration.

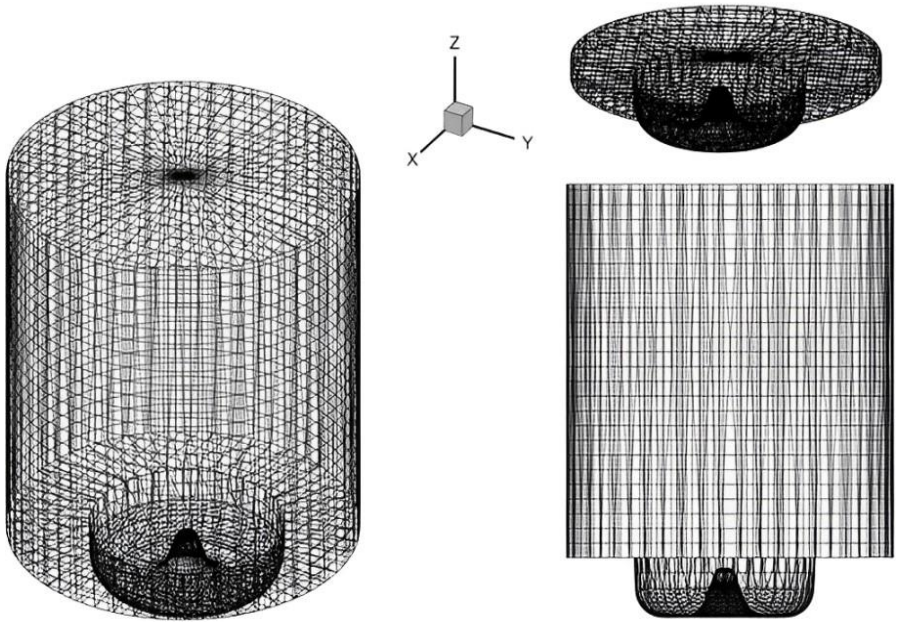


**Figure 4.6** Overview of the mesh of the combustion chamber.

The present simulations were done in the LTE laboratory (Environmental Technology Research Laboratory). We used a 64-bit Windows-based machine (Z400 workstation), featuring a 3.2 GHz CPU, 8 GB of RAM, and a graphics card with 4 GB capacity.

The average computational time for diesel and B30 simulations was respectively, 23h11m and 56h29m; a balanced trade-off between numerical accuracy and computational cost.

### 4.3.6 Model validation

Model validation was conducted by comparing experimentally measured exhaust gas temperature (EGT) with CFD-predicted in-cylinder temperature. A direct quantitative comparison is not possible, as these quantities correspond to different locations and thermodynamic states. Consequently, validation is based on expected temperature hierarchy and qualitative trends supported by established engine theory.

According to Heywood (2018), the mass-averaged in-cylinder gas temperature during the exhaust process is typically 200–300 K higher than the mass-averaged exhaust port temperature, due to gas expansion, heat transfer to the walls, and mixing effects.

As shown in Figure 4.7, the simulated in-cylinder temperature decreases significantly during the expansion and exhaust strokes for both diesel fuel and the B30 blend, whereas the experimentally measured EGT remains substantially lower, which is consistent with diesel exhaust

thermodynamics described in the literature. Furthermore, both CFD and experimental results exhibit the same fuel-dependent trend, with neat diesel showing higher temperatures than B30, reflecting the lower heating value of the biodiesel blend.

Although this validation is qualitative in nature, the correct temperature ordering between in-cylinder and exhaust gases, together with consistent fuel trends, confirms that the combustion and heat transfer processes are physically well represented by the numerical model.

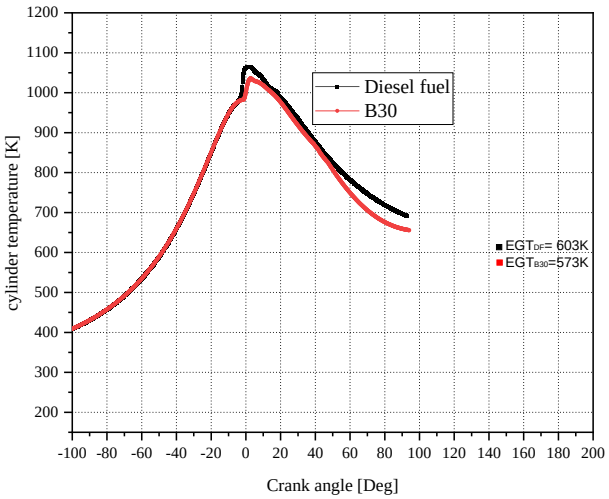


**Figure 4.7** Experimentally measured exhaust gas temperature (EGT) and CFD-predicted in-cylinder temperature profiles for diesel fuel and B30 at 50% engine load.

## 4.4 Simulations results and discussion

This section presents CFD simulation results for a diesel engine fuelled with B30 waste cooking oil biodiesel-diesel blend at medium load. Engine performance, combustion behaviour, and emission characteristics are analysed using the previously described model.

### 4.4.1 Combustion characteristics

#### 4.4.1.1 Cylinder pressure

The in-cylinder pressure variation for diesel fuel and the B30 waste cooking oil biodiesel blend at 50% load is illustrated in Figure 4.8. Both fuels exhibit similar pressure evolution during compression and expansion, indicating stable combustion under the selected operating condition. Peak pressure occurs close to top dead center in both cases, confirming proper ignition timing. However, B30 produces a slightly lower peak pressure than diesel, mainly due to its lower heating value and higher viscosity, which reduce the intensity of premixed combustion

despite the oxygenated nature of the fuel. The close overlap of the pressure traces before ignition suggests a negligible influence of fuel type on the compression process, while the small deviation near peak pressure reflects differences in heat release behavior.

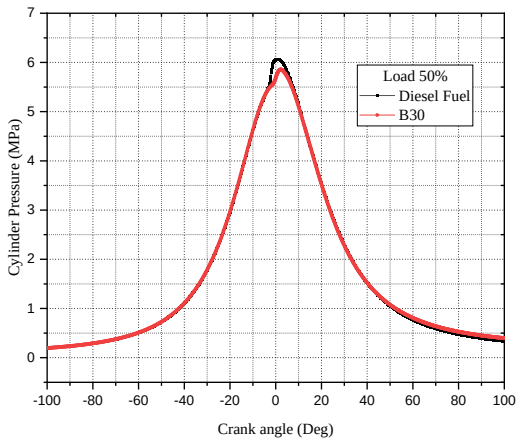


**Figure 4.8** cylinder pressure evolution at medium load for Biodiesel and Diesel fuel

#### 4.4.1.2 Heat release rate

The heat release rate profiles at 50% load in figure 4.9 show the typical two-stage combustion behavior for both diesel and the B30 blend. Diesel exhibits a sharper premixed combustion peak near TDC, indicating a larger fuel fraction accumulated during ignition delay. In contrast, B30 shows a lower and wider premixed peak, which can be attributed to its higher viscosity and lower volatility (Zhang et al., 2018). During the diffusion phase, B30 presents a more sustained heat release, reflecting the contribution of fuel-bound oxygen and smoother combustion. This behaviour is consistent with the lower peak pressure for the B30 blend in figure 4.7.

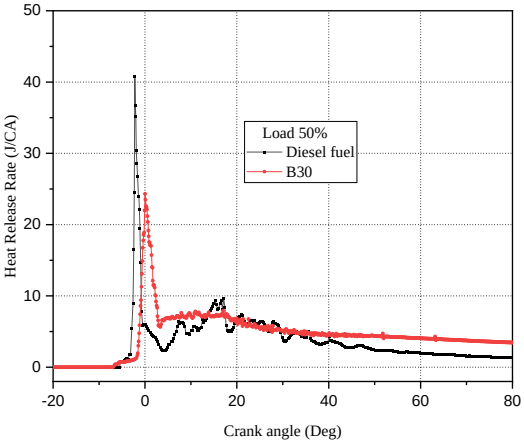


**Figure 4.9** Heat release rate evolution at medium load

### 4.4.1.3 Combustion duration and ignition delay

The fuels tested affect the combustion duration as shown in figure 4.10. Diesel fuel exhibited a combustion duration of 137.769°CA, while a marginally shorter duration of 136.52°CA was observed for the B30 blend. The reduced combustion duration of B30 can be associated with its higher cetane number, which promotes earlier ignition and a more rapid transition from pre-mixed to diffusion combustion (Can, 2014). This leads to a more controlled heat release and a faster completion of combustion.

Although biodiesel generally has higher viscosity and boiling point, which can slow down spray breakup and evaporation, the oxygenated nature of biodiesel enhances combustion efficiency, compensating for these physical limitations.

Then the impact of fuel on ignition delay is illustrated in figure 4.11. Ignition delay is a critical parameter in the combustion process. In the present study, B30 exhibited a shorter ignition delay than conventional diesel fuel. This behaviour is mainly attributed to the higher cetane number and oxygenated nature of biodiesel. Although biodiesel blends generally exhibit higher viscosity, it contains a small fraction of high-boiling components, such as diglycerides; under high in-cylinder temperatures, these high molecular weight ester compounds undergo thermal decomposition during injection. This process generates lighter, more volatile species that rapidly vaporize at the spray periphery, enhancing jet dispersion and air–fuel interaction. As a result, the formation of reactive combustion intermediates is accelerated, leading to earlier auto-ignition and a shorter ignition delay (Buyukkaya, 2010).

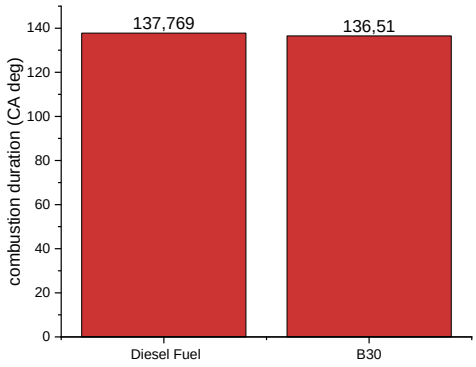


**Figure 4.10** impact of diesel fuel and B30 on combustion duration.

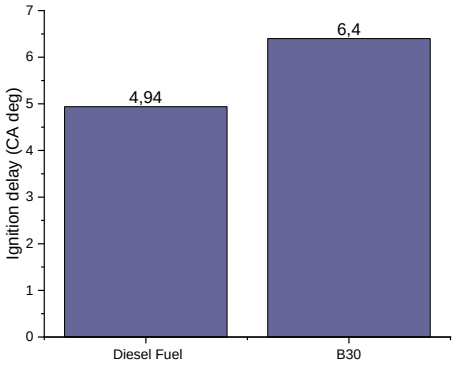


**Figure 4.11** Ignition delay of tested fuels on diesel engine at 1800 rpm and medium load.

### 4.4.2 Emission characteristics

#### 4.4.2.1 CO emissions

As depicted in figure 4.12, CO formation starts shortly after ignition for both fuels and increases rapidly during the early combustion phase. Overall, B30 shows slightly higher CO emissions than diesel, particularly during the late combustion period. This behaviour can be attributed to the higher viscosity and slower evaporation of biodiesel, which may lead to locally rich regions and incomplete oxidation despite its inherent oxygen content. The results are consistent with the experimental trends and indicate that CO emissions with B30 remain comparable to diesel under medium-load conditions (see figure 3.11).

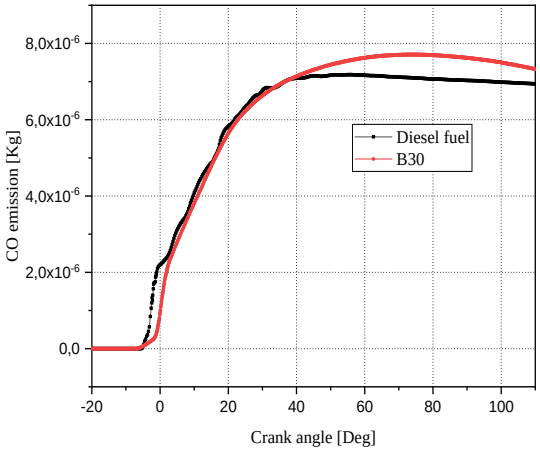


**Figure 4.12** Co emissions profiles at 50% load

#### 4.4.2.2 HC (unburned hydrocarbons) emissions

Figure 4.13 shows clear differences in their combustion characteristics for diesel and the B30 biodiesel blend in term of HC emissions. Both fuels display negligible HC levels before combustion begins, followed by a sharp rise after TDC, with B30 exhibiting a slightly earlier and higher peak due to its shorter ignition delay, higher viscosity and slower evaporation. However, during the expansion stroke, B30 consistently maintains lower HC levels than diesel, reflecting the blend's enhanced oxidation supported by its inherent oxygen content. Overall, although B30 produces a brief early increase in HC, it achieves lower residual emissions and demonstrates cleaner combustion compared with conventional diesel which is consistent with many studies (Loo et al., 2021;Sethuraman et al., 2023).

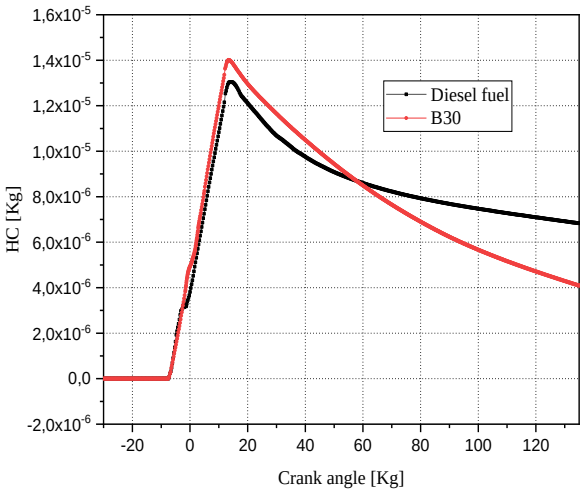


**Figure 4.13** HC emissions variations with crank angle degree at medium load

#### 4.4.2.3 Soot emissions

The applied model is capable of predicting soot emissions from an internal combustion engine operating on both diesel and biodiesel fuels. Figure 4.14 illustrates the crank-angle–resolved variation of soot emissions, showing that the B30 blend produces higher soot levels than conventional diesel at 50% engine load. This behavior is mainly attributed to the higher viscosity of B30, which adversely affects fuel spray formation and atomization, leading to increased soot formation. These findings are in agreement with the study of Wu et al. (2009), who reported that at high engine loads, fuel oxygen content has a more pronounced influence on soot emissions than viscosity, resulting in reduced soot formation with increasing oxygen content. Conversely, under low and mid-load conditions, differences in fuel viscosity become the dominant factor governing soot emissions.

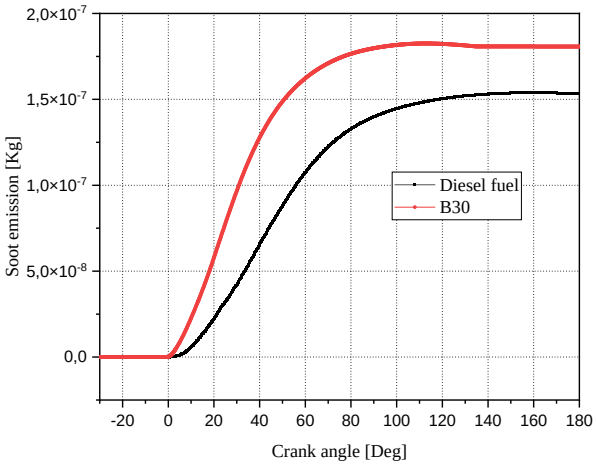


**Figure 4.14** Soot emissions variations with crank angle at medium load.

## 4.5 Conclusion

Chapter 4 presented the modelling study of IC engine performance and emissions using waste cooking oil biodiesel (B30) and conventional diesel. The chapter detailed the experimental scheme, boundary conditions, geometry, mesh generation, and the validation of the model against experimental data.

The results and discussion highlighted the influence of fuel type on key combustion characteristics, including ignition delay, combustion duration, in-cylinder pressure, and heat release rate (HHR). Emissions analysis focused on CO, HC, and soot formation.

The modeling provided a comprehensive dataset, extending beyond the experimental measurements, and captured the complex combustion phenomena effectively. Overall, B30 demonstrated good combustion performance and acceptable emissions characteristics, consistent with previous studies reported in the literature, confirming its potential as an alternative fuel in internal combustion engines.

# General conclusion and future perspectives

## 5.1 Conclusion

This thesis demonstrates that waste cooking oil (WCO) is a technically and environmentally promising feedstock for producing advanced alternative fuels. Its use directly contributes to addressing global challenges such as rising energy demand, fossil fuel depletion, climate change, and inefficient waste management practices. At the same time, it responds to specific issues related to the disposal of used oils and the environmental impacts associated with their uncontrolled release. Unlike biodiesel produced from edible oils, WCO-based biodiesel avoids the food-versus-fuel dilemma and supports principles of circularity and sustainable energy.

The main objectives of this work were to produce high-quality biodiesel from WCO, to optimize its production through transesterification, to characterize the resulting fuel according to international standards, and to evaluate its engine performance and emissions. Complementary combustion modelling using CONVERGE CFD was also initiated to enhance the understanding of in-cylinder processes.

Although transesterification is widely used, its efficiency is strongly influenced by the characteristics of the feedstock. This research therefore emphasises the critical importance of upstream stages (collection, storage, and pretreatment) which are often overlooked in the literature. The locally collected WCO exhibited significant variability in free fatty acid content, moisture, density, viscosity, and sensory properties (colour and odour). These variations were linked to frying conditions, exposure to air and light, moisture uptake, and inadequate storage practices. Through detailed assessment and appropriate pretreatment, including filtration and water removal, the oil was rendered suitable for base-catalysed transesterification.

Process optimisation formed a central component of this work. Base-catalysed transesterification with methanol proved effective, offering favourable reaction kinetics and facilitating alcohol recovery. Under the optimised conditions (methanol-to-oil molar ratio 6:1, 1% KOH catalyst, and 60 °C), the process yielded approximately 92% biodiesel. Subsequent purification by washing and centrifugation further improved fuel stability. The final product complied with major international standards, including EN 14214 and ASTM D6751.

This study clearly shows that the integration of careful pretreatment and controlled reaction conditions is essential for developing a clean, efficient, and economically viable production route. Together, these steps minimised soap formation, prevented catalyst neutralisation, avoided the need for excessive alcohol or catalyst quantities, reduced the number of washing cycles and overall water consumption, and improve the biodiesel quality.

Blending the produced biodiesel with petroleum diesel was found to be a practical pathway for immediate application. Biodiesel blends combine the environmental benefits of WCO-derived fuel (namely its lower sulphur content and higher oxygen levels) with the favourable cold-flow properties and higher energy density of conventional diesel. This results in a fuel fully compatible with existing diesel engines without requiring technical modifications.

Engine tests were conducted on a fully instrumented test bench following confirmation of biodiesel quality. The experimental programme applied a structured load–speed matrix, using commercial diesel as the baseline and applying identical operating conditions to biodiesel blends. Four load levels (25%, 50%, 75%, and 100%) and four engine speeds (1500, 1800, 2000, and 2300 rpm) were investigated. At each operating point, brake torque, brake power, brake-specific fuel consumption, exhaust gas temperature, and CO and $NO_x$ emissions were measured.

The results confirm that WCO-based biodiesel blends are viable substitutes for petroleum diesel, requiring no engine modification. As expected, the lower heating value of biodiesel led to slight reductions in power and torque and to a consistent increase in fuel consumption trends widely reported in the literature. However, two notable deviations were observed. First, $NO_x$ emissions decreased with increasing biodiesel proportion, contrary to the typical trend of $NO_x$ increase. Second, CO emissions increased slightly, despite biodiesel's oxygen content generally promoting CO reduction. These deviations may be attributed to the specific properties of the locally sourced WCO, the optimised transesterification conditions, and the influence of fuel viscosity and density.

Finally, the experimental engine results provide a robust foundation for the subsequent combustion modelling work mainly the essential validation data for CFD simulations. These simulations will enable a deeper exploration of spray behaviour, combustion dynamics, and pollutant formation, thereby complementing the experimental findings and supporting a more complete understanding of WCO-derived biodiesel combustion.

## 5.2 Perspectives

Building on the findings of this thesis, several research directions can be pursued to enhance the practical deployment, efficiency, and sustainability of WCO-derived biodiesel:

- Because this study was conducted at laboratory scale, it is also essential to examine scale-up effects. Developing a pilot unit would allow the process to be tested under industrially relevant mixing, heating, and separation conditions, and would help identify possible limitations. At this larger scale, operating parameters can safely exceed the laboratory limits; for example, higher reaction temperatures could be tested to improve conversion and yield.

- Although the applied filtration and water removal methods were effective, exploring alternative pretreatment technologies (adsorption, microwave-assisted dehydration, or enzymatic hydrolysis) may improve impurity removal.
- Further optimization could involve alternative catalysts (heterogeneous, enzymatic, or solid-base) to simplify post-processing, as well as advanced statistical and computational tools (RSM, neural networks, genetic algorithms) for multi-objective optimization.
- The integration of glycerol recovery and valorisation into the production chain should be explored. Upgrading this by-product and assessing its impacts through a full life cycle assessment (LCA) would offer a more complete view of the environmental and economic performance of WCO biodiesel.
- Further insight into the long-term behaviour of the fuel is needed. Since commercial deployment would involve storage, transport, and blending at fuel stations, future research should evaluate oxidation stability, storage stability, and cold-flow properties of both pure biodiesel and its blends.
- Engine-level investigations may also be deepened. The engine used in this work did not allow adjustment of injection timing, even though this parameter strongly affects combustion and emissions. Testing biodiesel blends on an engine with variable injection control would provide a more comprehensive evaluation. Similarly, the effect of fuel preheating for reducing viscosity and improving atomisation should be studied, especially for blends with higher biodiesel content.
- Engine evaluation should be extended to multi-cylinder, turbocharged engines. Long-duration endurance tests can assess deposit formation, wear, and performance under practical conditions. Comprehensive emissions analysis including HC, PM, and smoke opacity will provide a fuller understanding of environmental impacts.
- The modelling phase initiated in this work can be further developed by validating biodiesel surrogate mechanisms and performing parametric studies on injection pressure, timing, and boost conditions. CFD simulations offer insights into combustion optimization and pollutant formation that are difficult to capture experimentally.
- A detailed techno-economic analysis (TEA) and full life cycle assessment (LCA) of WCO biodiesel production are recommended to evaluate cost-effectiveness, environmental benefits, $CO_2$ reduction potential, energy balance, and waste valorisation, particularly in the Algerian context.

Finally, national strategies for WCO collection, decentralized biodiesel production units, and public awareness programs should be explored. Incentives and regulations supporting sustainable WCO valorisation are essential for scaling up and achieving meaningful environmental and energy benefits.

# References

Aarthy, M., Saravanan, P., Gowthaman, M. K., Rose, C., & Kamini, N. R. (2014). Enzymatic transester ification for production of biodiesel using yeast lipases: An overview. Chemical Engineering Research and Design, 92(8), 1591 1601. Available from https://doi.org/10.1016/j.cherd.2014.04.008.

Abbaszaadeh, A., Ghobadian, B., Omidkhah, M. R., & Najafi, G. (2012). Current biodiesel production technologies: A comparative review. Energy Conversion and Management, 63, 138 148. Available from https://doi.org/10.1016/j.enconman.2012.02.027.

Abd Rabu, R., Janajreh, I., & Honnery, D. (2013). Transesterification of waste cooking oil: Process optimization and conversion rate evaluation. Energy Conversion and Management, 65, 764–769. https://doi.org/10.1016/j.enconman.2012.02.031

Abed, K. A., El Morsi, A. K., Sayed, M. M., El Shaib, A. A., & Gad, M. S. (2018). Effect of waste cooking-oil biodiesel on performance and exhaust emissions of a diesel engine. Egyptian journal of petroleum, 27(4), 985-989.

Abomohra, A. E.-F., Wang, Q., & Huang, J. (Eds.). (2022). Waste-to Energy: Recent developments and future perspectives towards circular economy. Springer International Publishing. https://doi.org/10.1007/978-3-030-91570-4

Adenuga, A. A., Oyekunle, J. A. O., & Idowu, O. O. (2021). Pathway to reduce free fatty acid formation in Calophyllum inophyllum kernel oil: A renewable feedstock for biodiesel production. Journal of Cleaner Production, 316, 128222. https://doi.org/10.1016/j.jclepro.2021.128222

Adewale, P., Dumont, M. J., & Ngadi, M. (2015). Enzyme-catalyzed synthesis and kinetics of ultrasonic assisted methanolysis of waste choice white grease for fatty acid methyl ester production. Energy and Fuels, 29(10), 6412 6421. Available from https://doi.org/10.1021/acs.energyfuels.5b00849.

Adhikesavan, C., Ganesh, D., & Charles Augustin, V. (2022). Effect of quality of waste cooking oil on the properties of biodiesel, engine performance and emissions. Cleaner Chemical Engineering, 4(October), 100070. https://doi.org/10.1016/j.clce.2022.100070

Agarwal, A. K. (2007). Biofuels (alcohols and biodiesel) applications as fuels for internal combustion engines. Progress in Energy and Combustion Science, 33(3), 233–271. https://doi.org/10.1016/j.pecs.2006.08.003

Agarwal, D., Kumar, L., & Agarwal, A. K. (2008). Performance evaluation of a vegetable oil fuelled compression ignition engine. Renewable Energy, 33(6), 1147–1156. https://doi.org/10.1016/j.renene.2007.06.017

Agarwal, M., Chauhan, G., Chaurasia, S. P., & Singh, K. (2012). Study of catalytic behavior of KOH as homogeneous and heterogeneous catalyst for biodiesel production. Journal of the Taiwan Institute of Chemical Engineers, 43(1), 89–94. https://doi.org/10.1016/j.jtice.2011.06.003

Agence Nationale des Déchets. (2021). Rapport sur l'état de la gestion des déchets en Algérie. https://and.dz/rapport-sur-letat-de-la-gestion-des-dechets-en-algerie/

Al-Hamamre, Z., Yamin, J. (2014). Parametric study of the alkali catalyzed transesterification of waste frying oil for biodiesel production. Energy Conversion and Management, 79, 246–254. https://doi.org/10.1016/j.enconman.2013.12.027

Ali Ijaz Malik, M., Zeeshan, S., Khubaib, M., Ikram, A., Hussain, F., Yassin, H., & Qazi, A. (2024). A review of major trends, opportunities, and technical challenges in biodiesel production from waste sources. Energy Conversion and Management: X, 23(May), 100675. https://doi.org/10.1016/j.ecmx.2024.100675

Ali, M., & Akbar, N. (2020). Biofuel is a renewable environment friendly alternate energy source for the future. Modeling Earth Systems and Environment, 6(1), 557–565. https://doi.org/10.1007/s40808-019-00702-y

Alias, N. I., A/L JayaKumar, J. K., Md Zain, S. (2018). Characterization of waste cooking oil for biodiesel production. JurnalKejuruteraan, 2018(SI1(2)). https://doi.org/10.17576/jkukm-2018-si1(2)-10

Ambat, I., Srivastava, V., & Sillanpää, M. (2018). Recent advancement in biodiesel production methodol ogies using various feedstock: A review. Renewable and Sustainable Energy Reviews, 90, 356 369. Available from https://doi.org/10.1016/j.rser.2018.03.069.

Aransiola, E. F., Ojumu, T. V., Oyekola, O. O., Madzimbamuto, T. F., & Ikhu-Omoregbe, D. I. O. (2014). A review of current technology for biodiesel production: State of the art. Biomass and Bioenergy, 61, 276 297. Available from https://doi.org/10.1016/j.biombioe.2013.11.014.

Armas, O., Herna´ndez, J. J., & Ca´rdenas, M. D. (2006). Reduction of diesel smoke opacity from vegetable oil methyl esters during transient operation. Fuel, 85, 2427–2438.

Arous, S. A., Capone, R., Debs, P., Haddadi, Y., El Bilali, H., Bottalico, F., Hamidouche, M. (2017). Exploring household food waste issue in Algeria. Agrofor International Journal, 2(1), 55–67.

Arumugam, A. (2022). Biodiesel and its properties. In A. Arumugam (Ed.), Production of biodiesel from non-edible sources: Technological updates (pp. 25–58). Elsevier.

Atadashi, I. M., Aroua, M. K., Abdul Aziz, A. R., Sulaiman, N. M. N. (2011). The effects of catalysts in biodiesel production. Journal of Industrial and Engineering Chemistry, 19(1), 14–26.

Attaphong, C., Do, L., & Sabatini, D. A. (2012). Vegetable oil-based microemulsions using carboxylate based extended surfactants and their potential as an alternative renewable biofuel. Fuel, 94, 606 613. Available from https://doi.org/10.1016/j.fuel.2011.10.048.

Avhad, M. R., & Marchetti, J. M. (2015). A review on recent advancement in catalytic materials for bio diesel production. Renewable and Sustainable Energy Reviews, 50, 696 718. Available from https://doi. org/10.1016/j.rser.2015.05.038.

Awogbemi, O., Kallon, D. V. Von, Aigbodion, V. S., & Panda, S. (2021). Advances in biotechnological applications of waste cooking oil. Case Studies in Chemical and Environmental Engineering, 4, 100158. https://doi.org/10.1016/j.cscee.2021.100158

Aydin, H., & Bayindir, H. (2010). Performance and emission analysis of cottonseed oil methyl ester in a diesel engine. Renewable Energy, 35(3), 588–592. https://doi.org/10.1016/j.renene.2009.08.009

Ayetor, G., Sunnu, A., Parbey, J. (2015). Effect of biodiesel production parameters on viscosity and yield of methyl esters: Jatropha curcas, Elaeisguineensis, and Cocos nucifera. Alexandria Engineering Journal, 54(4), 1285–1290. https://doi.org/10.1016/j.aej.2015.09.011

Bae, C., Kim, J. (2017). Alternative fuels for internal combustion engines. Proceedings of the Combustion Institute, 36(3), 3389–3413. https://doi.org/10.1016/j.proci.2016.09.009

Bari, S., Hossain, S. N., Saad, I. (2020). A review on improving airflow characteristics inside the combustion chamber of CI engines to improve the performance with higher viscous biofuels. Fuel, 264, 116769. https://doi.org/10.1016/j.fuel.2019.116769

Bashir, M. A., Wu, S., Zhu, J., Krosuri, A., Khan, M. U., & Ndeddy Aka, R. J. (2022). Recent development of advanced processing technologies for biodiesel production: A critical review. Fuel Processing Technology, 227(October 2021), 107120. https://doi.org/10.1016/j.fuproc.2021.107120

Betiku, E., Okeleye, A. A., Ishola, N. B., Osunleke, A. S., & Ojumu, T. V. (2019). Development of a novel mesoporous biocatalyst derived from kola nut pod husk for conversion of kariya seed oil to methyl esters: A case of synthesis, modeling and optimization studies. Catalysis Letters, 149(7), 1772 1787. Available from https://doi.org/10.1007/s10562-019-02788-6.

Betiku,E.,Etim,A.O.,Pereao,O.,&Ojumu,T.V.(2017).Two-stepconversionofneem(Azadirachtaindica) seed oil into fatty methyl esters using a heterogeneous biomass-based catalyst: An example of cocoa pod husk. Energy and Fuels, 31(6), 6182 6193. Available from https://doi.org/10.1021/acs.energyfuels.7b00604.

Bhuiya, M., Rasul, M., Khan, M., & Ashwath, N. (2019). Performance and emission characteristics of a compression ignition (CI) engine operated with beauty leaf biodiesel. Energy Procedia, 160(2018), 641–647. https://doi.org/10.1016/j.egypro.2019.02.216

Bilgin, A., Gülüm, M., Koyuncuoglu, İ., Nac, E., Cakmak, A. (2015).Determination of transesterification reaction parameters giving the lowest viscosity waste cooking oil biodiesel. Procedia - Social and Behavioral Sciences, 195, 2492–2500. https://doi.org/10.1016/j.sbspro.2015.06.318

Bora, P., Boro, J., Konwar, L. J., & Deka, D. (2016). Formulation of microemulsion based hybrid biofuel from waste cooking oil A comparative study with biodiesel. Journal of the Energy Institute, 89(4), 560 568. Available from https://doi.org/10.1016/j.joei.2015.07.001.

BP p.l.c. (2019). BP Energy Outlook 2019 edition. BP.

Bruun, N., Tesfaye, F., Hemming, J., Dirbeba, M. J., Hupa, L. (2021). Effect of storage time on the physicochemical properties of waste fish oils and used cooking vegetable oils. Energies, 14(1), 101. https://doi.org/10.3390/en14010101

Buyukkaya, E. (2010). Effects of biodiesel on a di diesel engine performance, emission and combustion characteristics. Fuel, 89(10), 3099–3105. https://doi.org/10.1016/j.fuel.2010.05.034

Bwapwa, J. K., Anandraj, A., & Trois, C. (2017). Possibilities for conversion of microalgae oil into avia tion fuel: A review. Renewable and Sustainable Energy Reviews, 80, 1345 1354. Available from https:// doi.org/10.1016/j.rser.2017.05.224.

Cárdenas, J., Orjuela, A., Sánchez, D. L., Narváez, P. C., Katryniok, B., & Clark, J. (2021). Pre-treatment of used cooking oils for the production of green chemicals: A review. Journal of Cleaner Production, 289.https://doi.org/10.1016/j.jclepro.2020.125129

Chen, C., Chitose, A., Kusadokoro, M., Nie, H., Xu, W., Yang, F., Yang, S. (2021). Sustainability and challenges in biodiesel production from waste cooking oil: An advanced bibliometric analysis. Energy Reports, 7, 4022–4034. https://doi.org/10.1016/j.egyr.2021.06.084

Chen, Y., Zhang, J., Zhang, Z., Zhong, W., Zhao, Z., & Hu, J. (2023). Utilization of renewable biodiesel blends with different proportions for the improvements of performance and emission characteristics of a diesel engine. Heliyon, 9(9), e19196. https://doi.org/10.1016/j.heliyon.2023.e19196

Choe, E., & Min, D. B. (2007). Chemistry of deep-fat frying oils. Journal of Food Science, 72(5). https://doi.org/10.1111/j.1750-3841.2007.00352.x

Cihan, Ö. (2021). Experimental and numerical investigation of the effect of fig seed oil methyl ester biodiesel blends on combustion characteristics and performance in a diesel engine. Energy Reports, 7, 5846–5856. https://doi.org/10.1016/j.egyr.2021.08.180

Cordero-Ravelo, V., & Schallenberg-Rodriguez, J. (2018). Biodiesel production as a solution to waste cooking oil (WCO) disposal. Will any type of WCO do for a transesterification process? A quality assessment. Journal of Environmental Management, 228(August), 117–129. https://doi.org/10.1016/j.jenvman.2018.08.106

Daramola, M. O., Mtshali, K., Senokoane, L., & Fayemiwo, O. M. (2016). Influence of operating variables on the transesterification of waste cooking oil to biodiesel over sodium silicate catalyst: A statistical approach. Journal of Taibah University for Science, 10(5), 675–684. https://doi.org/10.1016/j.jtusci.2015.07.008

Demirbas A (2009) Progress and recent trends in biodiesel fuels. Energy Convers Manag 50:14–34. https://doi.org/10.1016/j.enconman.2008.09.001

Demirbas, A. (2005). Biodiesel production from vegetable oils via catalytic and non-catalytic supercritical methanol transesterification methods. Progress in Energy and Combustion Science, 31(5 6), 466 487. Available from https://doi.org/10.1016/j.pecs.2005.09.001.

Di Serio, M., Cozzolino, M., Giordano, M., Tesser, R., Patrono, P., & Santacesaria, E. (2007). From homogeneous to heterogeneous catalysts in biodiesel production. Industrial & Engineering Chemistry Research, 46(20), 6379–6384. https://doi.org/10.1021/ie070663q

Dinesh Kumar, M., Kavitha, S., & Banu, J. R. (2020). Valorization of food waste for biodiesel production. In J. R. Banu, G. Kumar, M. Gunasekaran, & S. Kavitha (Eds.), Food waste to valuable resources: Applications and management (pp. 75–95). Academic Press (Elsevier).

Duran, S. K. (2019). A review on oil extraction and biofuels production from various materials. Materials Today: Proceedings, 26, 261–265. https://doi.org/10.1016/j.matpr.2019.11.223

Eevera, T., Rajendran, K., & Saradha, S. (2009). Biodiesel production process optimization and characterization to assess the suitability of the product for varied environmental conditions. Renewable Energy, 34(3), 762–765. https://doi.org/10.1016/j.renene.2008.04.006

Enweremadu, C. C., & Rutto, H. L. (2010). Combustion, emission and engine performance characteristics of used cooking oil biodiesel—A review. Renewable and sustainable energy reviews, 14(9), 2863-2873.f

Erchamo, Y. S., Mamo, T. T., Workneh, G. A., & Mekonnen, Y. S. (2021). Improved biodiesel production from waste cooking oil with mixed methanol–ethanol using enhanced eggshell-derived CaO nano-catalyst. Scientific Reports, 11(1), 1–12. https://doi.org/10.1038/s41598-021-86062-z

Etim, A. O., Musonge, P., & Eloka-Eboka, A. C. (2021b). Transesterification via parametric modelling and optimization of marula (Sclerocarya birrea) seed oil methyl ester synthesis. Journal of Oleo Science, 70(1), 77 93. Available from https://doi.org/10.5650/jos.ess20258.

Fareed, A. F., El-Shafay, A. S., Mujtaba, M. A., Riaz, F., & Gad, M. S. (2024). Investigation of waste cooking and castor biodiesel blends effects on diesel engine performance, emissions, and combustion characteristics. Case Studies in Thermal Engineering, 60(June), 104721. https://doi.org/10.1016/j.csite.2024.104721

Felizardo, P., Baptista, P., Menezes, J. C., & Correia, M. J. N. (2007). Multivariate near infrared spectroscopy models for predicting methanol and water content in biodiesel. Analytica Chimica Acta, 595(1–2), 107–113. https://doi.org/10.1016/j.aca.2007.02.050

Fontaras, G., Karavalakis, G., Kousoulidou, M., Tzamkiozis, T., Ntziachristos, L., Bakeas, E., et al. (2009). Effects of biodiesel on passenger car fuel consumption, regulated and non-regulated pollutant emissions over legislated and real-world driving cycles. Fuel, 88, 1608–1617.

Freedman, B., Pryde, E.H. and Mounts, T.L. (1984) Variables Affecting the Yields of Fatty Esters from Transesterified Vegetable Oils. Journal of the American Oil Chemists Society, 61, 1638-1643.

Gad, M. S., El-Araby, R., Abed, K. A., El-Ibiari, N. N., El Morsi, A. K., & El-Diwani, G. I. (2018). Performance and emissions characteristics of C.I. engine fueled with palm oil/palm oil methyl ester blended with diesel fuel. Egyptian Journal of Petroleum, 27(2), 215–219. https://doi.org/10.1016/j.ejpe.2017.05.009

Gashaw, A., & Teshita, A. (2014). Production of biodiesel from waste cooking oil and factors affecting its formation: A review. International Journal of Renewable and Sustainable Energy, 3(5), 92–98. https://doi.org/10.11648/j.ijrse.20140305.12

Gaur, R. K., & Goyal, R. (2025). Performance, emission, combustion and economics analysis of CI engine fueled with mixed oil biodiesel blends from waste cooking oil and pongamia oil. Discover Applied Sciences, 7(6). https://doi.org/10.1007/s42452-025-07150-7

Gertz, C. (2000). Chemical and physical parameters as quality indicators of used frying fats. European Journal of Lipid Science and Technology, 102(8–9), 566–572.

GlobalData. (2023, September). UCO supply outlook [Report]. GlobalData. https://cleanfuels.org/wp-content/uploads/GlobalData_UCO-Supply-Outlook_Sep2023.pdf

Gopan, S. N., Rajan, A. V., Krishnan, B. R. (2020). Review of bio-diesel production from waste cooking oil and analysis of IC engine performance. Materials Today: Proceedings, 37(Part 2), 1208–1211. https://doi.org/10.1016/j.matpr.2020.06.373

Habibullah, M., Masjuki, H. H., Kalam, M. A., Rizwanul Fattah, I. M., Ashraful, A. M., & Mobarak, H. M. (2014). Biodiesel production and performance evaluation of coconut, palm and their combined blend with diesel in a single-cylinder diesel engine. Energy Conversion and Management, 87, 250–257. https://doi.org/10.1016/j.enconman.2014.07.006

Henein, N. A., Fragoulis, A. N. (1985). Correlation between physical properties and autoignition parameters of alternative fuels. SAE Paper 850266. https://doi.org/10.4271/850266

Heywood, J. B. (1988). Internal combustion engines: Fundamentals. McGraw-Hill.

Hosseinzadeh-Bandbafha, H., Nizami, A. S., Kalogirou, S. A., Gupta, V. K., Park, Y. K., Fallahi, A., Sulaiman, A., Ranjbari, M., Rahnama, H., Aghbashlo, M., Peng, W., Tabatabaei, M. (2022). Environmental life cycle assessment of biodiesel production from waste cooking oil: A systematic review. Renewable and Sustainable Energy Reviews, 161, 112411. https://doi.org/10.1016/j.rser.2022.112411

How, H. G., Masjuki, H. H., Kalam, M. A., Teoh, Y. H., & Chuah, H. G. (2018). Effect of Calophyllum Inophyllum biodiesel-diesel blends on combustion, performance, exhaust particulate matter and gaseous emissions in a multi-cylinder diesel engine. Fuel, 227(October 2017), 154–164. https://doi.org/10.1016/j.fuel.2018.04.075

IEA (2024), Demand of biogasoline and biodiesel, 1980-2022, IEA, Paris https://www.iea.org/data-and-statistics/charts/demand-of-biogasoline-and-biodiesel-1980-2022, Licence: CC BY 4.0

IEA (2025), Global investment in clean energy and fossil fuels, 2015-2025, IEA, Paris https://www.iea.org/data-and-statistics/charts/global-investment-in-clean-energy-and-fossil-fuels-2015-2025, Licence: CC BY 4.0

IEA. (2024). Oil 2024: Analysis and forecast to 2030. International Energy Agency. https://iea.blob.core.windows.net/assets/493a4f1b-c0a8-4bfc-be7b-b9c0761a3e5e/Oil2024.pdf

Jain, S., & Sharma, M. P. (2010). Biodiesel production from Jatropha curcas oil. Renewable and Sustainable Energy Reviews, 14(9), 3140. Available from https://doi.org/10.1016/j.rser.2010.07.047.

Kaisan, M. U., Anafi, F. O., Nuszkowski, J., Kulla, D. M., & Umaru, S. (2020). Calorific value, flash point and cetane number of biodiesel from cotton, jatropha and neem binary and multi-blends with diesel. Biofuels.

Kalogianni, E. P., Karapantsios, T. D., & Miller, R. (2011). Effect of repeated frying on the viscosity, density and dynamic interfacial tension of palm and olive oil. Journal of Food Engineering, 105(1), 169–179.

Kannan, G. R., Karvembu, R., & Anand, R. J. A. E. (2011). Effect of metal based additive on performance emission and combustion characteristics of diesel engine fuelled with biodiesel. Applied energy, 88(11), 3694-3703.

Kanwar Gaur, R., Goyal, R. (2022). A review: Effect on performance and emission characteristics of waste cooking oil biodiesel–diesel blends on IC engine. Materials Today: Proceedings, 63, 643–646. https://doi.org/10.1016/j.matpr.2022.04.447

Kaplan, C., Arslan, R., & Su¨rmen, A. (2006). Performance characteristics of sunflower methyl esters as biodiesel. Energy Sources Part A, 28, 751–755.

Karki, S., Sanjel, N., Poudel, J., Choi, J. H., & Oh, S. C. (2017). Supercritical transesterification of waste vegetable oil: Characteristic comparison of ethanol and methanol as solvents. Applied Sciences (Switzerland), 7(6). https://doi.org/10.3390/app7060632

Karki, S., Sanjel, N., Poudel, J., Choi, J. H., & Oh, S. C. (2017). Supercritical transesterification of waste vegetable oil: Characteristic comparison of ethanol and methanol as solvents. Applied Sciences (Switzerland), 7(6). https://doi.org/10.3390/app7060632

Kegl, B., Kegl, M., & Pehan, S. (2013). Green diesel engines: Biodiesel usage in diesel engines. Springer. https://doi.org/10.1007/978-1-4471-5325-2

Kesserwan, F., Ahmad, M. N., Khalil, M., El-Rassy, H., & CaO, H. (2020). Al2O3 aerogel as heterogeneous catalyst for biodiesel production. Chemical Engineering Journal, 385.

Khan, M., Chatterjee, R., Hasnain, S. M. M., & Giri, J. (2024). Results in Engineering Effect of fuel injection parameters on the performance & emissions of biodiesel based CI engine-A review. Results in Engineering, 24(October), 103180. https://doi.org/10.1016/j.rineng.2024.103180

Khodadadi, M. R., Malpartida, I., Tsang, C. W., Lin, C. S. K., & Len, C. (2020). Recent advances on the catalytic conversion of waste cooking oil. Molecular Catalysis, 494(July), 111128. https://doi.org/10.1016/j.mcat.2020.111128

Kulkarni, M. G., & Dalai, A. K. (2006). Waste cooking oil - An economical source for biodiesel: A review. Industrial and Engineering Chemistry Research, 45(9), 2901–2913. https://doi.org/10.1021/ie0510526

Lahane, S., Subramanian, K. A. (2015). Effect of different percentages of biodiesel–diesel blends on injection, spray, combustion, performance, and emission characteristics of a diesel engine. Fuel, 139, 537–545. https://doi.org/10.1016/j.fuel.2014.09.036

Liazid, A., Naima, K., Tazerout, M. L., Tarabet, L., Bousbaa, H. (2019). Eucalyptus biofuel study as alternative for diesel engine. International Journal of Renewable Energy Technology, 10(3), 247. https://doi.org/10.1504/IJRET.2019.10022907

Lisbona, P., Pascual, S. (2023). Waste to energy: Trends and perspectives. Cleaner Energy Systems, 14(April), 100494. https://doi.org/10.1016/j.ceja.2023.100494

Loo, D. L., Teoh, Y. H., How, H. G., Teh, J. S., Andrei, L. C., Starčević, S., & Sher, F. (2021). Applications characteristics of different biodiesel blends in modern vehicles engines: A review. Sustainability (Switzerland), 13(17), 1–32. https://doi.org/10.3390/su13179677

Lopresto, C. G. (2024). Sustainable biodiesel production from waste cooking oils for energetically independent small communities: An overview. International Journal of Environmental Science and Technology, 22(3), 1953–1974. https://doi.org/10.1007/s13762-024-05779-2

Lopresto, C. G., De Paola, M. G., Calabrò, V. (2024). Importance of the properties, collection, and storage of waste cooking oils to produce high-quality biodiesel – An overview. Biomass and Bioenergy, 189, 107363. https://doi.org/10.1016/j.biombioe.2024.107363

M.R. Teixeira, R. Nogueira, L.M. Nunes, Quantitative assessment of the valorisation of used cooking oils in 23 countries, Waste Manag. 78 (2018) 611–620, https://doi.org/10.1016/j.wasman.2018.06.039

Ma, F., Hanna, M. A. (1999).Biodiesel production: A review. Bioresource Technology, 70(1), 1–15. https://doi.org/10.1016/S0960-8524(99)00025-5

Macario, A., Giordano, G., Onida, B., Cocina, D., Tagarelli, A., & Giuffrè, A. M. (2010). Biodiesel production process by homogeneous/heterogeneous catalytic system using an acid–base catalyst. Applied Catalysis A: General, 378(2), 160–168. https://doi.org/10.1016/j.apcata.2010.02.016

Maheshwari, P., Haider, M. B., Yusuf, M., Klemeš, J. J., Bokhari, A., Beg, M., Al-Othman, A., Kumar, R., Jaiswal, A. K. (2022). A review on latest trends in cleaner biodiesel production: Role of feedstock, production methods, and catalysts. Journal of Cleaner Production, 355, 131588. https://doi.org/10.1016/j.jclepro.2022.131588

Maheshwari, P., Haider, M. B., Yusuf, M., Klemeš, J. J., Bokhari, A., Beg, M., Al-Othman, A., Kumar, R., & Jaiswal, A. K. (2022). A review on latest trends in cleaner biodiesel production: Role of feedstock, production methods, and catalysts. Journal of Cleaner Production, 355(March). https://doi.org/10.1016/j.jclepro.2022.131588

Mahmudul, H. M., Hagos, F. Y., Mamat, R., Adam, A. A., Ishak, W. F. W., & Alenezi, R. (2017). Production, characterization and performance of biodiesel as an alternative fuel in diesel engines – A review. Renewable and Sustainable Energy Reviews, 72(November 2016), 497–509. https://doi.org/10.1016/j.rser.2017.01.001

Mahmudul, H. M., Hagos, F. Y., Mamat, R., Adam, A. A., Ishak, W. F. W., & Alenezi, R. (2017). Production, characterization and performance of biodiesel as an alternative fuel in diesel engines – A review. Renewable and Sustainable Energy Reviews, 72(November 2016), 497–509. https://doi.org/10.1016/j.rser.2017.01.001

Malik, A. I., Zeeshan, S., Khubaib, M., Ikram, A., Hussain, F., Yassin, H., Qazi, A. (2024). A review of major trends, opportunities, and technical challenges in biodiesel production from waste sources. Energy Conversion and Management: X, 23, 100675. https://doi.org/10.1016/j.ecmx.2024.100675

Maroa, S. (n.d.). Semakula Maroa Freddie Inambao.

Medjahed, L., Bousbaa, H., Benramdane, M. et al. Integrated valorization of waste cooking oil into biodiesel: optimizing upstream processes and blend performance for sustainable energy. Model. Earth Syst. Environ. 11, 389 (2025). https://doi.org/10.1007/s40808-025-02509-6

Meng, X., Chen, G., Wang, Y. (2008). Biodiesel production from waste cooking oil via alkali catalyst and its engine test. Fuel Processing Technology, 89(9), 851–857. https://doi.org/10.1016/j.fuproc.2008.02.006

Mohadesi, M., Aghel, B., Maleki, M., Ansari, A. (2019). Production of biodiesel from waste cooking oil using a homogeneous catalyst: Study of semi-industrial pilot of microreactor. Re-newableEnergy, 136, 677–682. https://doi.org/10.1016/j.fuel.2020.117736

Mohammed, N. I., Kabbashi, N. A., Alade, A. O., & Sulaiman, S. (2018). Advancement in the utilization of biomass-derived heterogeneous catalysts in biodiesel production. Green and Sustainable Chemistry, 8, 74 91. Available from https://doi.org/10.4236/gsc.2018.81006.

Mueller, C. J., & Martin, G. C. (2010). Charles J. Mueller and Glen C. Martin*.

Muralidharan, K., Vasudevan, D., & Sheeba, K. N. (2011). Performance, emission and com-bustion characteristics of biodiesel fuelled variable compression ratio engine. Energy, 36(8), 5385–5393. https://doi.org/10.1016/j.energy.2011.06.050

Musa, I. A. (2016). The effects of alcohol to oil molar ratios and the type of alcohol on bio-diesel production using transesterification process. Egyptian Journal of Petroleum, 25(1), 21–31. https://doi.org/10.1016/j.ejpe.2015.06.007

Norjannah, B., Ong, H. C., Masjuki, H. H., Juan, J. C., & Chong, W. T. (2016). Enzymatic transesterification for biodiesel production: A comprehensive review. RSC Advances, 6(65), 60034–60055. https://doi.org/10.1039/c6ra08062f

O.B. Olmez, C. Gultekin, B. Balcik, A. Ekici, O.¨O. ¨Ozener, A variable neighborhood search based matheuristic for a waste cooking oil collection network design problem, Eur. J. Oper. Res. 302 (2022) 187–202, https://doi.org/ 10.1016/j.ejor.2021.12.018

Orege JI, Oderinde O, Kifle GA et al (2022) Recent advances in het- erogeneous catalysis for green biodiesel production by transesterification. Energy Convers Manag 258:115406

Orjuela, A. (2021). Industrial oleochemicals from used cooking oils (UCOs): Sustainability benefits and challenges. In Advances in carbon management technologies (pp. 74–96). CRC Press.

Ozsezen, A. N., Canakci, M., Turkcan, A., & Sayin, C. (2009). Performance and combustion characteristics of a DI diesel engine fueled with waste palm oil and canola oil methyl esters. Fuel, 88(4), 629–636. https://doi.org/10.1016/j.fuel.2008.09.023

Park, S. H., Cha, J., & Lee, C. S. (2012). Impact of biodiesel in bioethanol blended diesel on the engine performance and emissions characteristics in compression ignition engine. Applied Energy, 99, 334–343. https://doi.org/10.1016/j.apenergy.2012.05.050

Pourzolfaghar, H., Abnisa, F., Daud, W. M. A. W., & Aroua, M. K. (2016). A review of the enzymatic hydroesterification process for biodiesel production. Renewable and Sustainable Energy Reviews, 61, 245 257. Available from https://doi.org/10.1016/j.rser.2016.03.048.

Pydimalla, M., Husaini, S., Kadire, A., & Verma, R. K. (2023). Materials Today : Proceedings Sustainable biodiesel : A comprehensive review on feedstock , production methods , applications , challenges and opportunities. Materials Today: Proceedings, xxxx. https://doi.org/10.1016/j.matpr.2023.03.593

Qi, D. H., Geng, L. M., Chen, H., Bian, Y. Z., Liu, J., & Ren, X. C. (2009). Combustion and performance evaluation of a diesel engine fueled with biodiesel produced from soybean crude oil. Renewable Energy, 34(12), 2706–2713. https://doi.org/10.1016/j.renene.2009.05.004

Raheman, H., & Ghadge, S. V. (2007). Performance of compression ignition engine with mahua (Madhuca indica) biodiesel. Fuel, 86(16), 2568-2573.

Ramadhas, A. S. (2011). Alternative fuels for transportation (p. 463). Taylor & Francis.

Refaat, A.A., Attia, N.K., Sibak, H.A. et al. Production optimization and quality assessment of biodiesel from waste vegetable oil. Int. J. Environ. Sci. Technol. 5, 75–82 (2008). https://doi.org/10.1007/BF03325999

Sahar, S., Sadaf, S., Iqbal, J., Ullah, I., Bhatti, H. N., Nouren, S., Habib-ur-Rehman, M., Nisar, J., Iqbal, M. (2018). Biodiesel production from waste cooking oil: An efficient technique to convert waste into biodiesel. Sustainable Cities and Society, 41, 220–226. https://doi.org/10.1016/j.scs.2018.05.037

Saifuddin, N., Samiuddin, A., & Kumaran, P. (2015). A review on processing technology for biodiesel production. Trends in Applied Sciences Research, 10, 1 37. Available from https://doi.org/10.3923/ tasr.2015.1.37.

Saka, S., & Kusdiana, D. (2001). Biodiesel fuel from rapeseed oil as prepared in supercritical methanol. Fuel, 80(2), 225 231. Available from https://doi.org/10.1016/S0016-2361(00)00083-1.

Salamanca, M.; Mondragón, F.; Agudelo, J.R.; Santamaría, A. Influence of palm oil biodiesel on the chemical and morphological characteristics of particulate matter emitted by a diesel engine. Atmos. Environ. 2012, 62, 220–227. https://doi.org/10.1016/j.atmosenv.2012.08.031

Sanli, H., Canakci, M., & Alptekin, E. (2011). Characterization of Waste Frying Oils Obtained from Different Facilities. Proceedings of the World Renewable Energy Congress – Sweden, 8–13 May, 2011, Linköping, Sweden, 57, 479–485. https://doi.org/10.3384/ecp11057479

Saxena, P., Jawale, S., Joshipura, M. H. (2013). A review on prediction of properties of biodiesel and blends of biodiesel. Procedia Engineering, 51(NUiCONE 2012), 395–402. https://doi.org/10.1016/j.proeng.2013.01.055

Sethuraman, N., Karthikeyan, D., Vinodraj, S., Thamizhvel, R., & Kumarasamy, G. (2023). Performance and emission characteristics on CI engine by using waste cooking oil and waste transformer oil as substitute fuel with coconut shell as a catalyst. *Materials Today: Proceedings*, *72*, 2469–2475. https://doi.org/10.1016/j.matpr.2022.09.457

Shah, S., & Gupta, M. N. (2007). Lipase catalyzed preparation of biodiesel from Jatropha oil in a solvent free system. Process Biochemistry, 42(3), 409–414. https://doi.org/10.1016/j.procbio.2006.09.024

Sikorska, E., Caponio, F., Bilancia, M. T., Summo, C., Pasqualone, A., Khmelinskii, I. V., Sikorski, M. (2007). Changes in colour of extra-virgin olive oil during storage. Polish Journal of Food and Nutrition Sciences, 57, 495–498.

Silitonga, A. S., Mahlia, T. M. I., Ong, H. C., Riayatsyah, T. M. I., Kusumo, F., Ibrahim, H.,Gumilang, D. (2017). A comparative study of biodiesel production methods for Reutealis trisperma biodiesel. Energy Sources, Part A: Recovery, Utilization, and Environmental Effects, 39(20), 2006–2014. https://doi.org/10.1080/15567036.2017.1399174

Singh, B., & Guldhe, A. (Eds.). (2022). Waste and biodiesel: Feedstocks and precursors for catalysts. Elsevier. ISBN 978 0 12 823958 2.

Singh, D., et al. (2020). A review on feedstocks, production processes, and yield for different generations of biodiesel. Fuel, 262, 116553. https://doi.org/10.1016/j.fuel.2019.116553

Singh, R. S., Pandey, A., & Gnansounou, E. (Eds.). (2016). Biofuels: Production and future perspectives. CRC Press.

Sodhi, A. K., Tripathi, S., & Kundu, K. (2017). Biodiesel production using waste cooking oil: a waste to energy conversion strategy. Clean Technologies and Environmental Policy, 19(6), 1799–1807. https://doi.org/10.1007/s10098-017-1357-6

Su, J.; Zhu, H.; Bohac, S.V. Particulate matter emission comparison from conventional and premixed low temperature combustion with diesel, biodiesel and biodiesel-ethanol fuels. Fuel 2013, 113, 221–227. https://doi.org/10.1016/j.fuel.2013.05.068

Sunggyu, L. S., & Shah, Y. T. (2012). Biofuels and bioenergy: Processes and technologies. In Biofuels and Bioenergy: Processes and Technologies. https://doi.org/10.1201/b12510

Suzihaque, M. U. H., Alwi, H., Ibrahim, U. K., Abdullah, S., Haron, N. (2022). Biodiesel production from waste cooking oil: A brief review. Materials Today: Proceedings, 63, S490–S495. https://doi.org/10.1016/j.matpr.2022.04.527

Tabatabaei, M., & Aghbashlo, M. (2019). Biodiesel: From Production to Combustion. In Biodiesel. http://www.springer.com/series/11833

Tesfa, B., Mishra, R., Gu, F., Powles, N. (2010). Prediction models for density and viscosity of biodiesel and their effects on fuel supply system in CI engines. Renewable Energy, 35(12), 2752–2760.

Thangaraj, B., Solomon, P. R., Muniyandi, B., Ranganathan, S., & Lin, L. (2019). Catalysis in biodiesel production - A review. Clean Energy, 3(1), 2–23. https://doi.org/10.1093/ce/zky020

Topare, N. S., Jogdand, R. I., Shinde, H. P., More, R. S., Khan, A., Asiri, A. M. (2022). A short review on approach for biodiesel production: Feedstock's, properties, process parameters and environmental sustainability. Materials Today: Proceedings, 57, 1605–1612. https://doi.org/10.1016/j.matpr.2021.12.216

Topi, D. (2020). Transforming waste vegetable oils to biodiesel: Establishing a waste oil management system in Albania. SN Applied Sciences, 2, Article 2268. https://doi.org/10.1007/s42452-020-2268-4

Torres-Jimenez, E., Svoljsˇak-Jerman, M., Gregorc, A., Lisec, I., Dorado, M. P., & Kegl, B. (2010). Physical and chemical properties of ethanol–biodiesel blends for diesel engines. Energy & Fuels, 24, 2002–2009.

Ujong, A. E., Emelike, N. J. T., Owuno, F., & Okiyi, P. N. (2023). Effect of frying cycles on the physical, chemical and antioxidant properties of selected plant oils during deep-fat frying of potato chips. Food Chemistry Advances, 3(June), 100338. https://doi.org/10.1016/j.focha.2023.100338

Ullah, F., Dong, L., Bano, A., Peng, Q., & Huang, J. (2016). Current advances in catalysis toward sus tainable biodiesel production. Journal of the Energy Institute, 89(2), 282 292. Available from https:// doi.org/10.1016/j.joei.2015.01.018.

Verma, P., Sharma, M. P. (2016). Review of process parameters for biodiesel production from different feedstocks. Renewable and Sustainable Energy Reviews, 62, 1063–1071. https://doi.org/10.1016/j.rser.2016.04.054

Vicente, G., Martínez, M., & Aracil, J. (2004). Integrated biodiesel production: A comparison of different homogeneous catalyst systems. Bioresource Technology, 92(3), 297–305. https://doi.org/10.1016/j.biortech.2003.08.014

Vieira da Silva, M. A., Lagnier Gil Ferreira, B., da Costa Marques, L. G., Lamare Soares Murta, A., & Vasconcelos de Freitas, M. A. (2017). Comparative study of NOx emissions of biodiesel-diesel blends from soybean, palm and waste frying oils using methyl and ethyl transesterification routes. Fuel, 194, 144–156. https://doi.org/10.1016/j.fuel.2016.12.084

Vyas, A. P., Verma, J. L., & Subrahmanyam, N. (2010). A review on FAME production processes. Fuel, 89(1), 1–9. https://doi.org/10.1016/j.fuel.2009.08.014

Wu, F., Wang, J., Chen, W., & Shuai, S. (2009). A study on emission performance of a diesel engine fueled with five typical methyl ester biodiesels. *Atmospheric Environment*, *43*(7), 1481–1485. https://doi.org/10.1016/j.atmosenv.2008.12.007

Yaakob, Z., Mohammad, M., Alherbawi, M., Alam, Z., Sopian, K. (2013). Overview of the production of biodiesel from waste cooking oil. Renewable and Sustainable Energy Reviews, 18, 184–193. https://doi.org/10.1016/j.rser.2012.10.016

Yuan, M.-H., Chen, Y.-H., Chen, J.-H., & Luo, Y.-M. (2017). Dependence of cold filter plugging point on saturated fatty acid profile of biodiesel blends derived from different feedstocks. Fuel, 195, 59–68. https://doi.org/10.1016/j.fuel.2017.01.054

Zhang, H., Ozturk, U. A., Wang, Q., Zhao, Z. (2014). Biodiesel produced by waste cooking oil: Review of recycling modes in China, the US, and Japan. Renewable and Sustainable Energy Reviews, 38, 677–685. https://doi.org/10.1016/j.rser.2014.07.042

Zhang, J., Zhang, L., & Jia, L. (2012). Variables affecting biodiesel production from Zanthoxylum bungeanum seed oil with high free fatty acids. Industrial & Engineering Chemistry Research, 51(9), 3525–3530. https://doi.org/10.1021/ie200306w

Zhang, Z., E, J., Deng, Y., Pham, M. H., Zuo, W., Peng, Q., & Yin, Z. (2018). Effects of fatty acid methyl esters proportion on combustion and emission characteristics of a biodiesel fueled

marine diesel engine. Energy Conversion and Management, 159(November 2017), 244–253. https://doi.org/10.1016/j.enconman.2017.12.098

Ziejewski, M., Kaufman, K. R., Schwab, A. W., & Pryde, E. H. (1984). Diesel engine evaluation of a nonionic sunflower oil–aqueous ethanol microemulsion. Journal of the American Oil Chemists' Society, 61(10), 1620–1626. https://doi.org/10.1007/BF02541646